In-Situ observation of New Particle Formation (NPF) in the tropical tropopause layer of the 2017 Asian Monsoon Anticyclone: Part II - NPF ~~New particle formation~~ inside ice clouds~~: In-situ observations in the tropical tropopause layer of the 2017 Asian Monsoon Anticyclone~~

Kommentiert [WR1]: Part II - Änderung!

Kommentiert [WR2]: Part II - Änderung!

Ralf Weigel[1], Christoph Mahnke[2,6], Manuel Baumgartner[1,3], Martina Krämer[1,4], Peter Spichtinger[1], Nicole Spelten[4], Armin Afchine[4], Christian Rolf[4], Silvia Viciani[5], Francesco D'Amato[5], Holger Tost[1], and Stephan Borrmann[1,2]

[1]Institut für Physik der Atmosphäre, Johannes Gutenberg Universität, Mainz, Germany
[2]Partikelchemie, Max-Planck-Institut für Chemie, Mainz, Germany
[3]Zentrum für Datenverarbeitung, Johannes Gutenberg University, Mainz, Germany
[4]Institute of Energy and Climate Research (IEK-7), Forschungszentrum Jülich, Jülich, Germany
[5]National Institute of Optics - National Research Council (CNR-INO), Florence, Italy
[6]now at the Institute of Energy and Climate Research (IEK-8), Forschungszentrum Jülich, Jülich, Germany

Abstract

From 27 July to 10 August 2017, the airborne StratoClim mission took place in Kathmandu, Nepal where eight mission flights were conducted with the M-55 *Geophysica* up to altitudes of 20 km. New Particle Formation (NPF) was identified by the abundant presence of ~~ultrafine~~ nucleation-mode aerosols, with particle diameters d_p smaller than 15 nm, which were *in-situ* detected by means of condensation nuclei (CN) ~~counting~~ counter techniques. NPF fields in clear-skies as well as in the presence of cloud ice particles (d_p > 3 µm) were encountered at upper troposphere / lowermost stratosphere (UT/LS) levels and within the Asian Monsoon Anticyclone (AMA). NPF-generated ~~ultrafine~~nucleation-mode particles in elevated concentrations ($N_{~~uf~~nm}$) were frequently found together with cloud ice (in number concentrations N_{ice} of up to 3 cm^{-3}) at heights between ~ 11 km and 16 km. From a total measurement time of ~ 22.5 hours above 10 km altitude, in-cloud NPF was in sum detected over ~ 1.3 hours (~ 50 % of all NPF records throughout StratoClim). Maximum $N_{~~uf~~nm}$ of up to ~ 11000 cm^{-3} were detected coincidently with intermediate ice particle concentrations N_{ice} of 0.05 – 0.1 cm^{-3} at comparatively moderate carbon monoxide (CO) contents of ~ 90 - 100 nmol mol^{-1}. Neither under clear-sky nor during in-cloud NPF do the highest $N_{~~uf~~nm}$ concentrations correlate with the highest CO mixing ratios, suggesting that an elevated pollutant load is not a prerequisite for NPF. Under clear-air conditions, NPF with elevated $N_{~~uf~~nm}$ (> 8000 cm^{-3}) occurred slightly less often than within clouds. In the presence of cloud ice, NPF with $N_{~~uf~~nm}$ between 1500 – 4000 cm^{-3} were observed about twice as often as under clear air conditions. NPF was not found ~~W~~when ice water contents exceeded 1000 µmol mol^{-1} in very cold air (< 195 K) at tropopause levels~~ NPF was not found~~. This ~~may indicate~~indicates a reduction of NPF once ~~a strong~~deep convection~~ overshoot~~ is prevalent together with the presence of mainly

liquid-origin ice particles. Within *in-situ* cirrus near the cold point tropopause, recent NPF or intense events with mixing ration n_{nm} larger than 5000 mg^{-1} were observed only in about 6 % of the in-cloud NPF data. ~~In the presence of *in-situ* cirrus near the cold point tropopause very recent NPF or events of remarkable strength (mixing ratios n_{nf} > 5000 mg^{-1}) were rarely observed (~ 6 % of in-cloud NPF data).~~ In determining whether the cloud-internal NPF is attenuated or prevented by the microphysical properties of cloud elements, the integral radius (*IR*) of the ice cloud population turned out to be indicative. ~~For specifying the constraining mechanisms for NPF possibly imposed by the microphysical properties of the cloud elements, the integral radius (*IR*) of the ice cloud population was identified as the most practicable indicator~~. Neither the number of ice particles nor the free distance between the ice particles are clearly related. ~~Neither of both, the number of ice particles or the free distance between the ice particles, is clearly related~~ to the NPF-rate detected. While the increase of ice particles' mass per time ($\frac{dm}{dt}$) is proportional to the *IR* and mainly due to the condensation of water vapour, additional condensation of NPF precursor proceeds at the expense of the NPF rate as the precursor's saturation ratio declines. Numerical simulations show the impact of the *IR* on the supersaturation of a condensable vapour, such as sulphuric acid, and furthermore illustrate that the *IR* of the cloud ice determines the effective limitation of NPF-rates. ~~The results of a numerical simulation indicates how the *IR* affects the supersaturation of a condensable vapour, such as sulphuric acid, and that *IR* determines the effective limitation of NPF rates due to cloud ice.~~

Formatiert: Schriftart: Kursiv

Formatiert: Schriftart: Kursiv

Formatiert: Schriftart: Nicht Kursiv

Formatiert: Schriftart: Nicht Kursiv

Formatiert: Schriftart: Kursiv

Formatiert: Schriftart: Kursiv

Formatiert: Schriftart: Kursiv

1. Introduction

The process of gas-to-particle conversion, also denoted as homogeneous aerosol nucleation and most commonly known as new particle formation (NPF), ~~constitutes~~ is ~~one of the most effective sources~~ a major source of atmospheric aerosols and cloud condensation nuclei, which could promote the cloud formation at intermediate and upper tropospheric altitudes (e.g. Spracklen et al. (2006); Merikanto et al. (2009); Dunne et al. (2016); Gordon et al. (2017)). Sulphuric acid (H_2SO_4) and water (H_2O) are ~~presumably are~~ important chemical compounds involved in the NPF process. which~~, moreover,~~ is ~~likely~~ aided when ions come into play at elevated altitudes and cold temperatures within the atmosphere (Lee et al. (2003); Kazil et al. (2008); Weigel et al. (2011); Duplissy et al. (2016)). It was suggested that a ternary nucleation process involves, apart from sulphuric acid and water, an additional constituent such as ammonia (NH_3; Ball et al. (1999); Benson et al. (2009); Höpfner et al. (2019)). Experimental studies at the CLOUD (Cosmics Leaving OUtdoor Droplets) chamber confirmed that NPF rates are substantially elevated within this ternary H_2SO_4-H_2O-NH_3 System (e.g. Kirkby et al. (2011); Kürten et al. (2016); Kürten (2019)). In addition to sulphuric acid and ammonia, organic species (e.g. Metzger et al. (2010); Kerminen et al. (2010)) or amines (Kürten et al., 2018) may also promote particle

nucleation and growth. Considering the amounts of organic aerosols (Murphy et al., 2006) and ammonia species (Höpfner et al., 2019) that were frequently found in aerosol particles at UT/TTL heights in the AMA during StratoClim 2017, NPF is likely promoted by such species in the UT and TTL region.

~~From the CLOUD experiments, which were performed under a variety of controlled conditions, it can be deduced that the intensity of NPF (the formation rate of new particles per air volume and per time unit) depends on the concentration of the NPF precursors.~~ ~~T~~The results of individual CLOUD experiments ~~experiments~~ (Kürten et al. (2015); Kürten et al. (2016)) under a variety of controlled conditions and at different and elevated concentrations of the H_2SO_4 solution, always at supersaturated states, show how strongly ~~that~~ the nucleation rates are ~~strongly~~ associated with the precursor concentrations. The time series of a nucleation event within the CLOUD chamber (supplementary material of Kirkby et al. (2011)) shows that the nucleation rate remains elevated as long as the amount of precursors is kept at a constant level. Under real conditions in the atmosphere, however, the concentration of precursor material is spatially and temporally highly variable (e.g. Speidel et al. (2007), Ranjithkumar et al. (2021), or Höpfner et al. (2019)). Besides the precursor gas abundance, temperature determines the degree of supersaturation, which implies that even high precursor concentrations can yield weak NPF rates. Additionally, also temperature fluctuations at any (low) precursor concentrations can increase the local supersaturation and induce intense NPF (cf. Weigel et al. (2021a))~~T~~emperature determines the degree of supersaturation, which implies that even high precursor concentrations may result in a weak NPF rate, and vice versa.~~.~~

~~In particular, f~~For ternary or multi-component NPF, the degree of supersaturation as a function of temperature remains indeterminable if the respective concentration of the different substances is unknown as so far is the case for most atmospheric observations. T~~herefore, t~~he chamber experiments allow for studying the nucleation rate as a function of the precursor concentration at different temperatures, i.e. at varying supersaturation ratios, which are specific, but mostly unknown, with respect to the system of nucleating substances (involving H_2SO_4, H_2O, and NH_3). The complexity increases with sulphuric acid nucleation systems involving besides NH_3 also nitric acid (HNO_3) (Wang et al., 2020) or oxidised organic vapours (Riccobono et al., 2014), all of which ~~may~~ are reported as promoting ~~promote the~~ NPF ~~process~~ at supersaturations lower than required for pure H_2SO_4 solutions. The role of organic substances in connection with NPF ~~could be~~is of particular importance in the tropical UT/LS as has been indicated by (Schulz et al., 2018) and (Andreae et al., 2018). ~~The time series of a nucleation event within the CLOUD chamber (supplementary material of Kirkby et al. (2011)) shows, however, that the nucleation rate remains elevated as long as the amount of precursors is kept at a constant level as~~

~~investigated by means of the CLOUD experiments. Under real conditions in the atmosphere, however, the concentration of precursor material is spatially and temporally highly variableSpeidel et al. (2007)Rollins et al. (2017)Ranjithkumar et al. (2021)Höpfner et al. (2019)(Hopfner et al., 2019). Temperature fluctuations affect the degree of precursor supersaturation; hence, even low precursor concentrations may result in elevated supersaturations and intense NPF.~~ The influence of third or more substances possibly involved in the NPF process is not conclusively detectable or quantifiable~~The influence of third or multiple substances possibly involved in the NPF process is not unambiguously detectable or even quantifiable~~ in the ~~ultrafine~~ nucleation-mode particle population due to the current lack of instrumentation capable of directly analysing the chemical composition of such small particles ~~directly~~.

By means of ground based as well as airborne *in-situ* measurements, NPF was frequently observed to occur at various conditions and atmospheric altitudes (Kerminen et al., 2018). Recently, Williamson et al. (2019) compiled a comprehensive data set of *in-situ* NPF observations at altitudes from 180 m above sea level to up to ~ 12 km, thereby covering a latitude range from 80° North to 70° South alongside the Americas, and by probing air over both oceans, the Pacific and the Atlantic. In tropical regions, most of the *in-situ* NPF observations were made below the level of zero net radiative heating, i.e. at altitudes where subsidence or cloud formation is still well capable to efficiently remove or scavenge aerosol particles.

Investigations at high altitudes (i.e. > 12 km) concerning the occurrence of NPF within clouds~~,~~ or in their immediate vicinity~~,~~ are sparse; ~~and are~~ most of such observations ~~mainly~~are ~~limited to~~limited to ~~–~~tropospheric altitudes (e.g. Clarke and Kapustin (2002)). The region above tropospheric clouds seems favourable for NPF to occur, and possible reasons for this are discussed by Wehner et al. (2015). They found that the majority of their near-cloud NPF observations correlated with increased ultraviolet irradiance, so they concluded cloud edges to be a favourable environment for the production of precursor gases for the formation of new particles (*ibid.*). These authors argued that nucleation and particle growth is promoted by turbulences at the cloud edges, which also Radke and Hobbs (1991) already observed coincidently with abundant particles at increased relative humidity. Furthermore, NPF was found to be an important process inside the convective outflows (e.g. Twohy et al. (2002); Waddicor et al. (2012)). From measurements in the upper troposphere it is commonly assumed that the occurrence of NPF is directly connected to deep convective cloud systems (e.g. de Reus et al. (2001); Clarke and Kapustin (2002); Weigelt et al. (2009); Andreae et al. (2018)). The relationship between NPF and ice clouds is discussed in this study, whilst the immediate connection of NPF and deep convective events is addressed in Weigel et al. (2021a).

Formatiert: Schriftart: Kursiv

During *in-situ* measurements aboard the NASA high altitude research aircraft WB-57, Lee et al. (2004) observed nucleation events inside subtropical and tropical cirrus clouds between 7 and 16 km over Florida. The same authors summarise that they found recent occurrence of NPF in 72 % of their measurements within clouds. Despite the conceptual notion that the presence of cloud elements generally inhibits the formation of new particles, Kazil et al. (2007) demonstrated by means of model simulations that new sulphate aerosol can form within ice clouds such as cirrus. New particles are also produced in the anvil region and cirrus decks of Mesoscale Convective Systems (MCS) over West Africa (Frey et al., 2011). The particular role of mid-latitude MCS as a source of freshly formed aerosol within the upper troposphere was already suggested by Twohy et al. (2002), based on the detection of increased concentrations of particles with size diameter (d_p) greater than 25 nm, concurrently with elevated particle volatility. In the region of the Tropical Transition Layer (TTL) over South America, Australia and West Africa, the *in-situ* measurements by Weigel et al. (2011) revealed ~~nucleation~~ nucleation-mode particles in elevated number concentrations ~~likely resulting~~ from recent NPF. Based on coincident detections of abundant ~~nucleation~~ nucleation-mode particles together with cloud elements (i.e. ice particles of diameters 2.7 µm < d_p < 1.6 mm) ~~in~~ at ice~~ice~~ number concentrations always below ~ 2 cm^{-3} the authors concluded that the occurrence of NPF is mainly limited by the number of cloud particles. The underlying ~~concept~~ notation is that the surfaces of the cloud elements either scavenge the NPF-produced aerosol particles or remove the nucleating vapour molecules prior to the NPF process.

Regarding the occurrence of NPF in conjunction with the presence of upper tropospheric ice clouds~~, still~~ several unspecified details remain:

1) ~~what~~ What are the sets of chemical species acting as NPF precursor~~,~~?
2) ~~does~~ Does NPF ~~possibly~~ require (or not) contributions by cosmic radiation, by ions (Lovejoy et al. (2004); Kazil et al. (2008); Weigel et al. (2011)) ~~or,~~ or by chemical agents or catalysts (e.g. ~~Kürten (2019)),~~ Kürten (2019))?
3) ~~which~~ Which are the advantageous thermodynamic conditions for NPF within a cloud~~,~~ ?~~and~~
4) What are t~~t~~he conditions under which NPF is suppressed by the presence of ice particles of certain size and/or number?
5) What are the relative contributions from clear-air or in-cloud NPF to the aerosol population in the UT/LS?
6) Furthermore, it is of interest how the nucleation-mode particles from in-cloud NPF are processed:

Formatiert: Schriftfarbe: Schwarz

Formatiert: Schriftfarbe: Schwarz

Formatiert: Schriftfarbe: Schwarz

a. are the nucleation-mode particles dispersed as contribution to the clear-air background aerosol as soon as the cloud elements evaporate, or

4)b. are the nucleation-mode particles scavenged by present ice particles?

Comprehensive understanding of these processesComprehensive understanding of these relationships and their influences under real atmospheric conditions is necessary, particularly for modelling purposes. Such insights allow for narrowing down the cloud type and properties as well as the location in the cloud where NPF preferentially occurs in order to obtain estimates of the importance of NPF in the cloud. and their influences under real atmospheric conditions potentially contributes to narrow down the cloud type and the in-cloud location where NPF preferentially occurs, in order to obtain estimates (in particular for modelling purposes) concerning the importance of in-cloud NPF. Furthermore, the question could arise how the ultrafine particles generated by in-cloud NPF are processed: for example, if the ultrafine particles disperse as contribution to the clear air background aerosol as soon as the cloud elements evaporate, or if, in persistent clouds, the ultrafine particles are captured by present ice particles. In the context of the Asian Monsoon Anticyclone (AMA) it is important to clarify the origin of observed aerosol enhancements of aerosols in the embedded Asian Tropopause Aerosol Layer (ATAL, cf. Vernier et al. (2011); Vernier et al. (2018)). NPF could well beis an important source of aerosol particles which are then available for further processing to form the ATAL (Höpfner et al. (2019); He et al. (2019); Mahnke et al. (2021)). Furthermore, the relative contribution of in-cloud versus clear-air NPF is of importance in this context.

TThe Asian Monsoon Anticyclone (AMA) is a meteorological structure, which determines the regional circulation in constitutes one of the most important weather systems, which mainly determines the circulation in the Upper Troposphere/Lower Stratosphere (UT/LS) during monsoon season over the Indian subcontinentbetween June and September. The AMA is usually associated with extensive deep convection capable of transporting polluted air from the regional boundary layer (BL) to high altitudes. From the beginning of June through about the end of September, the large-scale anticyclone persists in the altitude level from the UT reaching up into LS regions (e.g. Randel and Park (2006); Park et al. (2007),) spanning over longitudes from East Asia to the Middle East/East Africa (e.g. Vogel et al. (2014); Vogel et al. (2019)). The system's anticyclonic rotation induces the development of a horizontal transport barrier within in the UT/LS (Ploeger et al., 2015) reducing isentropic exchange between the interior of the AMA and the anticyclone's surroundings. The vertical upward transport within the Asian monsoon circulation is understood as an effective pathway for young air from their of BL origin (Vogel et al., 2019) to rapidly reach UT/LS altitudes, accompanied by various constituents such as pollutants and, further gaseous material (Pan et al., 2016), and in particular water vapour

Formatiert

Formatiert: Schriftfarbe: Schwarz

(Ploeger et al., 2013). ~~To which extent the stratospheric entry of H_2O is supported by cirrus cloud particles (as a result of overshooting convection or ice formation due to local dynamics; de Reus et al. (2009); Corti et al. (2008)) is currently under debate (Ueyama et al. (2018), and references therein) and one of the subjects of a recent study by Krämer et al. (2020). Based on satellite investigations the existence of the ATAL was explored at tropopause altitudes within the AMA region (Vernier et al. (2011); Thomason and Vernier (2013)). Therefore, the~~ The constituents of the uplifted young air from ~~low~~ BL altitudes ~~may~~ also comprise ~~the~~ precursor material from anthropogenic (Vernier et al. (2015); Yu et al. (2015); Höpfner et al. (2019); Mahnke et al. (2021)) and other sources to develop and maintain the observed ~~aerosol layer~~ATAL~~, most likely due to NPF occurring at levels between approximately 14 km and the tropopause~~.

This study reports on the frequent occurrence of NPF in the presence of cloud ice in the tropopause region over the Indian subcontinent during the Asian monsoon season of the year 2017. All measurement data shown herein were acquired during StratoClim ~~2017~~ (in July/August 2017) based at Kathmandu, Nepal, and conducted with the M-55 *Geophysica* that operates up to 20 km altitude. NPF was observed with almost equivalent extent in clear-air as well as~~, under certain conditions,~~ in the midst of cloud ice particles. This investigation ~~aims at summarising~~summarises the various conditions under which NPF was observed coincidently with cloud ice particles. ~~Close examination of the measured data revealed that potential artefacts on the aerosol measurements due to the presence of ice particles, as suggested by Williamson et al. (2019), are largely excludable for the StratoClim data set (cf. Appendix A).~~ The caveats limiting the magnitude of encountered NPF are examined, as are the possibly constraining mechanisms imposed by the cloud elements' microphysical properties. The frequency of NPF observations in coincidence with elevated ice particle densities as well as in clear air ~~puts emphasis on the importance of the~~highlights the importance of the tropopause region within the AMA as an effective source region of ~~freshly nucleated~~ aerosols.

2 The StratoClim field campaign ~~in 2017~~, instruments and methods

During the Asian monsoon season, between 27 July and 10 August 2017, a total of eight scientific flights was conducted above parts of the Indian subcontinent, out of Kathmandu, Nepal (27° 42' 3'' N, 85° 21' 42'' E) throughout StratoClim 2017 (cf. Figure 1~~Figure 1~~). Some of these flights ~~partly~~ also led out of the Nepalese airspace, to east India, Bangladesh and the farthest north of the Bay of Bengal. The occurrence of NPF was encountered (cf. Figure 1~~Figure 1~~) during each flight, either in clear air or in the presence of cloud (ice) particles.

Formatiert: Schriftart: Nicht Fett, Englisch (Vereinigtes Königreich)

Formatiert: Schriftart: Nicht Fett, Englisch (Vereinigtes Königreich)

2.1 Number concentration of sub-micrometre sized particles

The 4-channel continuous flow condensation particle counter COPAS (COndensation PArticle counting System; Weigel et al. (2009)) ~~, which was operated with the chlorofluorocarbon (FC 43) as working liquid,~~ was used for measuring aerosol particle number concentrations. Particle detection and data storage occurred at 1 Hz frequency. Th~~For the reduction of the statistical noise in the raw signals, which are recorded directly from the scattered light detectors of the COPAS instrument, the 1-Hz raw data are pre-processed by a 15-second running average. Th~~e COPAS channels were set to different 50 %-detection particle diameters d_{p50} (i.e. 6 nm, 10 nm, and 15 nm). By counting aerosols (with d_{p50} = 10 nm) downstream of a heated (~ 270°C) sample flow line, a fourth COPAS channel measured particle concentrations of non-volatile (nv) or refractory particles (e.g. soot, mineral dust, metallic aerosol material as well as, e.g., organic material mixtures not evaporating at 270 °C, etc.). The measured data revealed that potential artefacts on the aerosol measurements due to the presence of ice particles, as suggested by Williamson et al. (2019), are largely excludable for the StratoClim data set (cf. Appendix A). For further details on the operation of COPAS during StratoClim 2017, the companion paper (Weigel et al., 2021a) provides further insights, as does the article with the technical introduction and characterisation of the COPAS device, the aerosol inlet system, and the particle vaporiser (Weigel et al., 2009).~~By means of laboratory experiments, the aerosol heating device was demonstrated to vaporise more than 98 % of H_2SO_4-H_2O particles at pressures between 70 and 300 hPa (Weigel et al., 2009). The aerosol sampling occurred via the forward facing aerosol inlet of COPAS, a custom-made reproduction of the inlet used on board the NASA ER-2 (Wilson et al., 1992). The use of this aerosol inlet also facilitated Lee et al. (2004) to measure in-cloud NPF. The inlet allows for aerosol sampling well outside the boundary layer of the aircraft. The inlet's geometry comprises two serial diffusors to sample air (at super-isokinetic conditions) with decelerated flow speed compared to the ambient free flow. The largest particle diameter that is detectable with the COPAS system is confined by the inlet geometry, and it is estimated that sub-micrometre sized particles enter the aerosol inlet and pass the aerosol lines without significant particle losses (Weigel et al., 2009). However, aerosol particles with diameter of up to 5 µm may occasionally be aspired by the COPAS inlet, but are clearly undersampled (Ebert et al., 2016). The COPAS measurement uncertainty is about 15 % for stratospheric particle concentrations, mainly due to uncertainties in the volume flow and as a result from particle counting statistics The~~ COPAS is an established instrument for high altitude application and ~~,~~ its ~~performance was characterised by Weigel et al. (2009) and COPAS~~ data were used and discussed in various studies (e.g. in Curtius et al. (2005); Borrmann et al. (2010); Frey et al. (2011); Weigel et al. (2011); Weigel et al. (2014); Schumann et al. (2017); Höpfner et al. (2019)).

Formatiert: Schriftart: Cambria

Formatiert: Schriftart: Cambria

2.2 Terminology and notations

Measured particle number concentrations N are provided in units of particle number per cubic centimetre of sampled air (ambient conditions). To compare aerosol observations from different pressure altitudes and, e.g., for correlations with mixing ratios of trace gases, COPAS measurements are also given as mixing ratio n in units of particles per milligram of air (mg^{-1}) as calculated based on the 1 Hz-resolved data of ambient static pressure and temperature (cf. Section 2.5). With N_6 (N_{15}) as the number concentration of submicrometre-sized particles with diameter greater than 6 nm (15 nm), t~~Hereafter, n_{10} denotes T~~he number concentration of ~~ultrafine~~nucleation-mode ~~aerosol~~ particles (~~hereafter~~ denoted as $N_{~~uf~~nm}$) is calculated from the difference N_6 - N_{15} = $N_{6\text{-}15}$~~, and~~This concentration of nucleation-mode particles ~~serves as an indication for~~indicates recent NPF if the designated NPF criterion (Equation 1) is met:

$$0.8 \cdot N_6 - 1.2 \cdot N_{15} > 0 \,. \qquad (1~~),~~)$$

This criterion was reassessed for the StratoClim 2017 data set and accounts for the COPAS detectors' signal-to-noise ratio and the counting statistics. Further ~~based on the principle definition used by Weigel et al. (2011).Further d~~details concerning the ~~corrections~~criterion and the corrections applied to ~~the measured~~ COPAS data~~, which were obtained, throughout the StratoClim 2017 mission are provided by Weigel et al. (2020a)~~are provided in Weigel et al. (2021a)~~, where the empirical parameters of 0.8 and 1.2 are introduced~~.

If compliant with the NPF criterion, a series of data points is a designated NPF *event* if measured number concentrations (or mixing ratios) of ~~ultrafine~~ nucleation-mode particles continuously remain greater than zero over at least five consecutive seconds. The term NPF *event duration* refers to the contiguous and uninterrupted measurement time (the sum of consecutive measurement seconds) for which the definition of in-cloud NPF applies.~~Caveats with this event definition are inherent for observations as short as 1 – 5 seconds.~~ Due to the detector's signal-to-noise-ratio and counting statistics, the given quantity and durations of too short events (over 1-5 seconds) bear uncertainties in the resulting number concentrations of newly formed particles and the event duration.~~maily.~~ ~~In addition, however, this event definition may prevent resolving very fine spatial structures (i.e. horizontally on 150 m-scales, vertically on 10 m-scales) of NPF fields.~~ With the mean airspeed of the M-55 *Geophysica* (~ 154 ± 39 m s^{-1}), the event definition implies that within five seconds a horizontal distance of ~ 770 m (in flight direction) is covered. The total of 308 individual detections of elevated $N_{~~uf~~nm}$ ~~coincident~~coincide ~~ly~~ with the presence of cloud elements, 104 of which fulfilled the event criterion. Note that the in-cloud NPF events discussed herein are partially embedded in larger NPF fields, which are identified by successive~~,~~ and uninterrupted detections of elevated $N_{~~uf~~nm}$. ~~Within this larger NPF fields the duration of simultaneous ice particles detection could be shorter or interrupted.~~ One or more in-cloud NPF

Formatiert: Schriftart: Kursiv
Formatiert: Tiefgestellt
Formatiert: Schriftart: Kursiv
Formatiert: Tiefgestellt
Formatiert: Schriftart: Kursiv
Formatiert: Schriftart: Kursiv
Formatiert: Schriftart: Kursiv
Formatiert: Schriftart: 11 Pt.

events ~~could~~ can be subsets of widespread NPF events ~~with continuously elevated N_{uf} concentration, which are generally~~as those discussed by Weigel et al. (2021a) where also ~~. They (*ibid.*) also present~~ further details are provided concerning the ~~duration of NPF events, the~~ persistence of the freshly formed particles in the ~~ultrafine~~ nucleation mode~~size range~~, and the presence of non-volatile particles under NPF conditions during StratoClim 2017.

The NPF-rate and, hence, the intensity of NPF varies with the degree of supersaturation of the NPF precursor (Kirkby et al. (2011), Kürten et al. (2016)). ~~Hereafter~~For the StratoClim 2017 data set~~,~~ the strength of a NPF event is classified as

(1) ~~*excessive*~~ *intense* NPF (often used synonymously with *most recent* NPF) if detected aerosol densities of ~~ultrafine~~ nucleation-mode particles exceed
   - mixing ratios of 10000 mg^{-1} or
   - number concentrations of 5000 cm^{-3},

(2) *intermediate* NPF when number densities of ~~ultrafine~~ nucleation-mode particles range at
   - mixing ratios of 1000 $mg^{-1} < n_{~~uf~~nm} < 10000\ mg^{-1}$ or
   - number concentrations of 500 $cm^{-3} < N_{~~uf~~nm} < 5000\ cm^{-3}$, and

(3) *weak* NPF when
   - mixing ratios $n_{~~uf~~nm}$ remain below 1000 mg^{-1}, or
   - number concentrations $N_{~~uf~~nm}$ of less than 500 cm^{-3} are detected.

~~(4) The notation *most intense* NPF is often used synonymously with *most recent* NPF in the following.~~

Formatiert: Standard, Keine Aufzählungen oder Nummerierungen

As the persistence of the particles in the ~~ultrafine size range~~nucleation mode is short (i.e. a few hours only due to coagulation, cf. ~~Weigel et al. 2020a~~ Weigel et al. (2021a)), an intense NPF event could still be in process when observed, or it had expired recently, i.e. 1-2 hours prior to the detection. For NPF encounters with low or intermediate $n_{~~uf~~nm}$ (or $N_{~~uf~~nm}$), the conclusions concerning the event's age remain ambiguous since they can result from an proceeding event with a low NPF rate or from an event that had ~~occurred~~ expired several hours ago.

2.3 Cloud particle and water vapour detection

The NIXE-CAPS (New Ice eXpEriment: Cloud and Aerosol Particle Spectrometer, in the following denoted as NIXE) was deployed during StratoClim for measuring the number size distribution in the cloud particles' diameter size range of 3 – 930 µm with 1 Hz resolution (Luebke et al. (2016); Costa et al. (2017)~~;). Comprehensive numerical analyses by means of computations fluid dynamics (CFD) were carried out by~~ Afchine et al. (2018) ~~to investigate the impact of the instrument's position underneath the aircraft wing on the cloud particle detection~~. The NIXE-

CAPS consist of two detectors: the NIXE-CAS-DPOL (Cloud and Aerosol Spectrometer with Detection of POLarization) and the NIXE-CIPg (Cloud Imaging Probe – grayscale). The ~~Compiling~~ compiled measurement~~d~~ data of both independent detectors delivers microphysical properties~~,~~ in terms of size and number, of particles with diameters ranging from 0.61 µm to 937 µm. The methods of post flight data processing and corrections were described by Luebke et al. (2016).

In the StratoClim 2017 data set, ~~C~~cloud particle detections were recognised as such when particles of diameters > 3 µm were encountered in numbers greater than zero. ~~Hereafter, t~~The number concentration of ice particles is denoted as N_{ice} (i.e. $N_{3\text{-}937\mu m}$, for the number concentration of ice particles with diameters of 3 µm < d_p < 937 µm). The data of ice water content (*IWC*) used herein were ascertained by using the relationship of cloud particles' mass (m_p) to diameter (d_p) (Krämer et al. (2016); Luebke et al. (2016); Afchine et al. (2018)).

The closed-path Lyman-α photo-fragment fluorescence hygrometer FISH (Fast In situ Stratospheric Hygrometer; cf. Zöger et al. (1999) and Meyer et al. (2015)) allows for 1 -~~H~~z -resolved measurements of the atmosphere's gaseous and solid phase water, denoted as total water or H_2O_{tot}. The FISH detection of H_2O_{tot} covers mixing ratios of 1 - 1000 µmol mol^{-1} over atmospheric pressures ranging from 50 hPa to 500 hPa with an accuracy and precision of 6 – 8 % and 0.3 µmol mol^{-1}. The ice water content (*IWC*) was calculated by subtracting the H_2O_{Gas} (measured by another Lyman-α detector, FLASH, the FLuorescent Airborne Stratospheric Hygrometer) from H_2O_{tot}. For further details concerning the data processing, see Afchine et al. (2018). Dependent on ambient temperatures, the smallest *IWC* detectable by the FISH instrument is approximately between ~~about~~ $1 \cdot 10^{-3}$ µmol mol^{-1} and $20 \cdot 10^{-3}$ µmol mol^{-1}, which corresponds to approximately $1 – 20 \cdot 10^{-4}$ mg m^{-3} (Afchine et al., 2018).

To cover the wide range of *IWC* observed during the StratoClim mission (from thousandths to thousands of µmol mol^{-1}) the complementary data sets of NIXE-CAPS and FISH concerning *IWC* were merged (cf. ~~. Thus, when large ice particles were abundant, causing *IWC* of hundreds to thousands of µmol mol^{-1}, mostly NIXE-CAPS data contributed to the resulting *IWC* data. In contrast, low numbers of small ice particles caused the FISH instrument to provide the most reliable *IWC*. The overall uncertainty of given *IWC* values were estimated to be ~ 20 %~~ Krämer et al. (2020)).

~~Based on cloud particle (NIXE-CAPS) and water vapour (FISH) measurements, ice particle shattering, which could be indicated e.g. by short bursts of small ice particles, remained unobserved throughout StratoClim (Krämer et al., 2020).~~

2.4 Carbon monoxide

In the troposphere, carbon monoxide (CO) is a component of atmospheric pollution (Park et al., 2009), the main sources of which are both natural and anthropogenic (including combustion, and the oxidation of hydrocarbons). Measured ~~It is assumed that the contributions to the tropospheric CO budget almost equivalently originate from: (1) its photochemical production and (2) directly from sources located at the surface. Mainly the oxidation with hydroxyl radical (OH) depletes CO within the atmosphere (Logan et al. (1981); Yin et al. (2015)).~~ CO mixing ratios are~~mixing ratios are well suitable and~~ often used as ~~tropospheric~~ dynamic tracer for air parcel ~~'s~~ transport~~. (a) within the troposphere, (b) across the tropopause, and (c) within the lower stratosphere~~ Typical CO ~~. In the free troposphere, CO mixing ratios~~ mixing ratios range from unpolluted 50 nmol mol^{-1} up to mixing ratios well exceeding 700 nmol mol^{-1} in close vicinity to emission sources (Clerbaux et al. (2008), Park et al. (2009)). Inside the AMA and up to 15 km altitude, CO mixing ratios remain comparatively high ($\gtrsim$ 100 nmol mol^{-1}), while between 15 km and 20 km altitude the CO mixing ratios decrease monotonically down to ~ 40 nmol mol^{-1} (Park et al., 2009).

During the StratoClim mission, the mixing ratio of CO was measured by means of the Tunable Diode Laser (TDL) technique implied in the revised version of the Cryogenically Operated Laser Diode (COLD) spectrometer. Compared to the previous instrument version (4 s temporal resolution, Viciani et al. (2008)), COLD-2 integrates improvements (Viciani et al., 2018) regarding:

1) an increased measurement's resolution by a factor of four,
2) an enhanced in-flight sensitivity of the COLD-2 spectrometer (ranging at ~ 2 nmol mol^{-1} at integration times of 1 s) , and
3) an accuracy of 3 % is specified for the CO measurement with COLD-2.

In the data set of simultaneous measurements of COPAS and COLD-2, ~~Within the data set of simultaneous measurements with COPAS, COLD-2 detected m~~minimum and maximum CO mixing ratios of 14 nmol mol^{-1} and 153 nmol mol^{-1}, are included ~~respectively~~.

2.5 Data of ambient temperature and static pressure

The atmospheric temperature and pressure data were taken from the Unit for Connection with the Scientific Equipment (UCSE, Sokolov and Lepuchov (1998)), a part of the navigational system of the M-55 *Geophysica*. UCSE data are provided as 1 -Hz - resolved ambient pressure (with an accuracy of ±1 hPa) and temperature (±2 K accuracy).

The potential temperature θ is calculated ~~correspondingly~~ with 1 -Hz resolution in compliance with the definition by the World Meteorological Organization (WMO, 1966). Note that for the

given vertical temperature gradients and over the θ -range covered during StratoClim 2017 (i.e. up to ~ 477 K), the WMO recommended calculation of θ differs only by up to ~ 1 K from the values obtained by using the recently reappraised θ-calculation (Baumgartner et al., 2020)~~(Baumgartner et al., 2020)~~.

3 Observations and results

During StratoClim 2017, eight mission flights were conducted with a total of 36.6 flight hours, whereas over a total of 6.42 hours ice clouds were encountered at air temperatures colder than 240 K. The cirrus cloud observations are described and ~~comprehensively~~ discussed by Krämer et al. (2020)~~, and thus are only briefly summarised herein~~. Most of the in-cloud measurements during StratoClim 2017 were performed at temperatures $\lesssim$ 205 K, corresponding to potential temperatures above ~ 355 K and geometric altitudes higher than ~ ~~14~~ 12 km~~, i.e. well within the TTL region~~. The clouds observed during the Asian monsoon season include: 1) *in-situ* cirrus, which had formed in ~~calm~~ dynamically calm situations associated with very slow updraught as well as 2) *liquid-origin* cirrus, the formation of which is connected to ~~overshooting~~ deep (including overshooting) convection with elevated uplift velocities (see Section 5.2), including ice clouds (e.g. anvils) associated with convective outflow.

At temperatures colder than 205 K, N_{ice} and *IWC* often reached values above their respective median of 0.031 cm^{-3} (blue dashed line in Figure 2~~Figure 2~~ c) and ~ 0.2 – 2 µmol mol^{-1} (cf. Figure 6~~Figure 6~~). The highest observed *IWC* values at these temperatures ~~are reached with~~reach ~~*IWC* of~~ up to 1000 µmol mol^{-1} ~~and a~~with a maximum N_{ice} as high as 30 cm^{-3}. Moreover, the ice crystal~~s~~ sizes (not shown here) exceed their corresponding median, hence, comparatively large ice crystals were found up to and around the cold point tropopause. Such large particles were detected during flights in strong convection.

3.1 The distribution of NPF and the presence of cloud ice particles over day time

During a total of ~ 22.5 hours of COPAS measurement time at altitudes above ~ 10 km ($\theta \gtrsim$ 350 K~~),~~) a total~~in general, a~~ duration of ~~about~~ 2 hours and 38 minutes was spent under NPF conditions in the TTL region (~ 11-17.5 km, ~ 355 – 400 K, cf. ~~Weigel et al 2020a~~ (Weigel et al., 2021a)). Throughout the ~~entire~~ StratoClim 2017 mission, elevated number densities of ~~ultrafine~~ nucleation-mode particles were observed coincidently with cloud particles (N_{ice} > 0 cm^{-3}) over a total of about 1 hour and 17 minutes (cf. Table 1~~Table 1~~). The encountered in-cloud NPF events at altitudes between approximately 11 km and 16.5 km (~ 355 – 385 K) had a mean event duration of 14.5 seconds (ranging from one second to a maximum of about 300 seconds, median duration: 2 seconds).

Formatiert: Schriftart: Kursiv

Kommentiert [WR3]:

Formatiert: Nicht Hervorheben

Formatiert: Nicht Hervorheben

In Figure 2~~Figure 2~~, all NPF detections throughout the StratoClim mission are compiled ~~with~~in a one-~~1-~~day time series ~~to illustrate the diurnal variability of the observations~~. The ~~scale~~ range of ~~the~~ this time series is limited to the ~~daytime as~~ schedules of the eight mission flights ~~were conducted~~ between 03:30 (UTC) and 12:30 (UTC)~~, which~~ correspond~~ing s~~ to local times of 09:15 LT to 18:15 LT. ~~Kathmandu local noon time corresponds to 22500 seconds of day, or 06:15 UTC, and is tagged with an orange line in Figure 2.~~ The encounter of NPF is considered as clear-air observation (black data points in Figure 2~~Figure 2, complete StratoClim data set~~) when ~~simultaneously detected~~ cloud (ice) particle number concentration N_{ice} remained at 0 cm^{-3}. Coincident observations of NPF and cloud (ice) particles (N_{ice} > 0 cm^{-3}) are highlighted ~~by~~ by red ~~data points~~points in Figure 2~~Figure 2~~ (Panels a and c). The number of in-cloud NPF encounters exceeding different thresholds of measured particle number concentration (N_{nm}, (500 cm^{-3}, 1000 cm^{-3}, and 5000 cm^{-3}, Panel b of Figure 2~~Figure 2~~) shows for StratoClim 2017 that the intense events of in-cloud NPF occurred predominantly in the late morning, well before local noon. The incidences of in-cloud NPF accumulate in the later morning hours as well as in the local afternoon~~The increased frequency of abundant cloud ice in the local afternoon may temporally coincide with the typically elevated convective activity during the second half of a day~~. ~~However, a t~~Temporal dependencies on daytime were not observed for the occurrence, severity or frequency of NPF~~emporal dependency was not observed for the occurrence, the strength or the frequency of NPF. Furthermore, there is no obvious indication that the number of ice particles present had a direct influence on the NPF strength~~. ~~The impression arises that even intense NPF happens almost unaffected only by the number of present cloud ice particles, as otherwise likely larger differences should be visible between the N_{uf} maxima in clear-air and under in-cloud conditions.~~

3.2 Vertical distribution of ~~ultrafine~~ nucleation-mode particles in presence/absence of cloud ice particles

Figure 3~~Figure 3~~ displays the vertical distribution of NPF-generated ~~ultrafine~~ nucleation-mode aerosols in terms of the mixing ratio n_{ufnm} as a function of potential temperature. The panel a) of Figure 3~~Figure 3~~ depicts the clear-air observations of elevated n_{ufnm} (black) together with those when coincidently ice particles were detected (red). The coincident observation of ice particles and ~~ultrafine~~ nucleation-mode aerosols is vertically limited to a range of potential temperatures from 355 K to 385 K (cf. also Table 1~~Table 1~~). Thereby, in-cloud NPF of intermediate strength was encountered together with convective overshooting up to altitudes above the mean tropopause height (~ 380 K, averaged over the StratoClim 2017 period and area of operation)~~Recent convective overshooting to altitudes above the mean tropopause height (~ 380 K, averaged over the period and operation area of StratoClim 2017) is indicated by θ values significantly larger than 380 K~~. Further above (above 385 K and up to ~ 400 K) and at

Formatiert: Englisch (Vereinigtes Königreich)
Formatiert: Englisch (Vereinigtes Königreich)
Formatiert: Englisch (Vereinigtes Königreich)
Formatiert: Schriftart: Kursiv
Formatiert: Tiefgestellt
Formatiert: Hochgestellt
Formatiert: Englisch (Vereinigtes Königreich)
Formatiert: Englisch (Vereinigtes Königreich)
Formatiert: Englisch (Vereinigtes Königreich)

altitudes below 355 K, exclusively ~~C~~clear-air NPF was sampled ~~also at higher altitudes, i.e. at potential temperatures above 385 K and up to ~ 400 K, or at lower altitudes, below 355 K~~. As already indicated by ~~the time series shown in~~ Figure 2~~Figure 2~~, also the vertical profiles in Figure 3~~Figure 3~~ suggest that the strength of NPF was largely independent from the presence of cloud elements. The intermediate panels (c and d) in Figure 3~~Figure 3~~ show the StratoClim NPF data after their separation into clear-air and in-cloud conditions ~~upon detection~~. ~~The data in~~ Figure 3~~Figure 3~~~~cb~~ shows that in-cloud NPF observations were made during each of the eight mission flights (cf. Figure 1~~Figure 1~~). During the first four flights (from 27 July through 02 August) no in-cloud NPF was found above 365 K, ~~-~~since deep convection occurred more sparsely in the first half of the StratoClim mission period than in the second half ~~consistent with the finding that deep convection occurred more sparsely in the first half of the mission than in the second half (Stroh et al., 2021)~~ (Bucci et al., 2020). ~~Accordingly, d~~During the second half of the mission flights (04 to 10 August), the frequency and the spatial extent of in-cloud NPF events were increased. ~~Over the StratoClim observation period, in-cloud NPF was a frequently occurring phenomenon within the AMA associated with predominantly large convective cloud systems over the Himalayan foothills. Apparently, in-cloud NPF is a common phenomenon in connection with the AMA and in presence of prevailing large convective cloud systems over the Himalayan foothills. The separation of in-cloud and clear-air conditions of NPF observation is illustrated with the intermediate panels (c and d) of Figure 3. In this way, the in-cloud NPF observations (c), which occurred in the altitude interval of ~ 355 < Θ < 385 K, are opposed to NPF observations that were exclusively made under clear-air conditions (d) over a vertical range between 355 K and 400 K.~~

The comparison of CO mixing ratios ~~(as indicator for the air masses' pollutant load)~~ and NPF occurrence in the tropical UT/LS over West Africa (Weigel et al., 2011)~~(Abdelhady and Weigel, 2011)~~ suggested a link between NPF-rate and ground-level sources of NPF precursors. These precursors ~~(mainly sulphur compounds, possibly also organics)~~ (likely sulphur compounds, possibly also organics) are thought to be efficiently lifted into the TTL region by convection and not completely removed by scavenging. ~~The relationship between CO mixing ratios and NPF occurrence in the tropical UT/LS over West Africa (Weigel et al., 2011) indicated a relationship between NPF and ground sources of gaseous NPF precursor substances (mainly sulphur compounds, potentially also organics) that are efficiently lifted into the TTL region via convective transport, and not entirely removed by scavenging. Tost et al. (2010) revealed a substantial underestimation of simulated sulphur dioxide (SO_2)~~SO_2 ~~compared to flight observations throughout the SCOUT-O3 mission in 2005. These authors utilised global chemistry climate model simulations independent of the representation of deep convection, the results of which indicated that the scavenging of SO_2 is weaker less effective than expected and that the~~

Formatiert: Englisch (Vereinigtes Königreich)

Formatiert: Englisch (Vereinigtes Königreich)

Formatiert: Englisch (Vereinigtes Königreich)

Formatiert: Schriftart: Nicht Fett

~~impact of the SO_2 retention is not negligible (*ibid.*). However, a s~~Substantial fractions ~~of the well soluble sulphur dioxide (SO_2) may~~ do ~~not~~ reach UT/LS altitudes via convectiionve events. ~~Cloud-resolving numerical modelling revealed a fraction of 40-90 % of SO_2, that is capable of reaching the deep convection's outflow region (Barth et al., 2001), largely consistent with the estimates by Crutzen and Lawrence (2000). The results of o~~Other model studies (Ekman et al., 2006) ~~showed~~ suggest ~~that only 30 % of SO_2 from the boundary layer reach cloud top levels. Experimental studies by Jost et al. (2017) found moderate retention coefficients (0.2 – 0.5) of SO_2 in the ice phase of clouds, while~~ compared to those of hydrochloric acid (HCl), ~~and nitric acid (HNO_3), or ammonia (NH_3), which~~ are almost entirely retained under ~~in the~~ ice cloud ~~conditions~~ ice (*ibid.*). ~~(Jost et al., 2017)~~In essence, ~~O~~once the cloud particles freeze, large ~~fractions of the in-cloud dissolved SO_2 could~~ can leave the cloud ice composite. ~~The SO_2, which remaining~~ remained in the cloud ice composite, is released as soon as the ice sublimates in the ~~region of convective outflow, or underneath, while the ice particles sediment.~~ Hence.

NPF should most frequently occur in air enriched with precursor material and which experienced ~~rapid~~ vertical uplift. ~~An indicator for the air masses' pollutant load and/or contact with the boundary layer and recent vertical uplift is provided by air's carbon monoxide (CO) content.~~ According to the ~~CO mixing ratio when n_{ufnm} mixing ratios were elevated (colour coding in~~ panels e and f of Figure 3~~Figure 3)~~, ~~none of the different~~neither of both, clear-air or in-cloud NPF, ~~conditions, in clear air or in the presence of ice particles, shows~~ exhibit n_{nm} ~~the highest number of ultrafine~~ nucleation-mode ~~particles together with~~maxima coincidently with highest CO mixing ratios. Th~~at thi~~is is not a typical characteristic of only in-cloud NPF as is discussed in more detail in ~~the companion paper based on the dataset of all StratoClim 2017 NPF observations~~Weigel et al. (2021a). ~~In fact, t~~During in-cloud NPF, the~~he~~ highest densities of ~~ultrafine~~ nucleation-mode particles were observed at ~~comparatively~~ moderate CO mixing ratios of ~ 90 - 100 nmol mol^{-1}. ~~This largely agrees with the in situ measurements of correlations between CO mixing ratio and NPF obtained at similar altitudes in the region of Mesoscale Convective Systems during the West African Monsoon (Frey et al. (2011), Weigel et al. (2011)) although based on a smaller data set of coincident CO and particle detections.~~ ~~Moderately high or intermediate CO mixing ratios may result from the dilution of young, CO-enriched air with aged and processed air masses, which would reduce both the CO content of the air and its NPF precursor concentration. As soon as the thermodynamic conditions for NPF are reached during transport, the formation process may be initialised, while the content of diluted CO could indicate an unremarkable pollution state of the probed air.~~ In air masses with lowest CO content (~ 40 - 60 nmol mol^{-1}), NPF was observed only above the tropopause (θ > 380 K) and in the absence of ice particles with n_{ufnm} ranging from 300 mg^{-1} to a maximum of 2000 mg^{-1}. ~~(Weigel et al., 2021a).~~

Formatiert: Nicht Hervorheben
Formatiert: Nicht Hervorheben
Formatiert: Nicht Hervorheben
Formatiert: Nicht Hervorheben
Formatiert: Nicht Hervorheben
Formatiert: Nicht Hervorheben
Formatiert: Nicht Hervorheben
Formatiert: Nicht Hervorheben
Formatiert: Nicht Hervorheben
Formatiert: Nicht Hervorheben
Formatiert: Nicht Hervorheben
Formatiert: Hervorheben
Formatiert: Hervorheben
Formatiert: Hervorheben
Formatiert: Hervorheben
Formatiert: Hervorheben

Most intense NPF, i.e. with highest densities of ~~ultrafine~~ nucleation-mode aerosols~~ particles~~, were found below the tropopause (~ 380 K). In the presence of ice particles (as in clear air), ~~elevated~~ intermediate $n_{~~u~~fnm}$ values were also encountered at ~~low~~ CO mixing ratios~~,~~ below ~ 70 nmol mol^{-1}~~,~~ at potential temperatures of 370 - 380 K. Under clear-air conditions, NPF ~~occurs~~ occurred even at much lower CO mixing ratios (mainly from measurements on 29 and 31 July), which is shown by the $n_{~~u~~fnm}$ vertical ~~profile~~ profile at altitudes above 385 K (Figure 3~~Figure 3~~f). ~~The results of~~According to Figure 3~~Figure 3~~, ~~indicate that~~ in-cloud NPF was predominantly ~~occurred~~ found in an altitude band between ~~350~~ 355 K and ~~380~~ 385 K (corresponding to ~ ~~8.5~~9 – 16.5 km) with $n_{~~u~~fnm}$ in the range of about 1000 to 50000 mg^{-1} (~ 500 – 11000 cm^{-3}). The $n_{~~u~~fnm}$ values of NPF in ice clouds do generally not differ from those of NPF under clear-sky conditions.

3.3 Statistics of NPF events in the presence of ice particles

The frequency of NPF occurrence in coincidence with ice particles is illustrated in Figure 4~~Figure 4~~. The upper panel (Figure 4~~Figure 4~~a) exhibits the absolute ~~occurrence~~ frequency of occurrence of number concentrations $N_{~~u~~fnm}$ observed during NPF events. The graphs compile all measurements (more than 4600 samples of 1 ~~-~~Hz ~~-~~ resolved data, cf. Table 1~~Table 1~~), which comply with the NPF criterion (black), for a comparison with clear-air NPF events (green) and those, which were coincidently detected with ice particles (red). At heights of in-cloud NPF observations (i.e. between ~~350~~ 355 K and ~~380~~ 385 K), the number concentrations of particles larger than the ~~ultrafine~~ nucleation mode, i.e. N_{15} and N_{65}, ranged (by median) at ~ 200 cm^{-3} < N_{15} < 1000 cm^{-3} (COPAS) and ~ 60 cm^{-3} < N_{65}< 150 cm^{-3} (UHSAS-A, Mahnke et al. (2021)). Two features are apparent:

1) Number concentrations $N_{~~u~~fnm}$ of more than ~ 8000 cm^{-3} seem ~~more~~ to be ~~frequently~~ observed more frequently (about 1.5 times more often) in clear-air conditions. ~~However,~~ ~~a~~As the number of in-cloud NPF observations with $N_{~~u~~fnm}$ > 8000 cm^{-3} is comparably low (≤ 10 encounters), the statistics is likely insufficient for drawing ~~additional~~ further conclusions from this. Whether ~~or not~~ the presence of cloud ice ~~confines~~ constrains the chance to detect very recent NPF (resulting in high $N_{~~u~~fnm}$), is discussed in Section 6.
2) For NPF in the presence of cloud ice, number concentrations $N_{~~u~~fnm}$ between 1500 - 4000 cm^{-3} were observed about twice as often as under clear-air conditions (Figure 4~~Figure 4b~~a).

~~Plausibly, h~~Highest $N_{~~u~~fnm}$ values are ~~particularly~~ found mainly in the absence of deposition surfaces, which ice particles would provide. It seems~~, however,~~ less understandable why NPF should generate a particular range of $N_{~~u~~fnm}$ more frequently in the presence of cloud ice. Further discussion on this issue is provided in Section 6.

Formatiert: Englisch (Vereinigtes Königreich)

Formatiert: Hochgestellt

Formatiert: Englisch (Vereinigtes Königreich)

Formatiert: Englisch (Vereinigtes Königreich)

Until this point, the presence or absence of ice particles was distinguished by the criteria $N_{ice} = 0$ cm^{-3} or $N_{ice} > 0$ cm^{-3}, respectively. Figure 4~~Figure 4~~b ~~exhibits~~ depicts the occurrence frequency of $N_{~~uf~~nm}$ with ice particles $N_{ice} > 0$ cm^{-3} normalised to the occurrence frequency of $N_{~~uf~~nm}$ of all NPF events (black curve in Figure 4~~Figure 4~~a). More than 75 % of observed NPF cases with 2000 cm^{-3} < $N_{~~uf~~nm}$ < 4000 cm^{-3} (~ 200 samples) were detected ~~occurred~~ while ice particles were present. In Figure 4~~Figure 4~~c, the occurrence frequencies of $N_{~~uf~~nm}$ are compiled for various levels of number densities N_{ice}, which were normalised to $N_{~~uf~~nm}$ at $N_{ice} > 0$ cm^{-3} (red curve in Figure 4~~Figure 4~~a). Thresholds of N_{ice} are set with stepwise increasing number concentrations (by one order of magnitude), to investigate whether the ~~occurrence of~~ NPF is eventually ~~confined~~ constrained or ~~significantly~~ influenced by the ice particle number density.

Although very faint, so called sub-visible cirrus clouds were found to comprise very small ice particle number concentrations of 10^{-5} cm^{-3} (corresponding to 0.1 per litre, cf. Kübbeler et al. (2011); Spreitzer et al. (2017)). Sub-visible cirrus ~~clouds~~ with $N_{ice} < 10^{-3}$ cm^{-3} are assumed to have negligible influence on the NPF process, as is also to conclude from Figure 4~~Figure 4~~c. Therefore, a first threshold level is set to $N_{ice} > 10^{-3}$ cm^{-3} (magenta curve), followed by ~~a second~~the threshold ~~at~~ level of $N_{ice} > 10^{-2}$ cm^{-3} (corresponding to 1 – 10 ice particles per litre, blue curve), which still represents a comparatively small amount of N_{ice} within sub-visible cirrus clouds (cf. Thomas et al. (2002); Peter et al. (2003); Davis et al. (2010); Frey et al. (2011)). The maximum observed N_{ice} reached up to ~ 3 cm^{-3}. Concerning the frequency of observed $N_{~~uf~~nm}$, the difference between $N_{ice} > 0$ cm^{-3} and $N_{ice} > 10^{-3}$ cm^{-3} appears negligibly small. This leaves to conclude, that elevated $N_{~~uf~~nm}$ were mostly observed coincidently with ice crystal number densities greater than 10^{-3} cm^{-3}. With rising N_{ice} level (above 10^{-2} cm^{-3}), the occurrence frequency of the highest $N_{~~uf~~nm}$ (> ~ 5000 cm^{-3}) decreased. When N_{ice} exceeds 10^{-1} cm^{-3}, the occurrence of $N_{~~uf~~nm} > 4500$ cm^{-3} is significantly reduced and $N_{~~uf~~nm} > 8500$cm^{-3} were absent. At the highest observed N_{ice} of ~ 3 cm^{-3}, NPF with $N_{~~uf~~nm} > 250$ cm^{-3} were not detected anymore.

Hence, events with highest NPF-rates ~~seem to~~ occurred preferentially at low~~er~~ ice particle concentrations or in clear air. At a certain N_{ice} level (~ 3 cm^{-3}), the process of NPF ~~seems~~ appears to be suppressed~~. This is~~ in general agreement with earlier findings (Weigel et al., 2011)~~, which~~ indicat~~ed~~ing the ~~confinement~~ limitation of NPF by ~~number densities above~~ 2 cm^{-3} of cloud ice particles with diameter larger than 2 µm. Among other ~~incidents~~incidences, a singularly observed event was discussed (*ibid.*), during which NPF ~~was very likely~~appeared to be suppressed by ~~the excessive presence of~~abundant cloud ice particles~~, , which then,~~while on leaving the cloud the NPF re-emerged at almost previously observed concentrations of nucleation mode particles ~~on leaving the cloud, re-emerged with amounts of ultrafine particles of almost previously observed magnitude~~. ~~Although an ultimate observational evidence is~~

Formatiert: Englisch (Vereinigtes Königreich)

Formatiert: Englisch (Vereinigtes Königreich)

Formatiert: Englisch (Vereinigtes Königreich)

Formatiert: Englisch (Vereinigtes Königreich)

~~currently lacking, however, t~~These findings suggest that NPF is entirely prevented in cases when N_{ice} ~~substantially~~ exceeds 2 - 3 cm^{-3}.

4 In-cloud NPF related to *IWC* and cloud particle number densities

4.1 The relationship between cloud ice and aerosols

Based on *in-situ* measurements over northern Australia and over West Africa, de Reus et al. (2009) investigated the relationship between the number density of submicron aerosol particles and the abundance of cloud particles at UT/LS levels. The authors provided aerosol and ice particle number concentrations~~, which were~~ averaged over the duration of various cloud encounters ~~in order~~ to ~~measure the~~determine the ~~fraction~~ proportion of submicrometre-sized particles that potentially convert into cloud ice. ~~Concerning~~ In the context of~~the~~ homogeneous ice nucleation ~~process~~, a specific relationship between the number concentration of aerosol and of ice particles cannot be expected (Kärcher and Lohmann, 2002), whereas such a relationship is inherent in the ice clouds' heterogeneous freezing process. From their analyses, de Reus et al. (2009) concluded that a ~~very~~ similar range of ice-aerosol-ratios is observable in the convective outflow of both, ordinary tropical convection (Australia) as well as of large, mesoscale convective systems (MCSs, West Africa).

Formatiert: Schriftart: Cambria

~~The measurements from StratoClim 2017 were compiled correspondingly to de Reus et al. (2009) and are depicted in~~ Figure 5~~Figure 5~~ depicts the StratoClim 2017 data correspondingly to the data presentation by de Reus et al. (2009) from UT measurements in 2005 during SCOUT-O3, over Darwin, Australia. ~~To ease the recognition of the relationship between the measured number concentrations of ice particles and total aerosol (N_{10}), r~~Reference lines are included ~~in Figure 5,~~ which indicate the number of encountered cloud particles per number of submicrometre-sized aerosol particles~~. In addition to the density ratios of 1 : 300 and 1 : 30 000 (as in de Reus et al. (2009)), here also the 1 : 500 000 and the 1 : 5 000 000 ratios are marked~~. The two panels in Figure 5~~Figure 5~~ comprise the ~~same~~ identical set of data points~~set~~ of ice cloud encounters ~~from~~ during StratoClim 2017, each of which are~~. The data were~~ averaged over at least 10 seconds and ~~over~~ up to ~ 23 minutes.

Several occasions were identified by de Reus et al. (2009) when comparatively high ratios with up to a few hundreds of aerosol particles remained non-activated per single ice particle. The cloud ice – aerosol – ratios, which were found in the Asian monsoon's convective outflow region, ~~are in general agreement~~agree with previous observations (de Reus et al., 2009) ~~most of,~~ which were limited to the blue shaded area in Figure 5~~Figure 5~~. ~~In agreement with previous findings, t~~Total aerosol numbers of significantly less than a few hundreds per single ice particle were not observed during StratoClim 2017, not either by de Reus et al. (2009). Up to N_{10} of 700 cm^{-3}

almost all StratoClim data result from measurements at mean ambient temperatures colder than -75 °C (i.e. the temperatures, ~~correspondingly to the~~ at which the observations by de Reus et al. (2009) were made~~, shaded area~~). Frequent observations were made at aerosol concentrations below 1000 cm^{-3}. Compared to previous findings, ~~however,~~ the StratoClim data set comprises ~~a lot~~ more observations at cloud ice – aerosol - ratios between 1 : 3 000 and 1 : 500 000, including frequent events of elevated N_{10}~~aerosol number concentrations~~ (> 10^3 cm^{-3}). High ~~*total aerosol number concentrations*~~N_{10} of more than 6000 cm^{-3}, were observed at *IWC* values mostly below 10 µmol mol^{-1} (i.e. log (*IWC,* µmol mol^{-1}) ≈ 1, Figure 5~~Figure 5~~a). The majority of observations were made at mean *IWC* values below ~ 300 µmol mol^{-1} (i.e. log (*IWC,* µmol mol^{-1}) ≈ 2.5), which rules out ~~largely minimises the probability~~ that the measured N_{10} were impacted by shattering artefacts from ice particles (cf. Appendix A). The majority of NPF occurrences (mostly at ambient air temperatures between – 50 °C and – 80 °C) coincide with cloud ice – aerosol – ratios between 1 : 3 000 and 1 : 500 000 (cf. Figure 5~~Figure 5~~b). ~~In particular, t~~The ~~abundance of~~ data points with in-cloud NPF concentrate~~s~~ between ratios of 1 : 30 000 and 1 : 500 000 because as a consequence of NPF, the aerosol proportion in the cloud ice – aerosol – ratio is strongly elevated~~, which may not further surprise, as the large aerosol number concentrations are indicative to result from NPF~~. Concentrations N_{10} of more than 1000 cm^{-3} were not detected at ratios greater than 1 : 3 000. For N_{10} above 500 cm^{-3} and for cloud ice – aerosol - ratios smaller than 1 : 30 000, i.e. where elevated total aerosol concentrations mostly coincide with lower ice particles densities (~ 10^{-3} – 10^{-1} cm^{-3}), the observations ~~predominantly~~ occurred during NPF. ~~However, c~~Cloud ice – aerosol – ratios greater than 1 : 3 000 were reached mostly in the absence of NPF.

As pointed out by de Reus et al. (2009), there are caveats inherent with this kind of analyses. The strength or efficiency of the aerosol activation is not straightforward to deduce from provided ratios of total aerosol and cloud particle numbers. Many interdependencies exist that may impact the illustrated relationship, such as

1) the altering of the aerosol particles (coagulation, condensation) or of the cloud elements (sedimentation) or
2) the mixing of air masses with different aerosol and/or variable vapour saturation characteristics (entrainment).

The type of ice formation process (*liquid origin* or *in-situ*) and the convection dynamics ~~may~~ additionally affect the relationship of cloud elements and interstitial aerosol. Assigning ~~ultrafine~~ nucleation-mode particles of thousands per cm^3 (or more) to result from NPF is ~~comparatively~~ straightforward. In contrast, $N_{~~u~~fnm}$ of a few 10 - 100 cm^{-3} are potentially filtered by the NPF criterion, and are probably not identified as NPF event ~~,~~ if detected together with ~~at~~ total aerosol concentrations (N_{10}) of comparable numbers. Apart from demonstrating the reproducibility of earlier findings (de Reus et al., 2009), the dataset was extended by new observations at different

Formatiert: Schriftart: Kursiv

Formatiert: Tiefgestellt

conditions (including NPF) obtained from StratoClim measurements.~~the StratoClim mission allowed for extending this data set by new observations at different conditions, particularly by including NPF.~~

~~In essence, these findings confirm that the occurrence of NPF is constrained by the cloud ice microphysical properties such as particle size and number (both implied in the *IWC*). Total aerosol number concentrations N_{10} of a few hundreds per cubic centimetre were measured even at highest cloud particle number concentrations ($N_{ice} > 2 \cdot 10^{-1}$ cm^{-3}) whereas, under such conditions, NPF encounters remain exceptional. The following approach aims to narrow down the cloud particle microphysical properties that limits the occurrence of in-cloud NPF.~~

4.2 NPF in the *IWC-T* parameter space

Analyses in earlier cirrus-related studies concerning the clouds' ice water content (*IWC*) as a function of ambient air temperature provide insight into the processes inherent with the cirrus formation (Krämer et al., 2016). As introduced by Luebke et al. (2016), Krämer et al. (2016), and Wernli et al. (2016), a distinction of cirrus clouds regarding their formation mechanism is obtainable within the *IWC-T* parameter space. The cirrus forms *in-situ* at elevated altitudes and instantaneously at sufficiently cold temperatures. The *liquid-origin* cirrus cloud forms on convective uplift from initially liquid droplets at lower altitudes (and less cold temperatures). More specifically Wernli et al. (2016) distinguishes:

- *liquid-origin* cirrus: initially well-sized liquid cloud droplets freeze at almost thermodynamic equilibrium in the ambient temperature range 235 K < T < 273 K under nearly saturated conditions with respect to liquid water (relative humidity RH_w of ~ 100 %), but at high supersaturation with respect to ice ($RH_i \gg 100$ %), while at freezing level, the water can coexist in each of its three phases ~~(vapour, liquid, and ice)~~.
- *in-situ* cirrus: under exclusion of pre-existing large liquid cloud droplets, ice crystals nucleate heterogeneously (due to deposition freezing) or freeze homogeneously from tiny super-cooled aqueous solution droplets (Koop et al., 2000), which are designated as "too small to be considered as cloud droplets" (Wernli et al., 2016).

~~The main goal of juxtaposing *IWC* and ambient air temperature is to investigate differences in the characteristics of ice clouds, which may influence the cirrus clouds' radiative properties. Additionally, those cirrus clouds' properties can be investigated, which arise from the dynamics and conditions in which the cirrus ice particles have formed.~~

In Figure 6~~Figure 6~~ the *IWC*~~s~~ versus ambient air temperatures ~~are~~ is displayed for all cloud encounters throughout StratoClim 2017 as a function (colour code) of

a) the mixing ratio of ~~ultrafine~~ nucleation-mode particles (i.e. $n_{6\text{-}15} = n_{\text{~~uf~~nm}}$; Figure 6~~Figure 6~~a),

Formatiert: Abstand Vor: 12 Pt.

b) the total mixing ratio n_6 of particles with d_p > 6 nm (Figure 6~~Figure 6~~b) and
c) the CO mixing ratio (Figure 6~~Figure 6~~c), respectively.

The upper panel of Figure 6~~Figure 6~~ includes two data sets: (1) all data from StratoClim 2017 in 1 ~~-~~Hz ~~- -~~resolution (grey data points) and (2) only the resulting $n_{~~u~~fnm}$ complying with the NPF criterion (colour coded data points). ~~Mainly a~~At very low ambient air temperatures (~ 200 K and colder) and for comparatively high *IWC* values, the $n_{6\text{-}15}$ (grey) data were available but many failed the NPF criterion. The absolute values of the mixing ratio n_6 of submicrometre-sized particles were relatively high (Figure 6~~Figure 6~~b). The detection of likewise excessive mixing ratios n_{15} (without illustration) resulted in $n_{6\text{-}15}$~~, which did not exceed the threshold given with the NPF criterion~~ that did not exceed the specified threshold of the NPF criterion (cf. Section 1.1). Nevertheless, most of the $n_{6\text{-}15}$ data points, which failed the NPF criterion (cf. the grey points in Figure 6~~Figure 6~~a), coincide with the mixing ratios n_6 reaching up to several thousands of mg^{-1}. It is not deducible from COPAS measurements how the enriched particle densities (n_6 and n_{15}) distribute over the diameter spectrum of the submicrometre-sized aerosols. It therefore remains open whether the restrained $n_{6\text{-}15}$ ~~this observation is~~ are due to ~~an~~ expired NPF ~~event~~ with ~~subsequent~~particles' rapid coagulation (with background aerosol and cloud ice) ~~of particles from~~out of the ~~ultrafine~~ nucleation-mode size range (Weigel et al., 2021a), or whether the particle enrichment (consistently in n_6 and n_{15}) is due to larger particles that were ~~entered~~ lifted ~~with the~~with deep convection ~~overshooting~~. The main findings from these juxtapositions can be summarised as follows:

- The absence of NPF ~~at with excessively high~~ *IWC* exceeding 1000 µmol mol^{-1} ~~within~~ at very cold air (Figure 6~~Figure 6~~) suggests that NPF is ~~confined~~ constrained as soon as ~~strong~~ deep convection~~overshooting~~ prevails, due to the presence of predominantly *liquid-origin* ice particles. ~~Excessive~~ *IWC* ~~(>~~exceeding ~~-~~1000 µmol mol^{-1}~~)~~ at air temperatures colder than 200 K indicates that ~~strong, vertically overshooting~~deep convection had occurred. ~~T~~These high *IWC* ~~most likely~~ originated from cloud ice~~, which~~ that ~~had~~ formed from liquid droplets at lower altitudes, ~~levels~~ as the amount of water vapour in the air at such cold temperatures is not sufficient to achieve comparable *IWC* ~~from liquid droplets. The amount of water vapour that is required to form ice clouds of comparable *IWC*~~ values. Thus, the~~at these air temperatures is too large to explain the~~ formation of encountered cirrus cannot be attributed to any other than the ~~by another than the~~ *liquid-origin* process. This feature was observed~~-~~ during the ~~the StratoClim~~ flights on 27 July and on 10 August 2017, respectively. Within the same temperature range (T < 200 K), only a few NPF events with ~~moderately elevated~~intermediate $n_{~~u~~fnm}$ of more than ~ 4000 mg^{-1} (log ($n_{~~u~~fnm}$, mg^{-1}) ≳ 3.6, yellow and reddish colours in Figure 6~~Figure 6~~a) were encountered offside from strong ~~vertical overshooting~~convection.

Formatiert: Schriftart: Kursiv
Formatiert: Tiefgestellt
Formatiert: Schriftart: Kursiv
Formatiert: Tiefgestellt
Formatiert: Schriftart: Nicht Kursiv
Formatiert: Schriftart: Kursiv
Formatiert: Hervorheben

765 ● In the presence of *in-situ* formed cirrus particles at cold temperatures (185 – 200 K), i.e. in or
766 around the cold point tropopause region, NPF events ~~of remarkable strength (~~with n_{ufnm} > 5000~~,~~
767 ~~(~~i.e. log (n_{ufnm}, mg^{-1}) > 3.7, orange and reddish colours in Figure 6a) or ~~very~~ recent NPF bursts
768 were rarely observed. When the cloud ice has ~~likely~~ formed *in-situ* (CO < 80 nmol mol^{-1}, yellow,
769 greenish and blue colours in Figure 6~~Figure 6~~c), mostly weak NPF ~~of reduced strength was~~
770 ~~observed (~~with n_{ufnm} < 1500 mg^{-1}~~, (~~i.e. log (n_{ufnm}, mg^{-1}) < 3.2, bluish colours of data points in
771 Figure 6~~Figure 6~~a) was observed. ~~This~~ These data also indicate~~s~~ that NPF ~~occurs~~ proceeds in air
772 with low CO content~~, i.e. with comparatively low pollutant load~~.

773 ● Suppression of NPF by cloud particles (due to ~~the~~ the large total surface area from their
774 number density and ~~and~~ particle size ~~of ice particles~~) could explain why the number of ~~ultrafine~~
775 nucleation-mode particles remained below the NPF criterion threshold at ~~comparatively~~ high
776 *IWC*~~,~~ albeit ~~the~~ total particle mixing ratios (n_6 ~~or~~ and n_{15}) were significantly elevated. It is
777 unlikely that the abundance of submicrometre-sized particles of up to 11000 cm^{-3} originates
778 from interstitial (non-activated) aerosols carried in the cloud without contributions from NPF. ~~It~~
779 ~~is not likely that a high number of interstitial, non-activated aerosol is accountable for the~~
780 ~~abundance of submicrometre-sized particles.~~ The large particle quantities observed (10^3 -
781 10^4 mg^{-1}) and the ~~comparatively~~ moderate CO content of the air sampled (≲ 100 nmol mol^{-1})
782 indicate a source of these particles at high altitudes. ~~Very few hours a~~About 4 hours after an ~~fter~~
783 ~~a completed~~ NPF event ~~(≳ 4 h), however~~has expired, the event may not be detectable anymore
784 due to the short persistence of the particles in the ~~ultrafine~~ nucleation-mode size range ~~(Weigel~~
785 ~~et al., 2020a)~~ (Weigel et al., 2021a). Hence, ~~I~~if the *IWC* values remained high over several hours
786 due to ~~strong overshooting~~deep convection, and if NPF had happened more than four hours
787 prior to the measurements, then the nucleation mode particles have certainly coagulated to sizes
788 beyond 15 nm in diameter~~then ultrafine particles could have coagulated to diameter sizes~~
789 ~~beyond 15 nm, hence, NPF would not have been identifiable anymore with COPAS~~.

790 ● Air's low pollutant load is indicated by comparatively moderate or low CO mixing ratios
791 between 50 and about 100 nmol mol^{-1} at ambient air temperatures of < 200 K (Figure 6~~Figure~~
792 ~~6~~c). For comparison, the NPF observed during the West African monsoon were associated with
793 CO levels between 60 and 90 nmol mol^{-1} (Weigel et al., 2011). Observation of ~~moderate~~
794 intermediate NPF (n_{ufnm} < 1500 mg^{-1}, log (n_{ufnm}, mg^{-1}) ≲ 3.3) in the midst of *in-situ* formed cloud
795 ice in air with ~~comparatively~~ low pollutant load (CO < 80 nmol mol^{-1}) indicates that recent
796 convective uplift of polluted air is not a prerequisite for NPF to occur. Advection of air from
797 elsewhere or chemical and/or photochemical conversion cause the accumulation of NPF
798 precursors at UT/LS levels~~Slow processes, which cause an accumulation of NPF precursors at~~
799 ~~UT/LS altitudes, such as advection from elsewhere or the chemical and/or photo-chemical~~

Formatiert: Hochgestellt

Formatiert: Schriftart: Kursiv

~~conversion, likely suffice to supply a reservoir of precursor material~~. In air with the highest CO content (> 100 nmol mol^{-1}), the *IWC*-*T*-values (for T > 200 K, i.e. at lower altitudes) remain in expected ranges and they scatter within the limits of most frequent observations (dashed black lines in Figure 6~~Figure 6~~) as obtained from earlier analyses (Krämer et al., 2016). At the highest CO content (> 100 nmol mol^{-1}), the $n_{~~uf~~nm}$ values ~~remained~~ predominantly remained below 5000 mg^{-1}.

Formatiert: Tiefgestellt, Nicht Hervorheben

5 The dependency of NPF on the proximity to ice particles

5.1 NPF as a function of mean free distance between ice elements

Surfaces, such as those of ice particles, ~~represent a~~constitute ~~potential~~ sinks for the gaseous precursor species such as the H_2SO_4-H_2O system~~, since the ice particles' coating~~ (Bogdan et al. (2006); Bogdan et al. (2013)) ~~offers the necessary attachment points for the molecules of a condensable vapor. Consequently,~~ and ~~an~~ the abundance of condensation surface ~~should~~ reduces or even prevents the NPF process. ~~Cloud ice particles provide a comparatively large surface for coating, which raises the question whether NPF is affected by the presence of these particles.~~

The free distance between the ice particles is quantified based on the measurements of N_{ice} and of the ice particles' mean mass radius $\overline{r_{ice}}$, (consider $\overline{r_{ice}}^3 \sim \frac{IWC}{N_{ice}}$). The mean free volume in between the ice particles (the inter-crystal volume, *ICV* per cm^3 of air) is calculated with the number N_{ice}^* of ice particles ~~per air volume~~ (instead of the particles' number concentration) as:

$$ICV = \frac{V - \frac{4}{3}\pi \cdot \overline{r_{ice}}^3 \cdot N_{ice}^*}{N_{ice}^*} \quad (2)$$

Formatiert: Englisch (Vereinigtes Königreich)

which basically subtracts the total ice volume from the sampled air volume (V = 1 cm^3) and the division by N_{ice}^* yields the *ICV*. Consequently, the *ICV* represents the mean particle-free volume assuming ~~the~~ a homogeneous distribution of ice crystals within the air volume~~ as homogeneous~~. ~~As long as the particle number and size remain small, subtracting the total ice volume from the air volume in equation (2) yields results without significant contribution.~~ With a maximum of measured ice particles (N_{ice}^* = 3~~ cm^{-3}~~) together with the maximum detected ice particle radius of 100 µm, the subtraction $V - \frac{4}{3} \cdot \pi \cdot \overline{r_{ice}}^3 \cdot N_{ice}^*$ corresponds by the order of magnitude ~~to~~to a subtraction of ~~1 cm^{-3}~~ 10^{-11} cm^{-3}~~.~~ ~~f~~rom 1 cm^{-3}. Hence, the volume of ice is insignificant compared to the volume of air, and the *ICV* may be considered as a function of N_{ice}^*~~ N_{ice}~~ only. The mean inter-crystalline distance (*ICD,* in cm) is then calculated by:

$$ICD = \sqrt[3]{\frac{ICV}{\left(\frac{4}{3}\pi\right)}} \quad (3)$$

and the *ICV* is assumed as a sphere around ~~every~~ each individual ice particle. The radius of each sphere ~~constitutes~~ represents the mean ice-free distance in~~to~~ any direction from the individual ice particle. Conceptually, this approach corresponds to the definition of the cloud elements' distance provided by Baumgartner and Spichtinger (2018).

~~,~~Figure 7~~Figure 7~~a depicts the number concentration of ~~ultrafine~~ nucleation-mode particles ($N_{~~uf~~nm}$) as a function of the calculated ~~*ice particles' mean free distance*~~*ICD* ~~from each other~~. The continuous colour transition of the data points ~~from red to blue~~in x-direction together with unchanged colouring in y-direction demonstrates ~~indicates~~ the independence of N_{nm} ~~the number of ultrafine particles in reference to~~from ~~the~~ ~~ice particles' mean free distance~~the *ICD* and rather ~~documents~~ illustrates the ~~obvious relationship~~correlation between the number of ice particles and their distance. The present ice particles compete for the limited amount of available water vapour ~~,~~ such that~~consequently,~~ elevated number concentrations of ice particles ~~are associated with many~~ mainly result ~~small~~ from the abundance of small ice particles. Hence, by means of ~~In essence, only~~ the number of ice particles ~~N_{ice}~~ only, it ~~would not be~~ is not possible ~~able~~ to constrain the occurrence and/or strength of NPF~~,~~ as ~~under encountered atmospheric conditions,~~ a wide scattering of $N_{~~uf~~nm}$ concentrations was observed at any *ICD* between about 1 cm and 10 cm.

~~,~~Figure 7~~Figure 7~~b shows the ice particles' mean mass radius $\overline{r_{ice}}$ as a function of the *ICD* and the number of nucleation-mode~~ultrafine~~ particles. By means of the mean mass radius $\overline{r_{ice}}$, two different cases were distinguished:

a) ~~In the~~For smallest ice particle size ~~ranges~~ (~ 3µm < $\overline{r_{ice}}$ < ~ 20 µm, log ($\overline{r_{ice}}$, µm) ≲ 1.3), a dependency of the *ICD* on the particle size was discernible. For instance, smallest ice particles (bluish $\overline{r_{ice}}$) predominantly coincided with short *ICD* of about 1 cm at elevated N_{ice}. Towards larger *ICD*, ice particle sizes continuously increased up to $\overline{r_{ice}}$ ≈ 20 µm, which ~~again~~ reflects the competition of the ice crystals for the available water vapour. ~~However, w~~Within the same interval of ice particle sizes ($\overline{r_{ice}}$ < ~ 20 µm), the concentrations $N_{~~uf~~nm}$ scattered over almost two orders of magnitude (from ~ 100 cm^{-3} to ~ 10 000 cm^{-3}) up to *ICD* of ~ 10 cm without any obvious systematic.

b) In the presence of larger ice particles, $\overline{r_{ice}}$ > ~ 30 µm (1.3 < log ($\overline{r_{ice}}$, µm) ≲ 1.4, orange and reddish colours), the *ICD* ranged from ~ 1 cm to values above ~ 10 cm. Hence, not only $\overline{r_{ice}}$ determined the resulting *ICD*, but N_{ice} increasingly contributed as well. ~~Unexpectedly, t~~The concentrations $N_{~~uf~~nm}$ were not at the highest when *ICD* values reached their maximum ~~of~~ at ~~slightly more than~~~ 10 cm. For largest particles sizes ($\overline{r_{ice}}$ > ~ 30 µm), the values of $N_{~~uf~~nm}$ accumulate at ~~number concentrations of~~ ~ 400 - 4000 cm^{-3} over the entire range of *ICDs*.

Formatiert: Schriftfarbe: Text 1, Englisch (Vereinigtes Königreich)

Formatiert: Schriftart: Kursiv

Formatiert: Englisch (Vereinigtes Königreich)

Formatiert: Schriftart: Kursiv

Formatiert: Englisch (Vereinigtes Königreich)

As long as the mean ice particle radius remained below a few dozen µm, NPF was encountered with almost any resulting N_{ufnm} concentration. ~~It was shown before (~~As shown in Figure 4~~Figure 4~~ and summarised in Section 4.4 ~~and Figure 4), that~~ a wide scatter of N_{nufm} was observed to occur largely independent from coincidently detected number N_{ice} of ice particles. Hence, the in-cloud NPF ~~– as found~~observed during StratoClim 2017 ~~- occurred~~was almost unaffected by the ice particle number, as long as the mean ice particle size remained small enough (i.e. with $\overline{r_{ice}}$ < 20 µm).

~~Instead of evaluating the number of ultrafine particles as an exclusive function either of ice crystal number or of the ice particle radius, respectively, t~~The *IWC* combines both microphysical parameters of the observed ice clouds, particle size and number concentration. ~~The particle mass (i.e. the particle radius to the third power, r^3) is proportional to *IWC* and N_{ice}.~~ I~~ndeed, i~~f N_{ufnm} over *ICD* are analysed as a function of *IWC*, ~~a certain~~ systematics become~~s~~ visible (Figure 7~~Figure 7~~c). At lower *IWC* (< 1 µmol mol^{-1}, log (*IWC*, nmol mol^{-1}) ≲ 0, bluish and green colours) the *ICD*s were at the largest and observed NPF was of the highest intensity (N_{ufnm} of several thousands per cm^3). Between 1 µmol mol^{-1} and 10 µmol mol^{-1} (yellow colours), the maximum of N_{ufnm} throughout observed NPF events was reduced. The maximum N_{ufnm} was further reduced when *IWC* ~~further~~ increased to values beyond 10 µmol mol^{-1}. This result ~~shows~~ demonstrates that the maximum N_{ufnm} reached throughout in-cloud NPF ~~was~~ is determined (in addition to the precursor gas concentration) by the combination of both, the ice particles' number concentration N_{ice} and their mean mass radius $\overline{r_{ice}}$.

5.2 NPF as a function of cloud elements' integral radius *IR*

~~Indications were found that both, number density and size of cloud ice particles, have a~~ The ~~complementary~~ combined effect of cloud ice particles' number density and size on the detectable ~~the amount of ultrafine particles (N_{ufnm}) resulting from~~ during in-cloud NPF~~. This~~ motivates ~~the compilation of~~to investigate N_{ufnm} values as a function of the integral radius $IR = \overline{r_{ice}} \cdot N_{ice}$ of the ice particle population. The parameter *IR* was described, e.g., by Manton (1979), or Politovich and Cooper (1988), and is frequently used to characterise clouds' microphysical properties (e.g. Korolev and Mazin (2003); or Krämer et al. (2009)). *IWC* and *IR* are expected to be strongly related (also visible by the systematic sorting of data in Figure 8~~Figure 8~~a) as the diffusive growth rate of an ice particle ($\frac{dm}{dt}$) is proportional to *IR* (see e.g. Pruppacher and Klett (2012)). The *IR* is the direct control variable for the mass increase per time by condensation (mainly of water vapour) on the surface of a cloud ice particle and thus for the particle's growth rate. At supersaturated NPF conditions, the NPF precursors condense on the cloud ice particles and the

Formatiert: Englisch (Vereinigtes Königreich)

Formatiert: Schriftart: Nicht Kursiv

Formatiert: Schriftart: Nicht Kursiv

Formatiert: Schriftart: Kursiv

change of the ice particle's mass ($\frac{dm}{dt}$) from the condensation of a gaseous precursor converts into a reduction of the gaseous precursor concentration.

~~The relationship between *IWC* and *IR* is also apparent from a systematic sorting of the data points displayed in Figure 8a. The probability should be high that weak NPF (generating low N_{uf}) often occurred in the presence of ice particles. In contrast, the occurrence of excessive NPF events in the cloud (with N_{uf} significantly exceeding several thousand per cm^3) was less likely.~~ For almost all *IR* below 1 µm cm^{-3}, ~~however,~~ the $N_{uf_{nm}}$ concentrations were unsystematically scattered over the entire interval between ~ 100 cm^{-3} and ~ 10 000 cm^{-3}.

Towards the highest *IR* (> 1 µm cm^{-3}), the maximum of observed $N_{uf_{nm}}$ continuously decreased. ~~Generally, t~~This ~~may~~ reflects a limiting influence by the cloud ice on the maximum strength of occurring NPF (indicated by the diagonal grey-shaded bars in Figure 8~~Figure 8~~). An exceptional feature is exhibited in Figure 8~~Figure 8~~a with a high signal of $N_{uf_{nm}}$ (~ 3000 – 4000 cm^{-3}) amongst elevated *IR* (between ~ 4 and 10 µm cm^{-3}). This cluster of data points resulted from the measurements of two individual mission flights, on 27 July (~ 3000 cm^{-3} < $N_{uf_{nm}}$ < ~ 3500 cm^{-3}) and on 06 August (~ 3500 cm^{-3} < $N_{uf_{nm}}$ < ~ 4000 cm^{-3}), respectively. During these measuring periods, ice particle densities (N_{ice}) and the mean ice particle sizes (i.e. the particles' mean mass radius $\overline{r_{ice}}$) did not rise above 0.1 - 0.3 cm^{-3} and 25 - 50 µm. Neither $N_{uf_{nm}}$ nor the ice microphysics exceeded the range of moderate values. The two independent exceptions in the observational data ~~may~~ indicate a local/temporal state of imbalance that could have been caused by:

1) ~~moderate~~ intermediate NPF, which was just proceeding when measured or which had been completed very recently (cf. Weigel et al. (2021a); ~~i~~in such a case, the observed $N_{uf_{nm}}$ should rapidly (< 1 h) decay ~~due to coagulation, within less than one hour,~~ to values of ~ 1000 cm^{-3}~~)~~ due to coagulation), or
2) ice particles, which sediment from high altitudes into an area of currently active NPF, or
3) cooling of air accompanied with nucleation of ice, while the cooling is due to the air parcel's vertical displacement, which results ~~possibly resulting~~ from ~~convective overshooting~~deep convection or gravity wave activity (cf. (Weigel et al., 2021a)~~Weigel et al. 2020a~~).

The ~~generally~~ limiting influence by the cloud ice on the maximum strength of NPF~~, that is~~ as indicated by the majority of observations~~,~~ is ~~possibly~~ explainable by ~~the~~the reduction of NPF precursor materials~~s~~ due to its condensation onto present ~~surfaces provided by the~~ ice particle surfaces~~s (maximum N_{ice}: 2 - 3 cm^{-3})~~. The question arises whether the distance between the ice particles allows efficient absorption and sustained reduction of NPF precursor molecules, or

Formatiert: Schriftart: Nicht Kursiv
Formatiert: Schriftart: Nicht Kursiv
Formatiert: Abstand Nach: 10 Pt.

whether such an effect ~~is~~ exists only ~~likely~~ in the immediate vicinity of an ice particle. ~~However,~~ ~~t~~The effectiveness of such a process strongly depends on the diffusivity of the NPF precursor ~~'s~~ molecules. If the molecules of the ~~main~~ NPF precursor are absorbed before the thermodynamic conditions for NPF are reached, then these molecules are removed and missing in the formation of molecular clusters as initial step in the nucleation process. ~~Sulphuric acid (H_2SO_4) is one of the most prominent condensable vapours and NPF precursors in the atmosphere.~~ Numerical analyses concerning the reduction of the saturation ratio of H_2SO_4 due to the presence of ice particles, which are coated with H_2SO_4 (as typical for cirrus particles at 10-20 km altitude; cf. Bogdan et al. (2006); Bogdan et al. (2013)) are described in Appendix B ~~Appendix B: Impact of ice particles on NPF precursors' saturation ratio~~(see also Figure B- 1~~Figure B- 1~~). Although the binary H_2SO_4-H_2O nucleation process alone is assumed as insufficient to explain atmospheric NPF (Bianchi et al. (2016); Kirkby et al. (2011)), the numerical analysis ~~may~~ qualitatively ~~apply~~ applies also ~~for~~ to saturated condensable vapours containing compounds other than ~~dissolved~~ H_2SO_4 (cf. Riccobono et al. (2014)).

The numerical analysis yielded that the precursor's saturation ratio decreases rapidly with increasing *IR*. As long as the ice particles' size remains small (radii < 10 µm) their influence on the saturation ratio of the NPF precursor is comparatively weak. ~~However, a~~As demonstrated for H_2SO_4 (cf. Appendix B), rising *IR* (combining ice particle size and number) cons~~ould crucially confine~~ trains the production of high $N_{\text{uf nm}}$, or inhibit NPF at all. ~~In particular, o~~Note, only completely uncoated ice particles of pure water (which are excluded to exist in the UT/LS; cf. Bogdan et al. (2006); Bogdan et al. (2013)) would be ineffective condensation surfaces for H_2SO_4 vapour~~, since attachment points for H_2SO_4 molecules were lacking on the surface of pure ice water. Hence, the frequent observations of in-cloud NPF is indicative for processes, which are capable of maintaining sufficiently high NPF precursor saturation ratios. Such processes could involve turbulent mixing of precursor enriched air (entrainment) or a cooling process as induced, e.g. by a temperature anomaly due to gravity wave activity (cf. Weigel et al. (2021a)). Otherwise, NPF observations should be less frequently observable in the view of ice particles' effective influence on the saturation ratio of NPF precursors~~

~~From~~ According to ~~the results shown in~~ Figure 8~~Figure 8~~a, ~~it may be concluded that~~ the $N_{\text{uf nm}}$-range of 500-3000 cm^{-3} is most frequently observed over the ~~entire extent~~range of detected *IR* values. ~~While this confirms the impression from~~Regarding Figure 4~~Figure 4~~, ~~(cf.~~ Section 4.4~~)~~, ~~the conclusions from~~ Figure 8~~Figure 8~~, ~~and~~ the simulation of Appendix B, the ~~allow~~following ~~for approaching a possible explanation~~ conclusions seem likely~~of the N_{uf}'s behaviour with *IR*~~:

1) The maximum $N_{\text{uf nm}}$ resulting from in-cloud NPF is determined by *IR*. Abundant ice particles of sufficient size are capable of reducing the saturation ratio of NPF precursors

Formatiert: Nicht Hervorheben

within time scales ranging from half an hour to a few hours. Consequently, ~~moderate~~ intermediate or weak NPF events with ~~less excessive~~low $N_{uf_{nm}}$ production ~~may~~ occur most frequently in the presence of cloud ice. ~~However, t~~The probability to instrumentally identify weak NPF events decreases with decreasing $N_{uf_{nm}}$.

~~1)~~ These NPF limitations by the *IR* result from the StratoClim 2017 dataset and may not necessarily be of general validity. Further investigations at other locations and under variable conditions and dedicated laboratory experiments are necessary to confirm these limitations marked as grey bars in Figure 8~~Figure 8~~, which do not represent sharply quantifiable relationships.

2)

~~2)~~3) ~~Furthermore, c~~Coagulation ~~also~~ additionally affects $N_{uf_{nm}}$ ~~i~~on time scales of a few ~~to dozens of~~ hours (cf. ~~Weigel et al. 2020a~~ Weigel et al. (2021a)), ~~very likely constituting the most efficient altering process of ultrafine particles from NPF.~~

~~At the time of observation, the age and processing progress of the ultrafine particles are unknown. Amongst the previously described effects, the temporal delay between the NPF event and the measurement may have a crucial but unquantifiable impact on the actually observed N_{uf}, as the altering of ultrafine particles is very effective in time scales of a few hours (Weigel et al., 2021a)(Weigel et al. 2020a). Hence, it is likely a matter of probability, that in-cloud NPF with moderately high N_{uf} (e.g. 500-3000 cm^{-3}) is most frequently observed.~~ According to the ~~data compiled~~results in Figure 8~~Figure 8~~, *IR* values of about 24 µm cm^{-3} (corresponding to N_{ice} of about 0.7-0.8 cm^{-3} and ~~mean mass radii~~ $\overline{r_{ice}}$ of about 32 µm) constituted ~~in general~~ the uppermost limit for in-cloud NPF observation during StratoClim 2017. Below the *IR* limits marked with grey bars, in-cloud NPF is encountered largely unaffected by the presence of ice particles. It is emphasised that the grey bars primarily mark a region in the *IR* – n_{nm} parameter space where the duration of an exceedance of marked levels decreases with increasing *IR* and/or n_{nm}. Hence, the detection of these points becomes less likely, or the probability increases to miss such events when the values cross the marked levels.

Figure 8~~Figure 8~~b depicts ~~Another processing of the same data set, i.e.~~ $N_{uf_{nm}}$ as a function of *IR*~~,~~ ~~implies a data sorting by means of~~ with reference to the CO mixing ratio ~~(Figure 8b)~~. ~~Apparently, n~~None ~~of the emerging samples, n~~either samples with highest $N_{uf_{nm}}$ nor samples with highest *IR*~~,~~ ~~was~~ were directly ascribable to polluted air~~, which was~~ recently lifted from the surface. ~~Strongest~~ Intense NPF (with $N_{uf_{nm}}$ > 5000 cm^{-3}) ~~were~~ was ~~exclusively~~ observed at CO mixing ratios ranging between ~ 90 and 100 nmol mol^{-1}, which indicates the air's moderate pollutant load or its moderate age. ~~Alternatively, these CO values may reflect certain mixing states of air masses of significantly different age.~~ In less polluted air (CO mixing ratios below ~ 70 nmol mol^{-1}), the *IR* reaches the highest values (up to ~ 24 µm cm^{-3}) which were observed together with

Formatiert: Schriftart: Kursiv

Formatiert: Schriftart: Kursiv

Formatiert: Schriftart: Kursiv

Formatiert: Schriftart: Kursiv

Formatiert: Tiefgestellt

Formatiert: Schriftart: Kursiv

Formatiert: Schriftart: Kursiv

Formatiert: Tiefgestellt

Formatiert: Abstand Nach: 12 Pt.

elevated *IWC* (up to ~750 µmol mol^{-1}, i.e. log (*IWC*, nmol mol^{-1}) ≈ 0.88). Within ~~pristine~~ low-polluted air, cloud ice particles mostly ~~likely~~ form *in-situ*. It is conceivable, that the *in-situ* cloud ice formation and NPF happens simultaneously~~, potentially~~ and induced by the same process: e.g. by updraughts due to subjacent convection (pileus effect) or by (local) cooling due to gravity waves (cf. Weigel et al. (2021a)~~Weigel et al. 2020a~~). ~~In such cases (~~At CO mixing ratios below ~~<~~ 70 nmol mol^{-1}~~)~~, the observed $N_{~~uf~~nm}$ ~~are systematically lower than 1000 cm^{-3} and they mostly~~ range at a few hundreds per cm^3~~.~~ but systematically below 1000 cm^{-3}.

Based on NPF encountered during StratoClim, the air masses with low pollutant loads therefore still contain sufficient amounts of precursor material ~~Hence, air masses with low pollutant loads obviously contain sufficient amounts of precursor material~~ to supply ~~moderate~~ intermediate NPF
(100 cm^{-3} < $N_{~~uf~~nm}$ < 1000 cm^{-3}) ~~which may strengthen the hypothesis that air's pollutant load is not an essential prerequisite for the occurrence of most intense NPF (N_{uf} > 5000 cm^{-3} at *IR* < 1 µm cm^{-3}) in the UT/LS region~~. This differs from earlier findings from ground-based measurements at high mountain sites (at about 5 km altitude) in the Himalaya region by Venzac et al. (2008) or at the Jungfraujoch station (~ 3.5 km altitude) in the Swiss Alps by Bianchi et al. (2016) ~~who~~ who attributed their frequent NPF observations to the advection of polluted air which rises up from the valleys towards the research stations. Williamson et al. (2019) ~~made their~~found ~~very~~ frequent NPF ~~observations based on a very comprehensive data set of airborne *in-situ*~~during measurements over ~~both oceans,~~ the Atlantic and the Pacific, i.e.~~,~~ ~~,~~in certain distance away from ~~from direct convective supply by~~sources of industrial pollution. ~~However, different atmospheric conditions and/or different chemical precursor species might play a role in the NPF processes occurring in the boundary layer or at UT/LS altitudes~~Like for StratoClim 2017, low levels of pollution here were sufficient to support NPF.

6 Summary and Conclusions

Between 27 July and 10 August 2017 the airborne StratoClim mission took place in Kathmandu, Nepal, comprising eight mission flights (~ 22.5 hours of COPAS measurement time above 10 km, $\theta \gtrsim 350$ K) up to altitudes of 20 km ($\theta \approx 475$ K) with the Russian high-altitude research aircraft M-55 *Geophysica*. ~~The present analysis includes the description and discussion of~~ New Particle Formation ~~(NPF)~~ in the presence of cloud ice particles was analysed, as it was encountered ~~as observed~~ in the UT/LS region of the Asian Monsoon Anticyclone (AMA) over northern India, Nepal and Bangladesh. Over the StratoClim observation period, in-cloud NPF was a frequently occurring phenomenon within the AMA associated with predominantly large convective cloud

Formatiert: Englisch (Vereinigtes Königreich)

systems over the Himalayan foothills. Elevated concentrations of ~~ultrafine~~ nucleation-mode particles ($N_{~~u~~fnm}$) generated by NPF were observed in hitherto ~~unexpected~~ unreported frequency together with ice particles ($N_{ice} > 0$ cm^{-3}) at altitudes between ~ 11 km and 16.5 km (~ 355 - 385 K) and mainly at ambient temperatures colder than ~ 230 K. During StratoClim 2017, a total number of 104 in-cloud NPF events was observed over a total duration of 1 hour and 17 minutes (~ 5 % of the total data set, ~ 49 % of all observed NPF cases). Maximum concentrations of ~~ultrafine~~ nucleation-mode particles of up to ~ 11000 cm^{-3} (≈ 50000 mg^{-1}) were detected coincidently with ice particles in concentrations N_{ice} of 0.05 – 0.1 cm^{-3} (correspondent to 50 - 100 ice particles per litre) at heights of approximately 15.5 km (~ 370 K).

The observations indicate the N_{nm}-range of 500-3000 cm^{-3} as most frequently observed during in-cloud NPF. Weak events with low NPF-rate occur most frequently in the presence of cloud ice, whilst the probability to instrumentally identify such weak events decreases with N_{nm}. Coagulation additionally affects elevated N_{nm} in time scales of a few hours (cf. Weigel et al. (2021a)). Consequently, the supposedly preferred N_{nm}-range results from superimposed effects, and it is a matter of probability and timing (delay between NPF event and observation) that the N_{nm}-range of 500-3000 cm^{-3} is most frequently observed in the presence of cloud ice.

Formatiert: Tabstopps: Nicht an 4.75 cm + 9.25 cm

Analyses of the StratoClim data set concerning the relationship between interstitial aerosol and the abundance of cloud particles in the UT/LS are consistent with the findings from earlier measurements (de Reus et al., 2009), and extended these by new observations under different conditions. When ice particles are abundant ($N_{ice} > 0.5$ cm^{-3}), total aerosol number concentrations (N_{10}) remain generally between ~ 200 cm^{-3} and 700 cm^{-3}. In agreement with earlier findings (de Reus et al., 2009), the ratio of ice particle number and the number of submicrometre-sized aerosols did not significantly rise above 300 submicrometre-sized ~~aerosols~~ aerosols per ice particle at low air temperatures (< 200 K). Intense NPF, generating ~~ultrafine~~ nucleation-mode particles of several thousands per cm^3, substantially decrease the ratio of number concentrations of ice particle~~-aerosol ratio substantially~~s to aerosols. However, such intense NPF was not observed at ratios larger than 1:3000, which indicates that the presence of cloud ice imposes limitations to ~~the occurrence of~~ NPF.

In-cloud NPF appears ~~confined~~ limited in the presence of predominantly *liquid-origin* ice particles with increased ice water content resulting from ~~strong convective overshooting~~deep convection up to cold point tropopause levels. This is confirmed by coincidently measured CO content of the air sample: air's pollutant load and/or its recent surface contact do not determine the strength of in-cloud NPF. Otherwise, the most intensive NPF events should ~~occur~~ be have been found more frequently ~~with~~in air masses with highest CO content. When the cloud ice has formed *in-situ,* at low CO mixing ratios, NPF was observed although with reduced strength.

However, it is not yet conclusively clarified whether the direct convective supply of precursor material from pollution in the boundary layer is an essential prerequisite for the occurrence of NPF in the UT/LS, or whether NPF together with the ice cloud formation are initialised in processed and diluted air masses. The observations suggest that sufficient amounts of NPF precursor accumulate at UT/LS altitude, which is not necessarily connected to air's recent vertical uplift. It remains speculative, and it should be subject of suitable numerical analyses, to which extent the vertically lifted ice particles themselves contribute as carrier for soluble NPF precursor gases such as SO_2, H_2SO_4, or others, e.g., if dissolved in the cloud elements' liquid phase at lower heights and ~~if~~ released again at TTL altitudes after the cloud ice has sublimated. Comparatively slow processes, as air mass transport from elsewhere or the chemical and/or photochemical conversion at elevated altitudes may suffice to supply the reservoir of NPF precursors at UT/LS altitudes. NPF of highest intensity, however, was observed at moderate CO mixing ratios~~, indicating a moderate pollutant load, and a certain age or mixing state of the air mass~~. Intense NPF seems ~~almost confined~~suppressed in strong convective updraughts (cf. Section 4.2), either because of the intense dynamics inherent with ~~overshooting~~ convection, or because the precursor's saturation ratio of recently uplifted air does not suffice for ~~immediate~~ NPF.

At the moment of observation, the age of the nucleation-mode aerosols (the delay between the NPF burst and the instrumental detection) as well as the aerosol's processing history is unknown. While the aerosol's persistence in the nucleation mode is limited, it is conceivable that the abundance of aerosols influences the local formation of ice particles, or that ice particles are coated by nucleation-mode aerosol material due to coagulation. Above certain sizes, the cloud ice elements are increasingly subject to sedimentation. On sedimentation to warmer ambient temperatures, the ice particles sublimate. The remnants of sublimated cloud ice consists of materials attributed to the initially NPF-generated nucleation-mode aerosols. It remains speculative whether or not, in terms of physico-chemical characteristics, the released aerosol material is comparable with the primary NPF-generated aerosol. The sublimation of coated ice particles and the release of aerosol material at intermediate altitudes provides nuclei for cloud entrainment and/or for cloud formation. It remains unquantified whether NPF near the surface (cf. Venzac et al. (2008) or Bianchi et al. (2016)) or the NPF at UT/LS altitudes contribute at the most to the availability of cloud condensation nuclei (CCN), which are supposed to promote cloud formation (Andreae et al., 2018) at the cloud condensation levels. The specific source contributions to the abundance of available CCN are as variable as the chemical species that may be involved in the NPF process.

~~The occurrence of NPF is strongly dependent on the precursor's saturation ratio.~~ Ice particles in sufficient number and size are well capable to reduce the saturation ratio of a NPF precursor such as H_2SO_4. This implies two conclusions: 1) in-cloud NPF is ~~confined~~ limited by abundant ice particles and 2) not only the number of ice particles limits the NPF occurrence but also the ice particles' size. The strength of in-cloud NPF ~~most clearly~~ depends on the integral radius *IR* ($= \overline{r_{\mathrm{ice}}} \cdot N_{\mathrm{ice}}$), which constitutes the control value of the ice particle's growth ($\frac{dm}{dt}$) ~~the product of the ice particles number concentration and the ice particles' mean mass radius~~. ~~The *IR* turned out as appropriate cloud ice related parameter to juxtapose with NPF data.~~ Up to *IR* of ~ 1 µm cm^{-3} the occurrence of NPF of any strength (with ~ 100 < $N_{\mathrm{uf\,nm}}$ < 10 000 cm^{-3}) seems independent on the presence of ice particles at all. At larger *IR* (> 1 µm cm^{-3}) the presence of ice particles limits the maximum of $N_{\mathrm{uf\,nm}}$ from NPF. This result refines earlier ~~findings~~ conclusions (Weigel et al., 2011) ~~that~~ according to which mainly the number of ice particles would limit the occurrence of NPF.

~~The observations indicate that a N_{uf} range of 500-3000 cm^{-3} was most frequently observed during in-cloud NPF. However, weak NPF generating only low N_{uf} may occur most frequently in the presence of cloud ice, whilst the probability to instrumentally identify such weak events decreases with decreasing N_{uf}. Additionally, coagulation affects large N_{uf} in time scales of a few to dozens of hours (cf. Weigel et al. 2020aWeigel et al. (2021a)). As a consequence, the supposedly preferred N_{uf} range likely results from superimposed effects, and it may be a matter of probability and timing (delay between NPF event and observation) that the N_{uf} range of 500-3000 cm^{-3} is most frequently observed in the presence of cloud ice.~~

~~At the moment of observation, the age of the ultrafine aerosol (the delay between the NPF burst and the instrumental detection) as well as the aerosol's processing history is unknown. While the aerosol's persistence in the ultrafine size range is limited, it is conceivable that the abundance of aerosols influences the local formation of ice particles, or that ice particles are coated by ultrafine aerosol material due to coagulation. Above certain sizes, the cloud ice elements are increasingly subject to sedimentation. At warmer ambient temperatures, the ice particles may sublimate. This could release the materials attributed to the initially NPF-generated ultrafine aerosol. It remains speculative whether or not, in terms of physico-chemical characteristics, the released aerosol material is comparable with the primary NPF-generated aerosol. However, the sublimation of coated ice particles and the release of aerosol material at intermediate altitudes could provide nuclei for entrainment and/or cloud formation. It remains unquantified, however, whether NPF near the surface (cf. Venzac et al. (2008) or Bianchi et al. (2016)) or the NPF at UT/LS altitudes contribute at the most to the availability of cloud condensation nuclei (CCN), which are supposed to promote cloud formation (Andreae et al.,~~

Formatiert: Schriftart: Nicht Kursiv

Formatiert: Schriftart: Nicht Kursiv

~~2018) at the cloud condensation levels. Most likely the specific source contributions to the abundance of available CCN are as variable as are the chemical species potentially involved in the NPF process.~~

Data availability:

The data shown in this study are available at the StratoClim campaign database at

https://stratoclim.icg.kfa-juelich.de/AfcMain/CampaignDataBase ;

alternatively, they may be provided by respective PI upon request.

Author contribution

RW evaluated and analysed the data, created the figures, and ~~draughted~~ drafted the manuscript with contributions by CM, MB, MK, HT and PS. SB participated in the data analyses and the manuscript ~~draughting~~drafting. Numerical simulations concerning the impact of ice particles on the saturation ratio of H_2SO_4 were performed by MB with contributions by HT. MK, NS, AA and CR contributed with cloud microphysical and water vapour data. SV and FD'A ~~took care of~~provided the CO data. The manuscript was critically reviewed by CM, MB, MK, PS, NS, AA, CR, SV, FD'A, HT, and SB.

Competing interests

The authors declare no competing interests.

Acknowledgements

The contributions from the workshops of the Max Planck Institute for Chemistry and of the Institute for Physics of the Atmosphere (Mainz University) were essential for this work. In particular, we acknowledge support of T. Böttger, M. Flanz, C. v. Glahn, H. Rott, and W. Schneider. Also acknowledged are the comprehensive and helpful discussions with M. Szakáll. We very much thank the crew of MDB (Myasishchev Design Bureau) and the M-55 *Geophysica* pilots. The extraordinary commitment of F. Stroh in realisation of the campaign and the leadership of the entire StratoClim project by M. Rex are gratefully acknowledged. Some of our research leading to the presented results received funding from the European Research Council under the European Union's Seventh Framework Program (FP/2007-2013)/ERC Grant Agreement No. 321040 (EXCATRO). The StratoClim project was funded by the EU (FP7/2007–2018 Grant No. 603557) and also supported by the German "Bundesministerium für Bildung und Forschung" (BMBF) under the joint ROMIC-project SPITFIRE (01LG1205A). M. Baumgartner acknowledges support by the DFG within the Transregional Collaborative Research CentreTRR165 "Waves to Weather", Project Z2. P. Spichtinger acknowledges support by the DFG within the research unit Multiscale Dynamics of Gravity Waves (MS-GWaves) through grant SP 1163/5-2. H. Tost acknowledges funding from the Carl-Zeiss foundation. We explicitly thank the officials of the Nepalese government authorities, research institutions and Tribhuvan Airport as well as of the German Embassy for their extraordinary support and hospitality, which enabled our field campaign and research.

Appendix A: Exclusion of sampling artefacts ~~on NPF observation~~ due to the presence of cloud ice

During the herein discussed NPF events, the detected total number concentration of cloud elements never exceeded ~2-3 cm^{-3}. Thus, the number density of cloud elements were always ~~significantly smaller (~~at least by two orders of magnitude~~)~~ smaller compared to detected aerosol number concentrations. At ambient air temperatures ranging ~~much colder than~~from 187 K to 235 K, ~~(and as cold as 187 K),~~ the clouds entirely consisted of ice particles. In other studies, however, the discussions on NPF are restricted to measurements under cloud-free (clear-air) conditions as the cloud particles are suspected to possibly impact onto the aircraft's hull or the aerosol inlet, this way possibly generating artefacts on the aerosol measurements (Williamson et al. (2019) referring to Weber et al. (1998)). Regarding the in-cloud NPF observations throughout StratoClim 2017, the following aspects are noteworthy:

1) At typical flight speeds of the M-55 *Geophysica* (154 ± 39 m s^{-1}), sub-micrometre-sized ~~ice~~ particles ~~should negligibly be~~are not subject to impaction on parts of the aircraft structure (nose, wing's leading edge, etc.) as the particles ~~are well capable to~~ follow the air stream around such flow obstacles (Kulkarni et al., 2011). Furthermore, ice particles in the diameter size range of a few micrometre (i.e. 1 µm < d_p < 10 µm) partially sublimate in the congestion region upstream of any aircraft structure (e.g. the wings leading edge, or the aerosol inlet). ~~Even though a single particle of the aforementioned size could randomly enter the COPAS aerosol inlet, t~~The diffuser-type entry of the aerosol inlet leads to a flow deceleration ~~of the air flow~~ inside the probe head ~~(Weigel et al., 2009)~~ accompanied with a sudden temperature increase ~~in the air sample~~ ~~(~~according to fluid dynamical simulations ~~of the inlet flow~~by up to 13°C on flow deceleration from 170 m s^{-1} to 60 m s^{-1}, cf. ~~;~~Weigel et al. (2009) and references therein). Hence, if a single particle with 1 µm < d_p < 10 µm randomly enters the COPAS aerosol inlet, rapid sublimation of such an ice particles ~~in the diameter size range of a few µm~~ can be expected to occur inside the aerosol inlet of COPAS. The entry of the sample air into the inlet's second diffuser additionally reduces the sampling of ice particle fragments. Due to additional heating of the air sample and during their passage through the aerosol line to the COPAS detector (less than about 0.5 seconds), the ice particles from shattering with diameters of a few µm evaporate even if they are present in large numbers.
2) The number concentration of ice particles with diameter d_p > 10 µm mostly remained below 0.4 cm^{-3} when coincidently detected with NPF. On impact and shattering of a single ice particle of such a size, the number of generated fragments is estimated to range at about 10-100 per cm^3 (Korolev et al., 2013). Hence, to substantially affect the

detected number concentration of ~~ultrafine~~ nucleation-mode particles (on magnitude order of hundreds to up to ten thousands per cm^3), the number of ice particles ~~possibly~~ emanating from shattering appears too low.

3) The probability that ice particles hit the sharp edged tips of the COPAS aerosol inlet (Weigel et al., 2009) appears negligibly small. The impaction surface provided by the COPAS aerosol inlet is mainly the inlet's ring-shaped entry with an opening diameter of ~ 7.3 mm and a wall thickness of ~ 100 µm. In the unlikely case that a single ice particle impact occurred, all generated fragments were required to endure the temperature rise within the inlet head (cf. first argument of this list) and the transport through the aerosol lines towards the COPAS detectors before they can cause any effect on the measurement.

An effect of shattered large ice particles on the detection of ~~ultrafine~~ nucleation-mode ~~aerosol~~ particles is ultimately not excludable. However, despite the reference by Williamson et al. (2019) in this context, ice particle fragmentation was not described by Weber et al. (1998). The same authors discuss the influence on NPF detections due to fragmentation of super-cooled liquid-water cloud droplets and suggest a careful discussion in such cases. In general, such an influence due to the fragmentation of ice particles was largely ruled out or estimated as much lower than that of liquid droplets (Weber et al., 1998). Concerning the analyses discussed herein, however, it seems a statistical exception that ice particle fragments emanating from shattered ice particles crucially affect the measurement of the numbers of ~~ultrafine aerosol~~nucleation-mode particles. Moreover, if the NPF detections were systematically affected by the presence of cloud ice, the observed quantities of ~~ultrafine~~ nucleation-mode particles would ~~probably~~ feature systematic and larger differences during in-cloud measurements compared to clear-air observations. None of the described artefacts ~~was~~ was observable in the data from StratoClim 2017.

Appendix B: Impact of ice particles on NPF precursors' saturation ratio

Calculations were made regarding the time scales in which the decrease of the supersaturation of H_2SO_4 vapour occurs in the presence of coated ice particles. ~~These serve as estimates concerning the efficiency of the diffusional loss of condensable materials, i.e. of the process competing with the gas-to-particle conversion of these vapours. The molecules of condensable and saturated (or supersaturated) vapours condense onto available surfaces, such as provided e.g. by an ice particle, whereas the combination of molecules into stable clusters requires significantly supersaturated conditions to form new particles out of the gas phase. However, it seems plausible that i~~In the closest vicinity of an ice particle, the condensational loss of a precursor gas like sulphuric acid (H_2SO_4) predominates over the NPF process. ~~For H_2SO_4, as a representative of the NPF precursors, the question arises how efficient the condensation of H_2SO_4 occurs onto provided surface.~~ The molecules' mobility and the condensation efficiency of

the H_2SO_4 molecules is mainly determined by their diffusivity under the given atmospheric conditions. The diffusivity of H_2SO_4 is about a factor of 0.2-0.5 of the diffusivity of water vapour (Tang et al., 2014). ~~Consequently, the condensational deposition of H_2SO_4 onto the coated particles surface causes the saturation ratio of H_2SO_4 to decrease within the environment of the ice particle, which likely suppresses the process of NPF within a certain range around the ice particle.~~

Presuming that the ice particles are coated with H_2SO_4 (Bogdan et al. (2006); Bogdan et al. (2013)), model simulations were performed to investigate the timescales ~~with~~in which the coated ice particles reduce various H_2SO_4 saturation ratios. The simulation results (shown in Figure B- 1~~Figure B- 1~~) are based on constant ambient temperature ($T \approx 200$ K) and pressure ($p = 110$ hPa) conditions. For the same temperature conditions, the saturation vapour pressure p_{sat} of H_2SO_4 is calculated according to Vehkamäki et al. (2002). ~~This~~ In this way, the degree of supersaturation is deducible from the H_2SO_4 molecules concentrations reported for the CLOUD (Cosmics Leaving OUtdoor Droplets) chamber experiments (cf. Kürten (2019), and references therein). According to this study, and in agreement with other references (H. Gordon, School of Earth and Environment, Leeds University, UK, personal communications Oct. 2019), molecule concentrations of $10^6 - 10^7$ cm^{-3} are required in the CLOUD chamber at temperatures of 208 K to induce NPF with nucleation rates of $10^{-2} - 100$ cm^{-3} s^{-1} (read out from Fig. 4 in Kürten (2019) from experiments at relative humidity of 38 %, *ibid.*). Keeping possible wall effects of the laboratory experiments in mind, for the occurrence of NPF under real atmospheric conditions, the lower bound of required molecule concentrations (10^6 cm^{-3}) may suffice, with an uncertainty of a factor five (H. Gordon, School of Earth and Environment, Leeds University, UK, personal communications Oct. 2019). At an ambient temperature of 208 K, the molecule concentrations of $10^6 - 10^7$ H_2SO_4 cm^{-3} (Kürten, 2019) correspond to saturation ratios of about $S \approx 10 - 100$. The following analysis, however, comprises a much wider range of saturation ratios between 10 and up to 5000 to account for a higher sensitivity of the temperature dependency of S.

Based on the expression formulated by Tsagkogeorgas et al. (2017) with the saturation vapour pressure p_{sat} of H_2SO_4 (above a flat surface) and with an accommodation coefficient of $\alpha = 0.65$ (Pöschl et al., 1998), the ~~ice particle's~~ change of the fully coated ice crystal with mass m per time unit ~~change of mass m per time unit~~ is calculated by:

$$\frac{dm}{dt} = \frac{4\pi D r (S-1)}{\left(\frac{L}{RT}-1\right)\frac{L}{T}\frac{D}{K} + \frac{RT}{\alpha p_{sat}}} \quad , \qquad (B-1)$$

which conceptually represents the change of mass (size) of the particles, onto which the H_2SO_4 condenses and which is also consistent with the finding that cirrus cloud elements are coated with a H_2SO_4-H_2O layer (Bogdan et al. (2006); Bogdan et al. (2013)). The diffusivity of H_2SO_4

Formatiert: Englisch (Vereinigtes Königreich)

Formatiert: Schriftart: Kursiv

Formatiert: Schriftart: Kursiv

molecules in air is denoted with D, and K refers to the thermal conductivity of air, while R and R_a are the gas constants of H_2SO_4 and the air, respectively. Since the ice particles grow predominantly by the uptake of water vapour and the effective contribution to $\frac{dm}{dt}$ by the condensing H_2SO_4 is of minor concern. The $\frac{dm}{dt}$ from the condensing H_2SO_4 converts instead to a reduction in the saturation ratio of gaseous H_2SO_4, the change of which is:

$$\frac{dS}{dt} = -\frac{R}{R_a}\frac{p}{p_{sat}} N_{ice} \frac{dm}{dt}, \quad (B-2)$$

with the latent heat of vaporisation which is assumed as constant:

$$L = \frac{67.59 \cdot 10^3 \text{ J mol}^{-1}}{M_{H2SO4}}, \quad (B-3)$$

and N_{ice} constitutes the number density of ice particles. Here, the sulphuric acid's molar mass is M_{H2SO4} = 0.098078 kg mol^{-1}. Note, the combination of the equations B−2 and B−1 depicts implies that $\frac{dS}{dt} \sim r \cdot N_{ice}$, i.e. the temporal change of the precursor's saturation ratio is proportional to the integral radius *IR* considered in Section 5.2.

In Figure B- 1Figure B- 1 the variability of two aspects is considered and in the panels (a-c) it is distinguished between three ice particle radii (1 µm, 10 µm, and 100 µm) and two different ice particle number concentrations (0.01 and 0.1 cm^{-3}). The study by Ueyama et al. (2020) revealed that ice particles (effective radii of about 15 µm) persist over 12 to 20 hours at convective outflow levels between 365 K and 370 K potential temperature in the 2017 AMA of the 2017 season.

Based on the simulation, apparently, the largest particles (r_p = 100 µm) are capable to efficiently suppress the NPF process. Particles of this size and in highest concentrations of 0.1 cm^{-3} cause the saturation ratio to rapidly abate to saturation level (i.e. S = 1) within 20-50 minutes. Even aAt lower concentrations (0.01 cm^{-3}) of particles of 100 µm radius, the saturation ratio is efficiently reduced by more than 70 % within 1 hour. Particles of 10 µm radius and in concentrations of 0.1 cm^{-3} appear to beare almost equally efficient in reducing the saturation ratio by ~ 70 % within 1 hour. Smaller number concentrations of the same particle size range, and smaller particles (r_p = 1 µm), in general, require considerably more time than 1 hour to significantly reduce the H_2SO_4 saturation ratio.

In essence, cloud ice particles can rapidly reduce the saturation ratio of H_2SO_4 andsands, very likely, also the saturation ratio of other condensable gases. The ranges of N_{ice} (0.01 - 0.1 cm^{-3}) and particle size (1 µm < r_p < 100 µm) considered in the simulation correspond to the characteristics of ice particles coincidently observed with NPF throughout the StratoClim 2017 mission (note,

Formatiert: Schriftart: Nicht Kursiv
Formatiert: Schriftart: Nicht Kursiv
Formatiert: Schriftart: Nicht Kursiv
Formatiert: Schriftart: Nicht Kursiv

away from NPF, higher N_{ice} ~~concentrations~~ and larger $\overline{r_{ice}}$ ~~sizes~~ were found, cf. Krämer et al. (2020)). About 71% of all ice cloud detections in coincidence with NPF had an *IR* (i.e. $\overline{r_{ice}} \cdot N_{ice}$) of less than 1 µm cm^{-3}, while only about 1.5 % of the ice particle samples reached *IR* values greater than 7.5 µm cm^{-3}; the maximum *IR* of 24 µm cm^{-3} was encountered once throughout the entire mission. In general, the cirrus cloud particles are expected as coated with a H_2SO_4/H_2O layer (Bogdan et al. (2006); Bogdan et al. (2013)) onto which sulphuric acid can condense. ~~However, i~~Impurities by weaker and substitutable acids (such as organic acids or HCl or HNO_3) also allow the H_2SO_4 uptake on the surface, which could reduce the gaseous H_2SO_4 concentration thereby ~~this way potentially suppressing~~ suppressing NPF. Hence, in certain abundance the presence of cloud ice particles restrains the NPF process, when condensation prevails over the competing gas-to-particle conversion. The efficiency of condensation onto the ice particles' surface ~~strongly~~ depends on

1) the size and number concentration of cloud ice particles and,
2) on the time interval during which the conditions remain at least saturated.

For the condensation of H_2SO_4, a partial coating of the ice particles' surface with sulphuric acid (or organic acids, HCl, or HNO_3) suffices to supply the gaseous H_2SO_4 with the required attachment points. To simplify the numerical simulation of the saturation decay, an ice particle is assumed as entirely coated (consistent with Bogdan et al. (2006); Bogdan et al. (2013)) and the (real) ice particle's habit (e.g. asphericity, porosity, etc.) remains unconsidered. Sporadic updraughts~~, such as initialised by~~ due to convective lifting well below the NPF level~~,~~ or gravity waves ~~could~~ cause small-scaled expansion and cooling which increases the precursor's supersaturation (Weigel et al., 2021a). ~~Hence, a c~~Certain concentrations of H_2SO_4 molecules ~~could~~ exceed the supersaturation threshold for NPF, even in the presence of abundant cloud ice, as long as the NPF process occurs faster than the reduction of *S* due to the present ice.

Kommentiert [WR4]:

References

Afchine, A., Rolf, C., Costa, A., Spelten, N., Riese, M., Buchholz, B., Ebert, V., Heller, R., Kaufmann, S., Minikin, A., Voigt, C., Zöger, M., Smith, J., Lawson, P., Lykov, A., Khaykin, S., and Krämer, M.: Ice particle sampling from aircraft - influence of the probing position on the ice water content, Atmos Meas Tech, 11, 4015-4031, 10.5194/amt-11-4015-2018, 2018.

Andreae, M. O., Afchine, A., Albrecht, R., Holanda, B. A., Artaxo, P., Barbosa, H. M. J., Borrmann, S., Cecchini, M. A., Costa, A., Dollner, M., Fütterer, D., Järvinen, E., Jurkat, T., Klimach, T., Konemann, T., Knote, C., Krämer, M., Krisna, T., Machado, L. A. T., Mertes, S., Minikin, A., Pöhlker, C., Pöhlker, M. L., Pöschl, U., Rosenfeld, D., Sauer, D., Schlager, H., Schnaiter, M., Schneider, J., Schulz, C., Spanu, A., Sperling, V. B., Voigt, C., Walser, A., Wang, J., Weinzierl, B., Wendisch, M., and Ziereis, H.: Aerosol characteristics and particle production in the upper troposphere over the Amazon Basin, Atmos Chem Phys, 18, 921-961, 10.5194/acp-18-921-2018, 2018.

Ball, S. M., Hanson, D. R., Eisele, F. L., and McMurry, P. H.: Laboratory studies of particle nucleation: Initial results for H_2SO_4, H_2O, and NH_3 vapors, J Geophys Res-Atmos, 104, 23709-23718, 10.1029/1999jd900411, 1999.

Baumgartner, M., and Spichtinger, P.: Towards a bulk approach to local interactions of hydrometeors, Atmos Chem Phys, 18, 2525-2546, 10.5194/acp-18-2525-2018, 2018.

Baumgartner, M., Weigel, R., Harvey, A. H., Ploeger, F., Achatz, U., and Spichtinger, P.: Reappraising the appropriate calculation of a common meteorological quantity: potential temperature, Atmos. Chem. Phys., 20, 15585-15616, 10.5194/acp-20-15585-2020, 2020.

Benson, D. R., Erupe, M. E., and Lee, S. H.: Laboratory-measured H_2SO_4-H_2O-NH_3 ternary homogeneous nucleation rates: Initial observations, Geophys Res Lett, 36, Artn L15818

10.1029/2009gl038728, 2009.

Bianchi, F., Tröstl, J., Junninen, H., Frege, C., Henne, S., Hoyle, C. R., Molteni, U., Herrmann, E., Adamov, A., Bukowiecki, N., Chen, X., Duplissy, J., Gysel, M., Hutterli, M., Kangasluoma, J., Kontkanen, J., Kürten, A., Manninen, H. E., Münch, S., Peräkylä, O., Petäjä, T., Rondo, L., Williamson, C., Weingartner, E., Curtius, J., Worsnop, D. R., Kulmala, M., Dommen, J., and Baltensperger, U.: New particle formation in the free troposphere: A question of chemistry and timing, Science, 352, 1109-1112, 10.1126/science.aad5456, 2016.

Bogdan, A., Molina, M. J., Sassen, K., and Kulmala, M.: Formation of low-temperature cirrus from H_2SO_4/H_2O aerosol droplets, J Phys Chem A, 110, 12541-12542, 10.1021/jp065898e, 2006.

Bogdan, A., Molina, M. J., Kulmala, M., Tenhu, H., and Loerting, T.: Solution coating around ice particles of incipient cirrus clouds, P Natl Acad Sci USA, 110, E2439-E2439, 10.1073/pnas.1304471110, 2013.

Borrmann, S., Kunkel, D., Weigel, R., Minikin, A., Deshler, T., Wilson, J. C., Curtius, J., Volk, C. M., Homan, C. D., Ulanovsky, A., Ravegnani, F., Viciani, S., Shur, G. N., Belyaev, G. V., Law, K. S., and Cairo, F.: Aerosols in the tropical and subtropical UT/LS: in-situ measurements of submicron particle abundance and volatility, Atmos Chem Phys, 10, 5573-5592, 10.5194/acp-10-5573-2010, 2010.

Bucci, S., Legras, B., Sellitto, P., D'Amato, F., Viciani, S., Montori, A., Chiarugi, A., Ravegnani, F., Ulanovsky, A., Cairo, F., and Stroh, F.: Deep-convective influence on the upper troposphere–lower stratosphere composition in the Asian monsoon anticyclone region: 2017 StratoClim campaign results, Atmos. Chem. Phys., 20, 12193-12210, 10.5194/acp-20-12193-2020, 2020.

Clarke, A. D., and Kapustin, V. N.: A pacific aerosol survey. Part I: A decade of data on particle production, transport, evolution, and mixing in the troposphere, Journal of the Atmospheric Sciences, 59, 363-382, 10.1175/1520-0469(2002)059<0363:Apaspi>2.0.Co;2, 2002.

Clerbaux, C., George, M., Turquety, S., Walker, K. A., Barret, B., Bernath, P., Boone, C., Borsdorff, T., Cammas, J. P., Catoire, V., Coffey, M., Coheur, P. F., Deeter, M., De Maziere, M., Drummond, J., Duchatelet, P., Dupuy, E., de Zafra, R., Eddounia, F., Edwards, D. P., Emmons, L., Funke, B., Gille, J., Griffith, D. W. T., Hannigan, J., Hase, F., Hopfner, M., Jones, N., Kagawa, A., Kasai, Y., Kramer, I., Le Flochmoen, E., Livesey, N. J., Lopez-Puertas, M., Luo, M., Mahieu, E., Murtagh, D., Nedelec, P., Pazmino, A., Pumphrey, H., Ricaud, P., Rinsland, C. P., Robert, C., Schneider, M., Senten, C., Stiller, G., Strandberg, A., Strong, K., Sussmann, R., Thouret, V., Urban, J., and Wiacek, A.: CO measurements from the ACE-FTS satellite instrument: data analysis and validation using ground-based, airborne and spaceborne observations, Atmos Chem Phys, 8, 2569-2594, 10.5194/acp-8-2569-2008, 2008.

Formatiert: Abstand Nach: 10 Pt.

Costa, A., Meyer, J., Afchine, A., Luebke, A., Gunther, G., Dorsey, J. R., Gallagher, M. W., Ehrlich, A., Wendisch, M., Baumgardner, D., Wex, H., and Kramer, M.: Classification of Arctic, midlatitude and tropical clouds in the mixed-phase temperature regime, Atmos Chem Phys, 17, 12219-12238, 10.5194/acp-17-12219-2017, 2017.

Curtius, J., Weigel, R., Vössing, H. J., Wernli, H., Werner, A., Volk, C. M., Konopka, P., Krebsbach, M., Schiller, C., Roiger, A., Schlager, H., Dreiling, V., and Borrmann, S.: Observations of meteoric material and implications for aerosol nucleation in the winter Arctic lower stratosphere derived from in situ particle measurements, Atmos Chem Phys, 5, 3053-3069, 10.5194/acp-5-3053-2005, 2005.

Davis, S., Hlavka, D. L., Jensen, E. J., Rosenlof, K., Yang, Q., Schmidt, S., Borrmann, S., Frey, W., Lawson, P., Voemel, H., and Bui, T. P.: In situ and lidar observations of tropopause subvisible cirrus clouds during TC4, Journal of Geophysical Research: Atmospheres, 115, 10.1029/2009jd013093, 2010.

de Reus, M., Krejci, R., Williams, J., Fischer, H., Scheele, R., and Strom, J.: Vertical and horizontal distributions of the aerosol number concentration and size distribution over the northern Indian Ocean, J Geophys Res-Atmos, 106, 28629-28641, Doi 10.1029/2001jd900017, 2001.

de Reus, M., Borrmann, S., Bansemer, A., Heymsfield, A. J., Weigel, R., Schiller, C., Mitev, V., Frey, W., Kunkel, D., Kurten, A., Curtius, J., Sitnikov, N. M., Ulanovsky, A., and Ravegnani, F.: Evidence for ice particles in the tropical stratosphere from in-situ measurements, Atmos Chem Phys, 9, 6775-6792, DOI 10.5194/acp-9-6775-2009, 2009.

Dunne, E. M., Gordon, H., Kürten, A., Almeida, J., Duplissy, J., Williamson, C., Ortega, I. K., Pringle, K. J., Adamov, A., Baltensperger, U., Barmet, P., Benduhn, F., Bianchi, F., Breitenlechner, M., Clarke, A., Curtius, J., Dommen, J., Donahue, N. M., Ehrhart, S., Flagan, R. C., Franchin, A., Guida, R., Hakala, J., Hansel, A., Heinritzi, M., Jokinen, T., Kangasluoma, J., Kirkby, J., Kulmala, M., Kupc, A., Lawler, M. J., Lehtipalo, K., Makhmutov, V., Mann, G., Mathot, S., Merikanto, J., Miettinen, P., Nenes, A., Onnela, A., Rap, A., Reddington, C. L. S., Riccobono, F., Richards, N. A. D., Rissanen, M. P., Rondo, L., Sarnela, N., Schobesberger, S., Sengupta, K., Simon, M., Sipilä, M., Smith, J. N., Stozkhov, Y., Tomé, A., Tröstl, J., Wagner, P. E., Wimmer, D., Winkler, P. M., Worsnop, D. R., and Carslaw, K. S.: Global atmospheric particle formation from CERN CLOUD measurements, Science, 354, 1119-1124, 10.1126/science.aaf2649, 2016.

Duplissy, J., Merikanto, J., Franchin, A., Tsagkogeorgas, G., Kangasluoma, J., Wimmer, D., Vuollekoski, H., Schobesberger, S., Lehtipalo, K., Flagan, R. C., Brus, D., Donahue, N. M., Vehkamaki, H., Almeida, J., Amorim, A., Barmet, P., Bianchi, F., Breitenlechner, M., Dunne, E. M., Guida, R., Henschel, H., Junninen, H., Kirkby, J., Kurten, A., Kupc, A., Maattanen, A., Makhmutov, V., Mathot, S., Nieminen, T., Onnela, A., Praplan, A. P., Riccobono, F., Rondo, L., Steiner, G., Tome, A., Walther, H., Baltensperger, U., Carslaw, K. S., Dommen, J., Hansel, A., Petaja, T., Sipila, M., Stratmann, F., Vrtala, A., Wagner, P. E., Worsnop, D. R., Curtius, J., and Kulmala, M.: Effect of ions on sulfuric acid-water binary particle formation: 2. Experimental data and comparison with QC-normalized classical nucleation theory, J Geophys Res-Atmos, 121, 1752-1775, 10.1002/2015jd023539, 2016.

Frey, W., Borrmann, S., Kunkel, D., Weigel, R., de Reus, M., Schlager, H., Roiger, A., Voigt, C., Hoor, P., Curtius, J., Kramer, M., Schiller, C., Volk, C. M., Homan, C. D., Fierli, F., Di Donfrancesco, G., Ulanovsky, A., Ravegnani, F., Sitnikov, N. M., Viciani, S., D'Amato, F., Shur, G. N., Belyaev, G. V., Law, K. S., and Cairo, F.: In situ measurements of tropical cloud properties in the West African Monsoon: upper tropospheric ice clouds, Mesoscale Convective System outflow, and subvisual cirrus, Atmos Chem Phys, 11, 5569-5590, DOI 10.5194/acp-11-5569-2011, 2011.

Gordon, H., Kirkby, J., Baltensperger, U., Bianchi, F., Breitenlechner, M., Curtius, J., Dias, A., Dommen, J., Donahue, N. M., Dunne, E. M., Duplissy, J., Ehrhart, S., Flagan, R. C., Frege, C., Fuchs, C., Hansel, A., Hoyle, C. R., Kulmala, M., Kürten, A., Lehtipalo, K., Makhmutov, V., Molteni, U., Rissanen, M. P., Stozkhov, Y., Tröstl, J., Tsagkogeorgas, G., Wagner, R., Williamson, C., Wimmer, D., Winkler, P. M., Yan, C., and Carslaw, K. S.: Causes and importance of new particle formation in the present-day and preindustrial atmospheres, Journal of Geophysical Research: Atmospheres, 122, 8739-8760, 10.1002/2017jd026844, 2017.

He, Q., Ma, J., Zheng, X., Yan, X., Vömel, H., Wienhold, F. G., Gao, W., Liu, D., Shi, G., and Cheng, T.: Observational evidence of particle hygroscopic growth in the upper troposphere–lower stratosphere (UTLS) over the Tibetan Plateau, Atmos. Chem. Phys., 19, 8399-8406, 10.5194/acp-19-8399-2019, 2019.

Höpfner, M., Ungermann, J., Borrmann, S., Wagner, R., Spang, R., Riese, M., Stiller, G., Appel, O., Batenburg, A. M., Bucci, S., Cairo, F., Dragoneas, A., Friedl-Vallon, F., Hünig, A., Johansson, S., Krasauskas, L., Legras, B., Leisner, T., Mahnke, C., Möhler, O., Molleker, S., Müller, R., Neubert, T., Orphal, J., Preusse, P., Rex, M., Saathoff, H., Stroh, F., Weigel, R., and Wohltmann, I.: Ammonium nitrate particles formed in upper troposphere from ground ammonia sources during Asian monsoons, Nat Geosci, 12, 608-612, 10.1038/s41561-019-0385-8, 2019.

Kärcher, B., and Lohmann, U.: A parameterization of cirrus cloud formation: Homogeneous freezing of supercooled aerosols, J Geophys Res-Atmos, 107, 4010, 10.1029/2001jd000470, 2002.

Kazil, J., Lovejoy, E. R., Jensen, E. J., and Hanson, D. R.: Is aerosol formation in cirrus clouds possible?, Atmos Chem Phys, 7, 1407-1413, DOI 10.5194/acp-7-1407-2007, 2007.

Kazil, J., Harrison, R. G., and Lovejoy, E. R.: Tropospheric new particle formation and the role of ions, Space Sci Rev, 137, 241-255, 10.1007/s11214-008-9388-2, 2008.

Kerminen, V. M., Petaja, T., Manninen, H. E., Paasonen, P., Nieminen, T., Sipila, M., Junninen, H., Ehn, M., Gagne, S., Laakso, L., Riipinen, I., Vehkamaki, H., Kurten, T., Ortega, I. K., Dal Maso, M., Brus, D., Hyvarinen, A., Lihavainen, H., Leppa, J., Lehtinen, K. E. J., Mirme, A., Mirme, S., Horrak, U., Berndt, T., Stratmann, F., Birmili, W., Wiedensohler, A., Metzger, A., Dommen, J., Baltensperger, U., Kiendler-Scharr, A., Mentel, T. F., Wildt, J., Winkler, P. M., Wagner, P. E., Petzold, A., Minikin, A., Plass-Dulmer, C., Poschl, U., Laaksonen, A., and Kulmala, M.: Atmospheric nucleation: highlights of the EUCAARI project and future directions, Atmos Chem Phys, 10, 10829-10848, 10.5194/acp-10-10829-2010, 2010.

Kerminen, V. M., Chen, X. M., Vakkari, V., Petäjä, T., Kulmala, M., and Bianchi, F.: Atmospheric new particle formation and growth: review of field observations, Environ Res Lett, 13, Artn 103003

10.1088/1748-9326/Aadf3c, 2018.

Kirkby, J., Curtius, J., Almeida, J., Dunne, E., Duplissy, J., Ehrhart, S., Franchin, A., Gagne, S., Ickes, L., Kurten, A., Kupc, A., Metzger, A., Riccobono, F., Rondo, L., Schobesberger, S., Tsagkogeorgas, G., Wimmer, D., Amorim, A., Bianchi, F., Breitenlechner, M., David, A., Dommen, J., Downard, A., Ehn, M., Flagan, R. C., Haider, S., Hansel, A., Hauser, D., Jud, W., Junninen, H., Kreissl, F., Kvashin, A., Laaksonen, A., Lehtipalo, K., Lima, J., Lovejoy, E. R., Makhmutov, V., Mathot, S., Mikkila, J., Minginette, P., Mogo, S., Nieminen, T., Onnela, A., Pereira, P., Petaja, T., Schnitzhofer, R., Seinfeld, J. H., Sipila, M., Stozhkov, Y., Stratmann, F., Tome, A., Vanhanen, J., Viisanen, Y., Vrtala, A., Wagner, P. E., Walther, H., Weingartner, E., Wex, H., Winkler, P. M., Carslaw, K. S., Worsnop, D. R., Baltensperger, U., and Kulmala, M.: Role of sulphuric acid, ammonia and galactic cosmic rays in atmospheric aerosol nucleation, Nature, 476, 429-U477, 10.1038/nature10343, 2011.

Formatiert: Abstand Nach: 10 Pt.

1484 Koop, T., Luo, B. P., Tsias, A., and Peter, T.: Water activity as the determinant for homogeneous
1485 ice nucleation in aqueous solutions, Nature, 406, 611-614, Doi 10.1038/35020537, 2000.

1486 Korolev, A., Emery, E., and Creelman, K.: Modification and tests of particle probe tips to mitigate
1487 effects of ice shattering, Journal of Atmospheric and Oceanic Technology, 30, 690-708,
1488 10.1175/JTECH-D-12-00142.1, 2013.

1489 Korolev, A. V., and Mazin, I. P.: Supersaturation of Water Vapor in Clouds, Journal of the
1490 Atmospheric Sciences, 60, 2957-2974, 10.1175/1520-0469(2003)060<2957:sowvic>2.0.co;2,
1491 2003.

1492 Krämer, M., Schiller, C., Afchine, A., Bauer, R., Gensch, I., Mangold, A., Schlicht, S., Spelten, N.,
1493 Sitnikov, N., Borrmann, S., de Reus, M., and Spichtinger, P.: Ice supersaturations and cirrus cloud
1494 crystal numbers, Atmos Chem Phys, 9, 3505-3522, 2009.

1495 Krämer, M., Rolf, C., Luebke, A., Afchine, A., Spelten, N., Costa, A., Meyer, J., Zöger, M., Smith, J.,
1496 Herman, R. L., Buchholz, B., Ebert, V., Baumgardner, D., Borrmann, S., Klingebiel, M., and
1497 Avallone, L.: A microphysics guide to cirrus clouds - Part 1: Cirrus types, Atmospheric Chemistry
1498 and Physics, 16, 3463-3483, 10.5194/acp-16-3463-2016, 2016.

1499 Krämer, M., Rolf, C., Spelten, N., Afchine, A., Fahey, D., Jensen, E., Khaykin, S., Kuhn, T., Lawson, P.,
1500 Lykov, A., Pan, L. L., Riese, M., Rollins, A., Stroh, F., Thornberry, T., Wolf, V., Woods, S., Spichtinger,
1501 P., Quaas, J., and Sourdeval, O.: A microphysics guide to cirrus – Part 2: Climatologies of clouds
1502 and humidity from observations, Atmos. Chem. Phys., 20, 12569-12608, 10.5194/acp-20-12569-
1503 2020, 2020.

1504 Kübbeler, M., Hildebrandt, M., Meyer, J., Schiller, C., Hamburger, T., Jurkat, T., Minikin, A., Petzold,
1505 A., Rautenhaus, M., Schlager, H., Schumann, U., Voigt, C., Spichtinger, P., Gayet, J. F., Gourbeyre, C.,
1506 and Krämer, M.: Thin and subvisible cirrus and contrails in a subsaturated environment, Atmos
1507 Chem Phys, 11, 5853-5865, 10.5194/acp-11-5853-2011, 2011.

1508 Kulkarni, P., Baron, P. A., and Willeke, K.: Aerosol measurement: principles, techniques, and
1509 applications, John Wiley & Sons, 2011.

1510 Kürten, A., Williamson, C., Almeida, J., Kirkby, J., and Curtius, J.: On the derivation of particle
1511 nucleation rates from experimental formation rates, Atmos Chem Phys, 15, 4063-4075,
1512 10.5194/acp-15-4063-2015, 2015.

1513 Kürten, A., Bianchi, F., Almeida, J., Kupiainen-Maatta, O., Dunne, E. M., Duplissy, J., Williamson, C.,
1514 Barmet, P., Breitenlechner, M., Dommen, J., Donahue, N. M., Flagan, R. C., Franchin, A., Gordon, H.,
1515 Hakala, J., Hansel, A., Heinritzi, M., Ickes, L., Jokinen, T., Kangasluoma, J., Kim, J., Kirkby, J., Kupc,
1516 A., Lehtipalo, K., Leiminger, M., Makhmutov, V., Onnela, A., Ortega, I. K., Petaja, T., Praplan, A. P.,
1517 Riccobono, F., Rissanen, M. P., Rondo, L., Schnitzhofer, R., Schobesberger, S., Smith, J. N., Steiner,
1518 G., Stozhkov, Y., Tome, A., Trostl, J., Tsagkogeorgas, G., Wagner, P. E., Wimmer, D., Ye, P. L.,
1519 Baltensperger, U., Carslaw, K., Kulmala, M., and Curtius, J.: Experimental particle formation rates
1520 spanning tropospheric sulfuric acid and ammonia abundances, ion production rates, and
1521 temperatures, J Geophys Res-Atmos, 121, 12377-12400, 10.1002/2015jd023908, 2016.

1522 Kürten, A., Li, C., Bianchi, F., Curtius, J., Dias, A., Donahue, N. M., Duplissy, J., Flagan, R. C., Hakala,
1523 J., Jokinen, T., Kirkby, J., Kulmala, M., Laaksonen, A., Lehtipalo, K., Makhmutov, V., Onnela, A.,
1524 Rissanen, M. P., Simon, M., Sipilä, M., Stozhkov, Y., Tröstl, J., Ye, P., and McMurry, P. H.: New
1525 particle formation in the sulfuric acid–dimethylamine–water system: reevaluation of CLOUD
1526 chamber measurements and comparison to an aerosol nucleation and growth model, Atmos.
1527 Chem. Phys., 18, 845-863, 10.5194/acp-18-845-2018, 2018.

1528 Kürten, A.: New particle formation from sulfuric acid and ammonia: nucleation and growth
1529 model based on thermodynamics derived from CLOUD measurements for a wide range of
1530 conditions, Atmos. Chem. Phys., 19, 5033-5050, 10.5194/acp-19-5033-2019, 2019.

1531 Lee, S. H., Reeves, J. M., Wilson, J. C., Hunton, D. E., Viggiano, A. A., Miller, T. M., Ballenthin, J. O.,
1532 and Lait, L. R.: Particle formation by ion nucleation in the upper troposphere and lower
1533 stratosphere, Science, 301, 1886-1889, DOI 10.1126/science.1087236, 2003.

1534 Lee, S. H., Wilson, J. C., Baumgardner, D., Herman, R. L., Weinstock, E. M., LaFleur, B. G., Kok, G.,
1535 Anderson, B., Lawson, P., Baker, B., Strawa, A., Pittman, J. V., Reeves, J. M., and Bui, T. P.: New
1536 particle formation observed in the tropical/subtropical cirrus clouds, J Geophys Res-Atmos, 109,
1537 Artn D20209

1538 10.1029/2004jd005033, 2004.

1539 Lovejoy, E. R., Curtius, J., and Froyd, K. D.: Atmospheric ion-induced nucleation of sulfuric acid
1540 and water, J Geophys Res-Atmos, 109, Artn D08204

1541 10.1029/2003jd004460, 2004.

1542 Luebke, A. E., Afchine, A., Costa, A., Grooss, J. U., Meyer, J., Rolf, C., Spelten, N., Avallone, L. M.,
1543 Baumgardner, D., and Krämer, M.: The origin of midlatitude ice clouds and the resulting
1544 influence on their microphysical properties, Atmospheric Chemistry and Physics, 16, 5793-5809,
1545 10.5194/acp-16-5793-2016, 2016.

1546 Mahnke, C., Weigel, R., Cairo, F., Vernier, J.-P., Afchine, A., Krämer, M., Mitev, V., Matthey, R.,
1547 Viciani, S., D'Amato, F., Ploeger, F., Deshler, T., and Borrmann, S.: The ATAL within the 2017
1548 Asian Monsoon Anticyclone: Microphysical aerosol properties derived from aircraft-borne in
1549 situ measurements, Atmos. Chem. Phys. Discuss., acp-2020-1241 2021.

1550 Manton, M. J.: On the broadening of a droplet distribution by turbulence near cloud base, Q J Roy
1551 Meteor Soc, 105, 899-914, 10.1002/qj.49710544613, 1979.

1552 Merikanto, J., Spracklen, D. V., Mann, G. W., Pickering, S. J., and Carslaw, K. S.: Impact of nucleation
1553 on global CCN, Atmos Chem Phys, 9, 8601-8616, 10.5194/acp-9-8601-2009, 2009.

1554 Metzger, A., Verheggen, B., Dommen, J., Duplissy, J., Prevot, A. S. H., Weingartner, E., Riipinen, I.,
1555 Kulmala, M., Spracklen, D. V., Carslaw, K. S., and Baltensperger, U.: Evidence for the role of
1556 organics in aerosol particle formation under atmospheric conditions, P Natl Acad Sci USA, 107,
1557 6646-6651, 10.1073/pnas.0911330107, 2010.

1558 Meyer, J., Rolf, C., Schiller, C., Rohs, S., Spelten, N., Afchine, A., Zöger, M., Sitnikov, N., Thornberry,
1559 T. D., Rollins, A. W., Bozoki, Z., Tatrai, D., Ebert, V., Kuhnreich, B., Mackrodt, P., Möhler, O.,
1560 Saathoff, H., Rosenlof, K. H., and Krämer, M.: Two decades of water vapor measurements with the
1561 FISH fluorescence hygrometer: a review, Atmos Chem Phys, 15, 8521-8538, 10.5194/acp-15-
1562 8521-2015, 2015.

1563 Murphy, D. M., Cziczo, D. J., Froyd, K. D., Hudson, P. K., Matthew, B. M., Middlebrook, A. M., Peltier,
1564 R. E., Sullivan, A., Thomson, D. S., and Weber, R. J.: Single-particle mass spectrometry of
1565 tropospheric aerosol particles, J Geophys Res-Atmos, 111, Artn D23s32

1566 Doi 10.1029/2006jd007340, 2006.

1567 Pan, L. L., Honomichl, S. B., Kinnison, D. E., Abalos, M., Randel, W. J., Bergman, J. W., and Bian, J.:
1568 Transport of chemical tracers from the boundary layer to stratosphere associated with the

Formatiert: Abstand Nach: 10 Pt.

Formatiert: Abstand Nach: 10 Pt.

Formatiert: Abstand Nach: 10 Pt.

dynamics of the Asian summer monsoon, Journal of Geophysical Research: Atmospheres, 121, 14.159-114.174, 10.1002/2016jd025616, 2016.

Park, M., Randel, W. J., Gettelman, A., Massie, S. T., and Jiang, J. H.: Transport above the Asian summer monsoon anticyclone inferred from Aura Microwave Limb Sounder tracers, J Geophys Res-Atmos, 112, Artn D16309

10.1029/2006jd008294, 2007.

Park, M., Randel, W. J., Emmons, L. K., and Livesey, N. J.: Transport pathways of carbon monoxide in the Asian summer monsoon diagnosed from Model of Ozone and Related Tracers (MOZART), J Geophys Res-Atmos, 114, Artn D08303

10.1029/2008jd010621, 2009.

Peter, T., Luo, B. P., Wirth, M., Kiemle, C., Flentje, H., Yushkov, V. A., Khattatov, V., Rudakov, V., Thomas, A., Borrmann, S., Toci, G., Mazzinghi, P., Beuermann, J., Schiller, C., Cairo, F., Di Donfrancesco, G., Adriani, A., Volk, C. M., Strom, J., Noone, K., Mitev, V., MacKenzie, R. A., Carslaw, K. S., Trautmann, T., Santacesaria, V., and Stefanutti, L.: Ultrathin Tropical Tropopause Clouds (UTTCs): I. Cloud morphology and occurrence, Atmos. Chem. Phys., 3, 1083-1091, 10.5194/acp-3-1083-2003, 2003.

Ploeger, F., Günther, G., Konopka, P., Fueglistaler, S., Müller, R., Hoppe, C., Kunz, A., Spang, R., Grooss, J. U., and Riese, M.: Horizontal water vapor transport in the lower stratosphere from subtropics to high latitudes during boreal summer, J Geophys Res-Atmos, 118, 8111-8127, 10.1002/jgrd.50636, 2013.

Politovich, M. K., and Cooper, W. A.: Variability of the Supersaturation in Cumulus Clouds, Journal of the Atmospheric Sciences, 45, 1651-1664, 10.1175/1520-0469(1988)045<1651:votsic>2.0.co;2, 1988.

Pöschl, U., Canagaratna, M., Jayne, J. T., Molina, L. T., Worsnop, D. R., Kolb, C. E., and Molina, M. J.: Mass Accommodation Coefficient of H_2SO_4 Vapor on Aqueous Sulfuric Acid Surfaces and Gaseous Diffusion Coefficient of H_2SO_4 in N_2/H_2O, The Journal of Physical Chemistry A, 102, 10082-10089, 10.1021/jp982809s, 1998.

Pruppacher, H. R., and Klett, J. D.: Microphysics of Clouds and Precipitation: Reprinted 1980, Springer Science & Business Media, 2012.

Radke, L. F., and Hobbs, P. V.: Humidity and Particle Fields around Some Small Cumulus Clouds, Journal of the Atmospheric Sciences, 48, 1190-1193, Doi 10.1175/1520-0469(1991)048<1190:Hapfas>2.0.Co;2, 1991.

Randel, W. J., and Park, M.: Deep convective influence on the Asian summer monsoon anticyclone and associated tracer variability observed with Atmospheric Infrared Sounder (AIRS), J Geophys Res-Atmos, 111, Artn D12314

10.1029/2005jd006490, 2006.

Ranjithkumar, A., Gordon, H., Williamson, C., Rollins, A., Pringle, K., Kupc, A., Abraham, N. L., Brock, C., and Carslaw, K.: Constraints on global aerosol number concentration, SO2 and condensation sink in UKESM1 using ATom measurements, Atmos. Chem. Phys., 21, 4979-5014, 10.5194/acp-21-4979-2021, 2021.

Riccobono, F., Schobesberger, S., Scott, C. E., Dommen, J., Ortega, I. K., Rondo, L., Almeida, J., Amorim, A., Bianchi, F., Breitenlechner, M., David, A., Downard, A., Dunne, E. M., Duplissy, J.,

Formatiert: Abstand Nach: 10 Pt.

Formatiert: Abstand Nach: 10 Pt.

Formatiert: Abstand Nach: 10 Pt.

1611 Ehrhart, S., Flagan, R. C., Franchin, A., Hansel, A., Junninen, H., Kajos, M., Keskinen, H., Kupc, A.,
1612 Kürten, A., Kvashin, A. N., Laaksonen, A., Lehtipalo, K., Makhmutov, V., Mathot, S., Nieminen, T.,
1613 Onnela, A., Petaja, T., Praplan, A. P., Santos, F. D., Schallhart, S., Seinfeld, J. H., Sipila, M., Spracklen,
1614 D. V., Stozhkov, Y., Stratmann, F., Tome, A., Tsagkogeorgas, G., Vaattovaara, P., Viisanen, Y., Vrtala,
1615 A., Wagner, P. E., Weingartner, E., Wex, H., Wimmer, D., Carslaw, K. S., Curtius, J., Donahue, N. M.,
1616 Kirkby, J., Kulmala, M., Worsnop, D. R., and Baltensperger, U.: Oxidation Products of Biogenic
1617 Emissions Contribute to Nucleation of Atmospheric Particles, Science, 344, 717-721,
1618 10.1126/science.1243527, 2014.

1619 Schulz, C., Schneider, J., Holanda, B. A., Appel, O., Costa, A., de Sa, S. S., Dreiling, V., Fütterer, D.,
1620 Jurkat-Witschas, T., Klimach, T., Knote, C., Krämer, M., Martin, S. T., Mertes, S., Pöhlker, M. L.,
1621 Sauer, D., Voigt, C., Walser, A., Weinzierl, B., Ziereis, H., Zöger, M., Andreae, M. O., Artaxo, P.,
1622 Machado, L. A. T., Pöschl, U., Wendisch, M., and Borrmann, S.: Aircraft-based observations of
1623 isoprene-epoxydiol-derived secondary organic aerosol (IEPOX-SOA) in the tropical upper
1624 troposphere over the Amazon region, Atmos Chem Phys, 18, 14979-15001, 10.5194/acp-18-
1625 14979-2018, 2018.

1626 Schumann, U., Kiemle, C., Schlager, H., Weigel, R., Borrmann, S., D'Amato, F., Krämer, M., Matthey,
1627 R., Protat, A., Voigt, C., and Volk, C. M.: Long-lived contrails and convective cirrus above the
1628 tropical tropopause, Atmos. Chem. Phys., 17, 2311-2346, 10.5194/acp-17-2311-2017, 2017.

1629 Sokolov, L., and Lepuchov, B.: Protocol of interaction between Unit for Connection with Scientific
1630 Equipment (UCSE) and on-board scientific equipment of Geophysica aircraft (Second edition),
1631 Myasishchev Design Bureau (MDB), 1998.

1632 Speidel, M., Nau, R., Arnold, F., Schlager, H., and Stohl, A.: Sulfur dioxide measurements in the
1633 lower, middle and upper troposphere: Deployment of an aircraft-based chemical ionization mass
1634 spectrometer with permanent in-flight calibration, Atmos Environ, 41, 2427-2437,
1635 10.1016/j.atmosenv.2006.07.047, 2007.

1636 Spracklen, D. V., Carslaw, K. S., Kulmala, M., Kerminen, V. M., Mann, G. W., and Sihto, S. L.: The
1637 contribution of boundary layer nucleation events to total particle concentrations on regional and
1638 global scales, Atmos Chem Phys, 6, 5631-5648, DOI 10.5194/acp-6-5631-2006, 2006.

1639 Spreitzer, E. J., Marschalik, M. P., and Spichtinger, P.: Subvisible cirrus clouds - a dynamical
1640 system approach, Nonlinear Proc Geoph, 24, 307-328, 10.5194/npg-24-307-2017, 2017.

1641 Tang, M. J., Cox, R. A., and Kalberer, M.: Compilation and evaluation of gas phase diffusion
1642 coefficients of reactive trace gases in the atmosphere: volume 1. Inorganic compounds, Atmos.
1643 Chem. Phys., 14, 9233-9247, 10.5194/acp-14-9233-2014, 2014.

1644 Thomas, A., Borrmann, S., Kiemle, C., Cairo, F., Volk, M., Beuermann, J., Lepuchov, B., Santacesaria,
1645 V., Matthey, R., Rudakov, V., Yushkov, V., MacKenzie, A. R., and Stefanutti, L.: In situ
1646 measurements of background aerosol and subvisible cirrus in the tropical tropopause region,
1647 Journal of Geophysical Research: Atmospheres, 107, AAC 8-1-AAC 8-14, 10.1029/2001jd001385,
1648 2002.

1649 Tsagkogeorgas, G., Roldin, P., Duplissy, J., Rondo, L., Tröstl, J., Slowik, J. G., Ehrhart, S., Franchin,
1650 A., Kürten, A., Amorim, A., Bianchi, F., Kirkby, J., Petäjä, T., Baltensperger, U., Boy, M., Curtius, J.,
1651 Flagan, R. C., Kulmala, M., Donahue, N. M., and Stratmann, F.: Evaporation of sulfate aerosols at
1652 low relative humidity, Atmos. Chem. Phys., 17, 8923-8938, 10.5194/acp-17-8923-2017, 2017.

1653 Twohy, C. H., Clement, C. F., Gandrud, B. W., Weinheimer, A. J., Campos, T. L., Baumgardner, D.,
1654 Brune, W. H., Faloona, I., Sachse, G. W., Vay, S. A., and Tan, D.: Deep convection as a source of new
1655 particles in the midlatitude upper troposphere, J Geophys Res-Atmos, 107, Artn 4560

10.1029/2001jd000323, 2002.

Ueyama, R., Jensen, E. J., Pfister, L., Krämer, M., Afchine, A., and Schoeberl, M.: Impact of Convectively Detrained Ice Crystals on the Humidity of the Tropical Tropopause Layer in Boreal Winter, Journal of Geophysical Research: Atmospheres, 125, e2020JD032894, 10.1029/2020JD032894, 2020.

Vehkamäki, H., Kulmala, M., Napari, I., Lehtinen, K. E. J., Timmreck, C., Noppel, M., and Laaksonen, A.: An improved parameterization for sulfuric acid–water nucleation rates for tropospheric and stratospheric conditions, Journal of Geophysical Research: Atmospheres, 107, AAC 3-1-AAC 3-10, 10.1029/2002jd002184, 2002.

Venzac, H., Sellegri, K., Laj, P., Villani, P., Bonasoni, P., Marinoni, A., Cristofanelli, P., Calzolari, F., Fuzzi, S., Decesari, S., Facchini, M. C., Vuillermoz, E., and Verza, G. P.: High frequency new particle formation in the Himalayas, P Natl Acad Sci USA, 105, 15666-15671, 10.1073/pnas.0801355105, 2008.

Vernier, J.-P., Fairlie, T. D., Deshler, T., Ratnam, M. V., Gadhavi, H., Kumar, B. S., Natarajan, M., Pandit, A. K., Raj, S. T. A., Kumar, A. H., Jayaraman, A., Singh, A. K., Rastogi, N., Sinha, P. R., Kumar, S., Tiwari, S., Wegner, T., Baker, N., Vignelles, D., Stenchikov, G., Shevchenko, I., Smith, J., Bedka, K., Kesarkar, A., Singh, V., Bhate, J., Ravikiran, V., Rao, M. D., Ravindrababu, S., Patel, A., Vernier, H., Wienhold, F. G., Liu, H., Knepp, T. N., Thomason, L., Crawford, J., Ziemba, L., Moore, J., Crumeyrolle, S., Williamson, M., Berthet, G., Jégou, F., and Renard, J.-B.: BATAL: The Balloon Measurement Campaigns of the Asian Tropopause Aerosol Layer, B Am Meteorol Soc, 99, 955-973, 10.1175/bams-d-17-0014.1, 2018.

Vernier, J. P., Thomason, L. W., and Kar, J.: CALIPSO detection of an Asian tropopause aerosol layer, Geophys Res Lett, 38, Artn L07804

10.1029/2010gl046614, 2011.

Vernier, J. P., Fairlie, T. D., Natarajan, M., Wienhold, F. G., Bian, J., Martinsson, B. G., Crumeyrolle, S., Thomason, L. W., and Bedka, K. M.: Increase in upper tropospheric and lower stratospheric aerosol levels and its potential connection with Asian pollution, J Geophys Res-Atmos, 120, 1608-1619, 10.1002/2014jd022372, 2015.

Viciani, S., D'Amato, F., Mazzinghi, P., Castagnoli, F., Toci, G., and Werle, P.: A cryogenically operated laser diode spectrometer for airborne measurement of stratospheric trace gases, Applied Physics B, 90, 581-592, 10.1007/s00340-007-2885-2, 2008.

Viciani, S., Montori, A., Chiarugi, A., and D'Amato, F.: A Portable Quantum Cascade Laser Spectrometer for Atmospheric Measurements of Carbon Monoxide, Sensors, 18, 2380, doi:10.3390/s18072380, 2018.

Vogel, B., Günther, G., Müller, R., Grooss, J. U., Hoor, P., Krämer, M., Müller, S., Zahn, A., and Riese, M.: Fast transport from Southeast Asia boundary layer sources to northern Europe: rapid uplift in typhoons and eastward eddy shedding of the Asian monsoon anticyclone, Atmos Chem Phys, 14, 12745-12762, 10.5194/acp-14-12745-2014, 2014.

Vogel, B., Müller, R., Günther, G., Spang, R., Hanumanthu, S., Li, D., Riese, M., and Stiller, G. P.: Lagrangian simulations of the transport of young air masses to the top of the Asian monsoon anticyclone and into the tropical pipe, Atmos Chem Phys, 19, 6007-6034, 10.5194/acp-19-6007-2019, 2019.

Waddicor, D. A., Vaughan, G., Choularton, T. W., Bower, K. N., Coe, H., Gallagher, M., Williams, P. I., Flynn, M., Volz-Thomas, A., Patz, H. W., Isaac, P., Hacker, J., Arnold, F., Schlager, H., and Whiteway,

Formatiert: Abstand Nach: 10 Pt.

Formatiert: Abstand Nach: 10 Pt.

J. A.: Aerosol observations and growth rates downwind of the anvil of a deep tropical thunderstorm, Atmos Chem Phys, 12, 6157-6172, 10.5194/acp-12-6157-2012, 2012.

Wang, M., Kong, W., Marten, R., He, X.-C., Chen, D., Pfeifer, J., Heitto, A., Kontkanen, J., Dada, L., Kürten, A., Yli-Juuti, T., Manninen, H. E., Amanatidis, S., Amorim, A., Baalbaki, R., Baccarini, A., Bell, D. M., Bertozzi, B., Bräkling, S., Brilke, S., Murillo, L. C., Chiu, R., Chu, B., De Menezes, L.-P., Duplissy, J., Finkenzeller, H., Carracedo, L. G., Granzin, M., Guida, R., Hansel, A., Hofbauer, V., Krechmer, J., Lehtipalo, K., Lamkaddam, H., Lampimäki, M., Lee, C. P., Makhmutov, V., Marie, G., Mathot, S., Mauldin, R. L., Mentler, B., Müller, T., Onnela, A., Partoll, E., Petäjä, T., Philippov, M., Pospisilova, V., Ranjithkumar, A., Rissanen, M., Rörup, B., Scholz, W., Shen, J., Simon, M., Sipilä, M., Steiner, G., Stolzenburg, D., Tham, Y. J., Tomé, A., Wagner, A. C., Wang, D. S., Wang, Y., Weber, S. K., Winkler, P. M., Wlasits, P. J., Wu, Y., Xiao, M., Ye, Q., Zauner-Wieczorek, M., Zhou, X., Volkamer, R., Riipinen, I., Dommen, J., Curtius, J., Baltensperger, U., Kulmala, M., Worsnop, D. R., Kirkby, J., Seinfeld, J. H., El-Haddad, I., Flagan, R. C., and Donahue, N. M.: Rapid growth of new atmospheric particles by nitric acid and ammonia condensation, Nature, 581, 184-189, 10.1038/s41586-020-2270-4, 2020.

Weber, R. J., Clarke, A. D., Litchy, M., Li, J., Kok, G., Schillawski, R. D., and McMurry, P. H.: Spurious aerosol measurements when sampling from aircraft in the vicinity of clouds, Journal of Geophysical Research: Atmospheres, 103, 28337-28346, 10.1029/98jd02086, 1998.

Wehner, B., Werner, F., Ditas, F., Shaw, R. A., Kulmala, M., and Siebert, H.: Observations of new particle formation in enhanced UV irradiance zones near cumulus clouds, Atmos Chem Phys, 15, 11701-11711, 10.5194/acp-15-11701-2015, 2015.

Weigel, R., Hermann, M., Curtius, J., Voigt, C., Walter, S., Bottger, T., Lepukhov, B., Belyaev, G., and Borrmann, S.: Experimental characterization of the COndensation PArticle counting System for high altitude aircraft-borne application, Atmos Meas Tech, 2, 243-258, 10.5194/amt-2-243-2009, 2009.

Weigel, R., Borrmann, S., Kazil, J., Minikin, A., Stohl, A., Wilson, J. C., Reeves, J. M., Kunkel, D., de Reus, M., Frey, W., Lovejoy, E. R., Volk, C. M., Viciani, S., D'Amato, F., Schiller, C., Peter, T., Schlager, H., Cairo, F., Law, K. S., Shur, G. N., Belyaev, G. V., and Curtius, J.: In situ observations of new particle formation in the tropical upper troposphere: the role of clouds and the nucleation mechanism, Atmos Chem Phys, 11, 9983-10010, 10.5194/acp-11-9983-2011, 2011.

Weigel, R., Volk, C. M., Kandler, K., Hosen, E., Gunther, G., Vogel, B., Grooss, J. U., Khaykin, S., Belyaev, G. V., and Borrmann, S.: Enhancements of the refractory submicron aerosol fraction in the Arctic polar vortex: feature or exception?, Atmos Chem Phys, 14, 12319-12342, DOI 10.5194/acp-14-12319-2014, 2014.

Weigel, R., Mahnke, C., Baumgartner, M., Dragoneas, A., Vogel, B., Ploeger, F., Viciani, S., D'Amato, F., Bucci, S., Legras, B., Luo, B., Belyaev, G. V., and Borrmann, S.: In-Situ observation of New Particle Formation (NPF) in the tropical tropopause layer of the 2017 Asian Monsoon Anticyclone: Part I - summary of StratoClim results Atmos. Chem. Phys. Discuss., acp-2020-1158, 2021a.

Weigelt, A., Hermann, M., van Velthoven, P. F. J., Brenninkmeijer, C. A. M., Schlaf, G., Zahn, A., and Wiedensohler, A.: Influence of clouds on aerosol particle number concentrations in the upper troposphere, J Geophys Res-Atmos, 114, Artn D01204

10.1029/2008jd009805, 2009.

Wernli, H., Boettcher, M., Joos, H., Miltenberger, A. K., and Spichtinger, P.: A trajectory-based classification of ERA-Interim ice clouds in the region of the North Atlantic storm track, Geophys Res Lett, 43, 6657-6664, 10.1002/2016gl068922, 2016.

Formatiert: Abstand Nach: 10 Pt.

Williamson, C. J., Kupc, A., Axisa, D., Bilsback, K. R., Bui, T., Campuzano-Jost, P., Dollner, M., Froyd, K. D., Hodshire, A. L., Jimenez, J. L., Kodros, J. K., Luo, G., Murphy, D. M., Nault, B. A., Ray, E. A., Weinzierl, B., Wilson, J. C., Yu, F., Yu, P., Pierce, J. R., and Brock, C. A.: A large source of cloud condensation nuclei from new particle formation in the tropics, Nature, 574, 399-403, 10.1038/s41586-019-1638-9, 2019.

WMO: International Meteorological Tables, WMO-No.188.TP97, edited by: Letestu, S., Secretariat of the World Meteorological Organization, Geneva, Switzerland, 1966.

Yu, P. F., Toon, O. B., Neely, R. R., Martinsson, B. G., and Brenninkmeijer, C. A. M.: Composition and physical properties of the Asian Tropopause Aerosol Layer and the North American Tropospheric Aerosol Layer, Geophys Res Lett, 42, 2540-2546, 10.1002/2015gl063181, 2015.

Zöger, M., Afchine, A., Eicke, N., Gerhards, M. T., Klein, E., McKenna, D. S., Morschel, U., Schmidt, U., Tan, V., Tuitjer, F., Woyke, T., and Schiller, C.: Fast in situ stratospheric hygrometers: A new family of balloon-borne and airborne Lyman alpha photofragment fluorescence hygrometers, J Geophys Res-Atmos, 104, 1807-1816, Doi 10.1029/1998jd100025, 1999.

Formatiert: EndNote Bibliography, Links, Abstand Vor: 0 Pt., Nach: 0 Pt.

Figure captions

Figure 1~~Figure 1~~: The flight patterns of the M-55 *Geophysica* during StratoClim 2017 over the Indian subcontinent. New particle formation (NPF) encountered in clear air along the flight tracks are indicated by orange colour in the main panel a). All NPF events coinciding with the detection of cloud (ice) particles are coloured in blue. The general perspective, b), exhibits the patterns of the eight StratoClim flights over Nepal, North - East India, Bangladesh, and the Bay of Bengal. For more details, see Table 1~~Table 1~~.

Figure 2~~Figure 2~~: ~~The 1-Hz – resolved n~~Number concentrations (1 Hz - resolved) of aerosol particles in the ~~ultrafine~~ nucleation-mode size range ($N_{\text{~~uf~~nm}}$) and of cloud (ice) particles (N_{ice}) of the eight StratoClim flights compiled in one time series ranging from 03:30 (UTC) to 12:30 (UTC). Kathmandu's (Nepal) local noontime is indicated by the vertical orange line (corresponding to 06:15 UTC, or 22500 seconds of day, UTC). Panel b): incidences of concentrations N_{nm} exceeding 500 cm^{-3}, 1000 cm^{-3}, and 5000 cm^{-3} within 15 minute time intervals. Data points of $N_{\text{~~uf~~nm}}$ in black whenever N_{ice} (cyan) equals zero, otherwise $N_{\text{~~uf~~nm}}$ is coloured in red. The blue dashed line (Panel c) indicates the median of N_{ice} (0.031 cm^{-3}) ~~for the entire dataset of~~over all cloud particle detections during StratoClim 2017 (Krämer et al., 2020).

Figure 3~~Figure 3~~: Vertical profiles of the mixing ratio (1 ~~-~~Hz – ~~-~~resolved) of aerosols in the ~~ultrafine~~ nucleation-mode size range ($n_{\text{~~uf~~nm}}$) versus the potential temperature (θ). a): all data separated concerning coincident detection of cloud (ice) particles (black: N_{ice} = 0 cm^{-3}, red: N_{ice} > 0 cm^{-3}) and b): all data coloured ~~correspondingly~~ in reference to the flight date, c): exclusively for N_{ice} > 0 cm^{-3}, and d): when N_{ice} = 0 cm^{-3}. In the panels at the bottom (e and f), in-cloud and clear-air measurements are distinguished ~~correspondingly to~~as in ~~the~~ intermediate panels (c and d) and coloured with reference to carbon monoxide (CO) mixing ratios.

Figure 4~~Figure 4~~: Histograms of the occurrence frequency of number concentrations $N_{\text{~~uf~~nm}}$ of all NPF detections (1 ~~-~~Hz ~~-~~ resolved) throughout StratoClim 2017. a): all data of $N_{\text{~~uf~~nm}}$ in general (black) and separated concerning coincident detection of cloud (ice) particles in the diameter size range 3 µm < d_{p} < 937 µm (green: N_{ice} = $N_{\text{3-937µm}}$ = 0 cm^{-3}, red: N_{ice} > 0 cm^{-3}). ~~Hence, t~~The sum of the green and red curve yield the black curve, the vertical bars of which represent the square ~~route~~ root of counts ~~values~~. b): relative occurrence frequency of $N_{\text{~~uf~~nm}}$ for in-cloud NPF (if detected coincidently with N_{ice} > 0 cm^{-3}) normalised with respect to all NPF detections, i.e. the ratio of the absolute occurrence frequencies (in red and black~~,~~ – in Panel a). c): relative occurrence frequency of $N_{\text{~~uf~~nm}}$ for in-cloud NPF, if detected coincidently with various N_{ice} levels, which were normalised with respect to those NPF detections with N_{ice} > 0 cm^{-3}, (in red, Panel b).

~~Figure 5Figure 5: The total aerosol number concentration versus cloud particle number concentration in accordance to de Reus et al. (2009).~~ StratoClim 2017 data of ~~T~~the total number concentration N_{10} ~~measured with one of four COPAS channels~~ together with coincident detections of N_{ice} (i.e. $N_{\text{3-937µm}}$) by the NIXE-CAPS. The vertical bars represent ~~. The data points are averaged over at least 10 s of flight time, and the bars exhibit~~ the standard deviation over the averaging periods. ~~The d~~Data points are colour-coded in a) with reference to *IWC*. b): NPF encounters (orange) throughout the averaging period (otherwise grey). ~~The b~~Blue-shaded areas in both panels indicate the range of most of the data points provided by de Reus et al. (2009). Reference lines for concentration ratios of 1 : 300 and 1 : 30 000 (as in de Reus et al. (2009)), and here additionally for 1 : 500 000 and 1 : 5 000 000 are provided.

Formatiert: Englisch (Vereinigtes Königreich)

Formatiert: Schriftart: +Überschriften (Cambria), Nicht Fett

Formatiert: Englisch (Vereinigtes Königreich)

Formatiert: Englisch (Vereinigtes Königreich)

Formatiert: Englisch (Vereinigtes Königreich)

Formatiert: Englisch (Vereinigtes Königreich)

Formatiert: Absatz-Standardschriftart, Schriftart: +Überschriften (Cambria)

Formatiert: Absatz-Standardschriftart, Schriftart: +Überschriften (Cambria)

Formatiert: Absatz-Standardschriftart, Schriftart: +Überschriften (Cambria)

Formatiert: Absatz-Standardschriftart, Schriftart: +Überschriften (Cambria)

Formatiert: Absatz-Standardschriftart, Schriftart: +Überschriften (Cambria)

Figure 6: NPF in the *IWC* - *T* parameter space (cf. Krämer et al. (2016)): measured ice water content (*IWC*) coincidently detected with COPAS data as a function of ambient air temperature throughout StratoClim 2017 (1 -Hz - resolved). - dData points are colour-coded referring to (a) the detected mixing ratios of ultrafine nucleation-mode particles, n_{ufnm}, (b) the total mixing ratio n_6 measured with one of four COPAS channels, -and (c) the carbon monoxide (CO) mixing ratio. Note: in (a), the data points are grey if data of $n_{6\text{-}15}$ are available, while colours are apportioned only to those n_{ufnm} (i.e. $n_{6\text{-}15}$) complying with the NPF criterion. Generally, the black lines represent the median (solid) and the upper-/lowermost bounds (dashed) of the core *IWC* band, respectively, as obtained from earlier measurements at other locations (Krämer et al. (2016)).

Figure 7Figure 7: The 1-Hz – resolved cConcentrations of in-cloud detected ultrafine nucleation-mode aerosols (N_{ufnm}) in 1 Hz – resolution as a function of the mean inter-crystal distance, *ICD*, between encountered cloud (ice) particles colour-coded with reference to (a) the number concentration of cloud ice particles, (b) to the *IWC*, and (c) to the mean ice particles' radius.

Formatiert: Englisch (Vereinigtes Königreich)

Figure 8Figure 8: The 1-Hz - resolved cConcentrations of nultrafine ucleation-mode aerosols (N_{ufnm}) in 1 Hz – resolution as a function of the cloud (ice) particles' integral radius, $IR = \overline{r_{ice}} \cdot N_{ice}$ (with $\overline{r_{ice}}$, ice particles' mean mass radius) colour-coded in correspondence to detected ice water content (*IWC*, panel a) and to measured CO mixing ratio (b); in the absence of CO values the data points are blackened. The diagonal, grey-coloured bars indicate a a break-off edgelimiting range, beyond -along which the probability of the NPF seems limited by the *IR* in generalobservations decreases, with two exceptional encounters of very recent or just proceeding NPF (see text for details).

Figure B- 1Figure B- 1: Simulated change of the H_2SO_4 vapour's saturation ratio as a function of time due to the presence of entirely H_2SO_4 - coated ice particle surfaces of various sizes and number concentrations. a): particles with radii r_p = 1 µm, b): r_p = 10 µm, c): r_p = 100 µm. Overall, this simulation covers a range of integral radii *IR* (= $\overline{\boldsymbol{r}_{ice}} \cdot \boldsymbol{N_{ice}}$) from 0.01 to 10 µm cm^{-3}. Note: a cloud (ice) particle is assumed as coated with H_2SO_4 (consistent with Bogdan et al. (2006); Bogdan et al. (2013)).

Formatiert: Schriftart: +Überschriften (Cambria), 11 Pt., Nicht Fett, Schriftfarbe: Automatisch, Englisch (Vereinigtes Königreich)

Figures

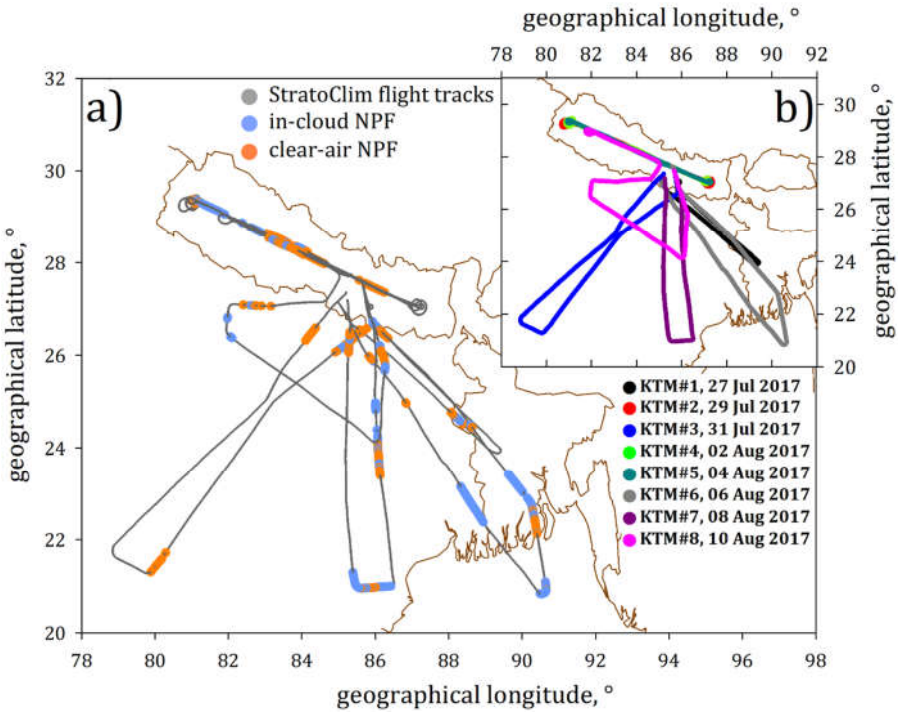

Figure 1

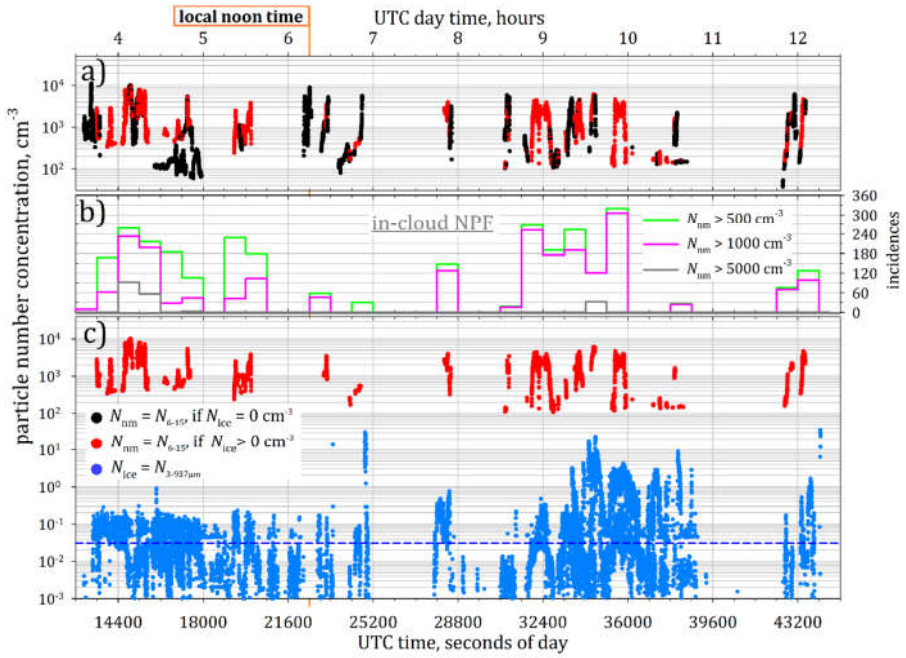
local noon time
UTC day time, hours
4
5
6
7
8
9
10
11
12
a)
b)
c)
in-cloud NPF
N_{nm} > 500 cm^{-3}
N_{nm} > 1000 cm^{-3}
N_{nm} > 5000 cm^{-3}
incidences
360
300
240
180
120
60
0
particle number concentration, cm^{-3}
$N_{nm} = N_{6\text{-}15}$, if N_{ice} = 0 cm^{-3}
$N_{nm} = N_{6\text{-}15}$, if N_{ice} > 0 cm^{-3}
$N_{ice} = N_{3\text{-}937\mu m}$
14400
18000
21600
25200
28800
32400
36000
39600
43200
UTC time, seconds of day

Figure 2

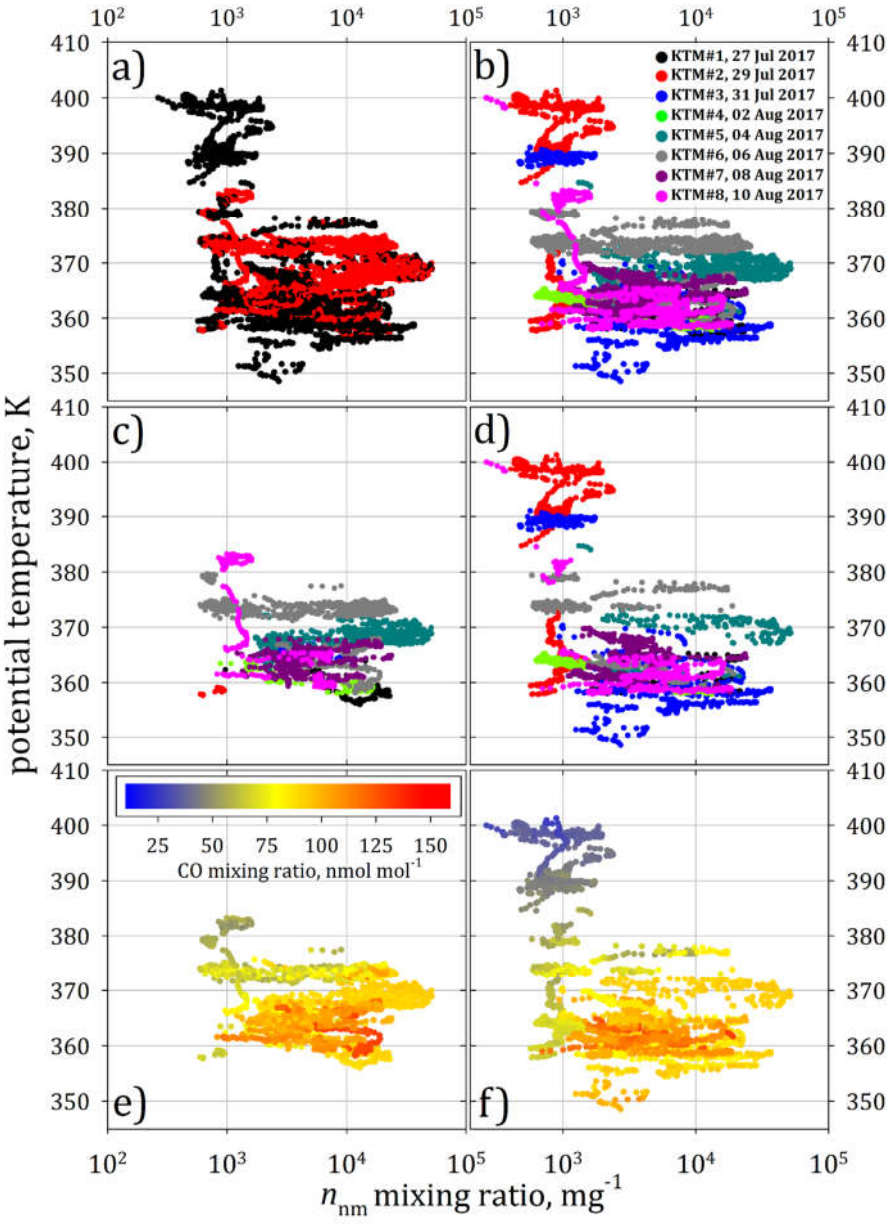
a)
b)
c)
d)
e)
f)
KTM#1, 27 Jul 2017
KTM#2, 29 Jul 2017
KTM#3, 31 Jul 2017
KTM#4, 02 Aug 2017
KTM#5, 04 Aug 2017
KTM#6, 06 Aug 2017
KTM#7, 08 Aug 2017
KTM#8, 10 Aug 2017
potential temperature, K
CO mixing ratio, nmol mol-1
25 50 75 100 125 150
nm mixing ratio, mg-1

Figure 3

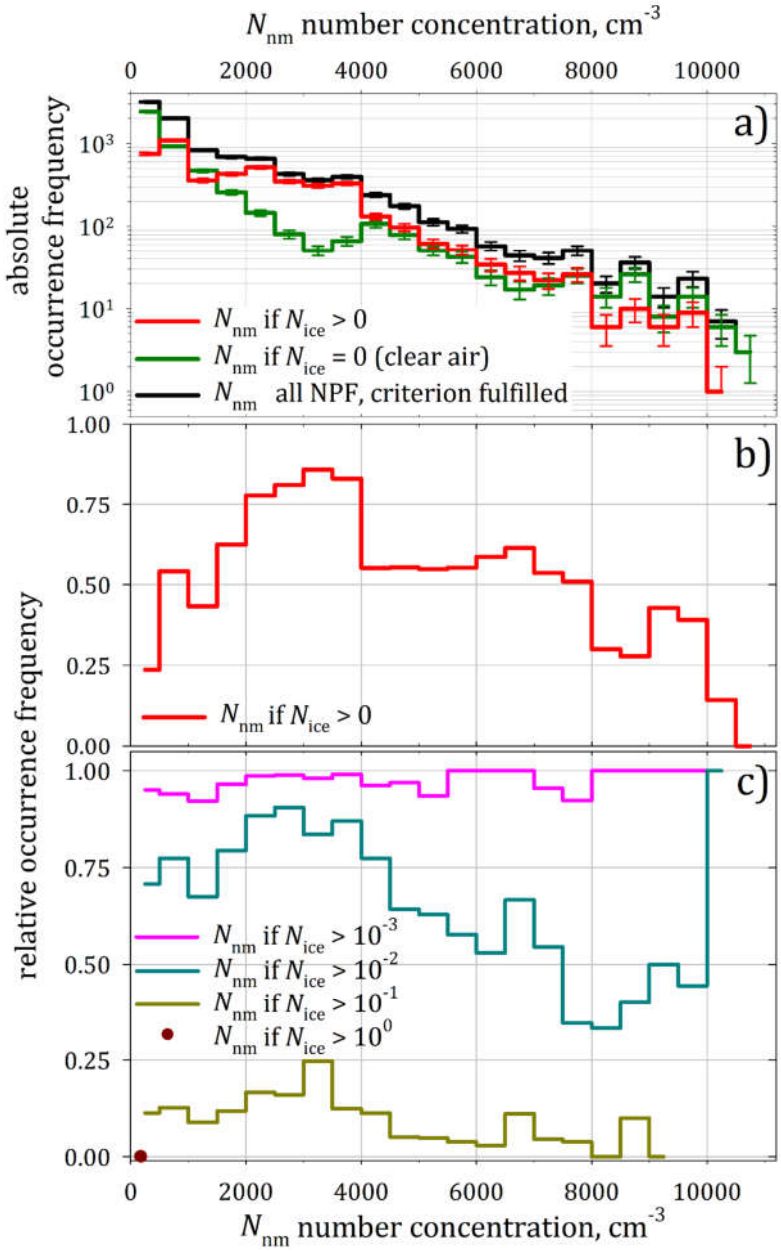
N_{nm} number concentration, cm^{-3}
0
2000
4000
6000
8000
10000
a)
absolute occurrence frequency
10^3
10^2
10^1
10^0
N_{nm} if $N_{ice} > 0$
N_{nm} if $N_{ice} = 0$ (clear air)
N_{nm} all NPF, criterion fulfilled
b)
relative occurrence frequency
1.00
0.75
0.50
0.25
0.00
N_{nm} if $N_{ice} > 0$
c)
N_{nm} if $N_{ice} > 10^{-3}$
N_{nm} if $N_{ice} > 10^{-2}$
N_{nm} if $N_{ice} > 10^{-1}$
N_{nm} if $N_{ice} > 10^{0}$
N_{nm} number concentration, cm^{-3}

Figure 4

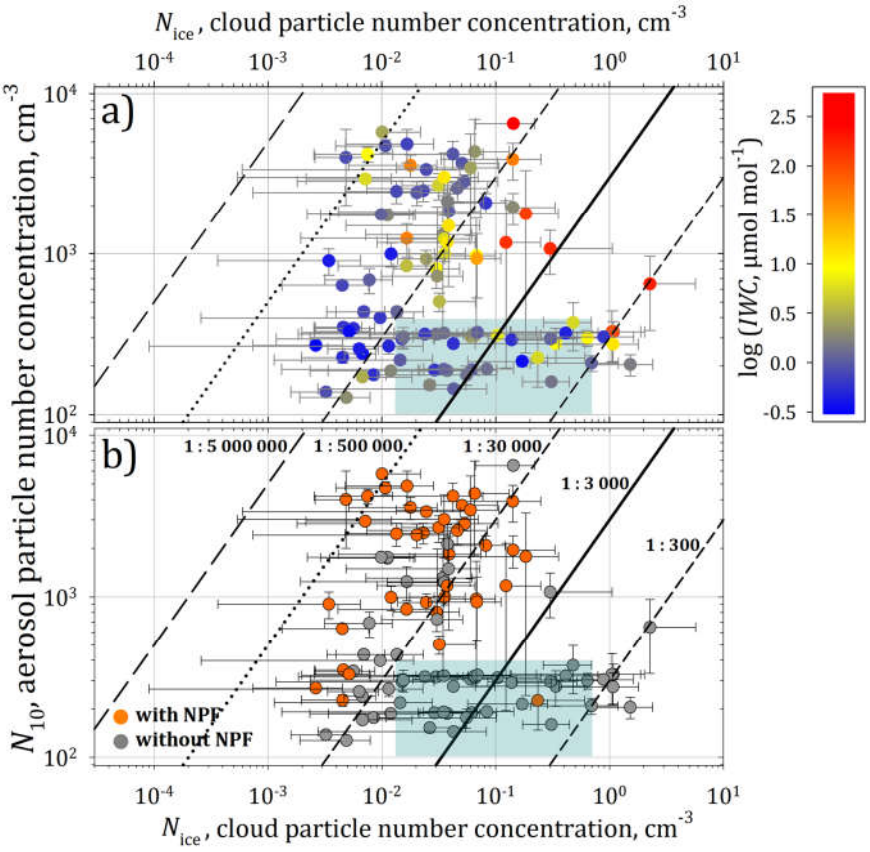
N_{ice}, cloud particle number concentration, cm^{-3}
a)
b)
N_{10}, aerosol particle number concentration, cm^{-3}
log (IWC, µmol mol^{-1})
1 : 5 000 000
1 : 500 000
1 : 30 000
1 : 3 000
1 : 300
with NPF
without NPF

Figure 5

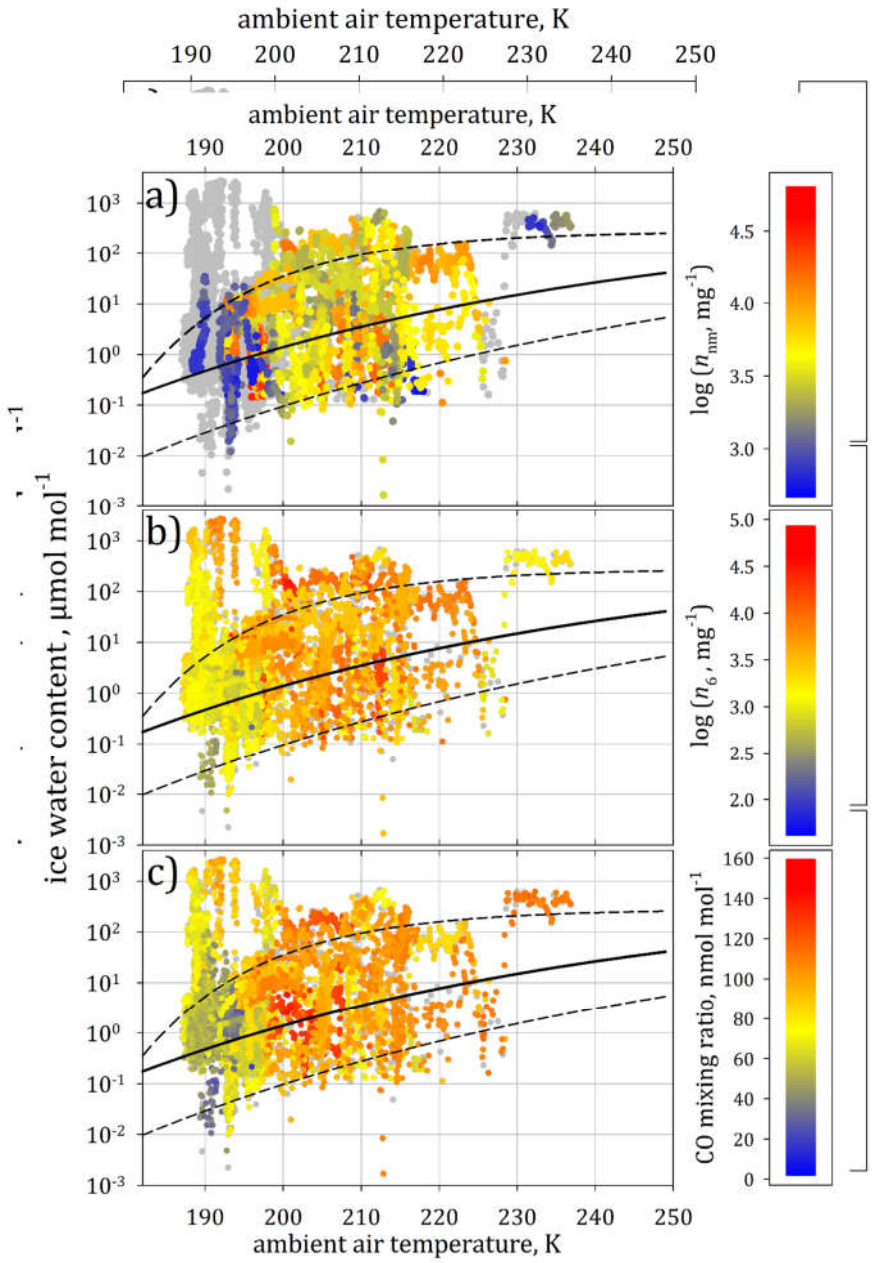
ambient air temperature, K
190 200 210 220 230 240 250
a)
b)
c)
ice water content , µmol mol-1
log (n_{nm}, mg-1)
log (n_6, mg-1)
CO mixing ratio, nmol mol-1

Figure 6

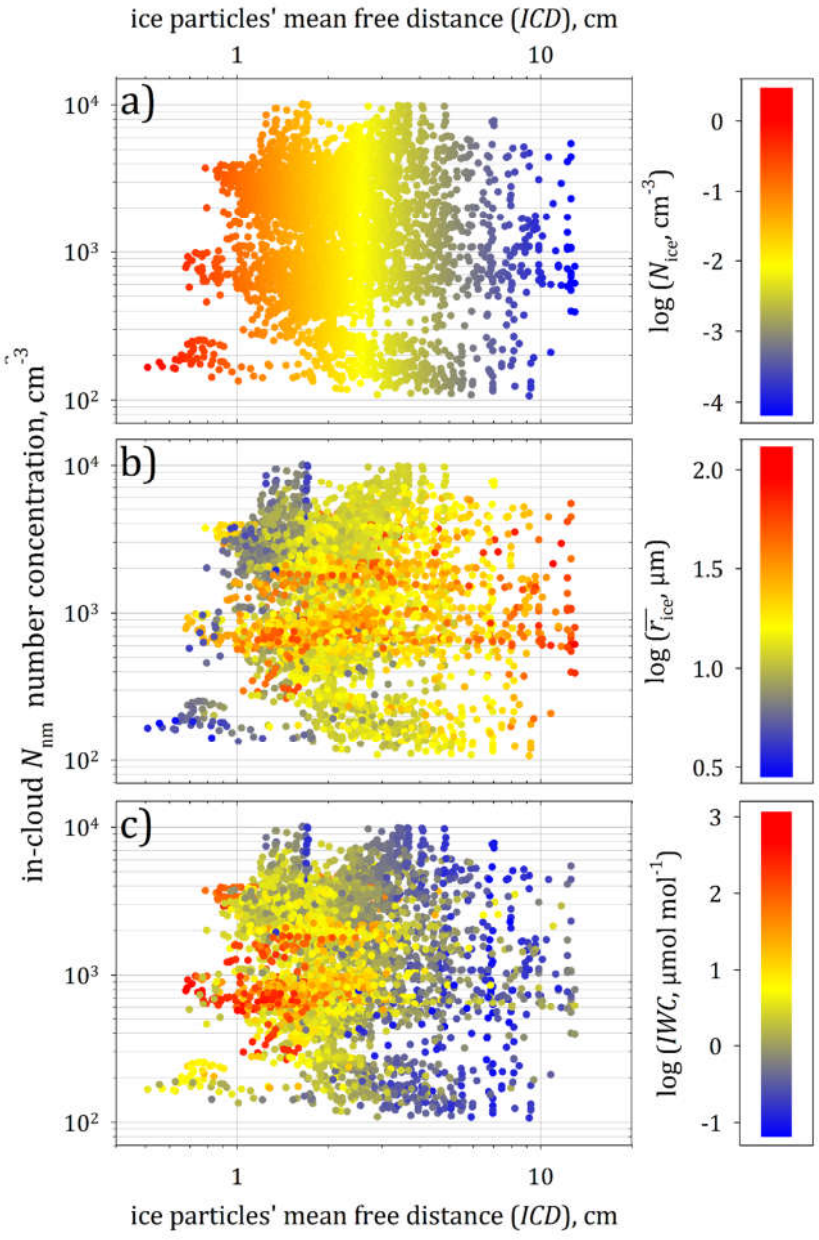
ice particles' mean free distance (ICD), cm
1
10
a)
b)
c)
in-cloud N_{nm} number concentration, cm^{-3}
10^4
10^3
10^2
log (N_{ice}, cm^{-3})
0
-1
-2
-3
-4
log ($\overline{r_{ice}}$, µm)
2.0
1.5
1.0
0.5
log (IWC, µmol mol^{-1})
3
2
1
0
-1
ice particles' mean free distance (ICD), cm

Figure 7

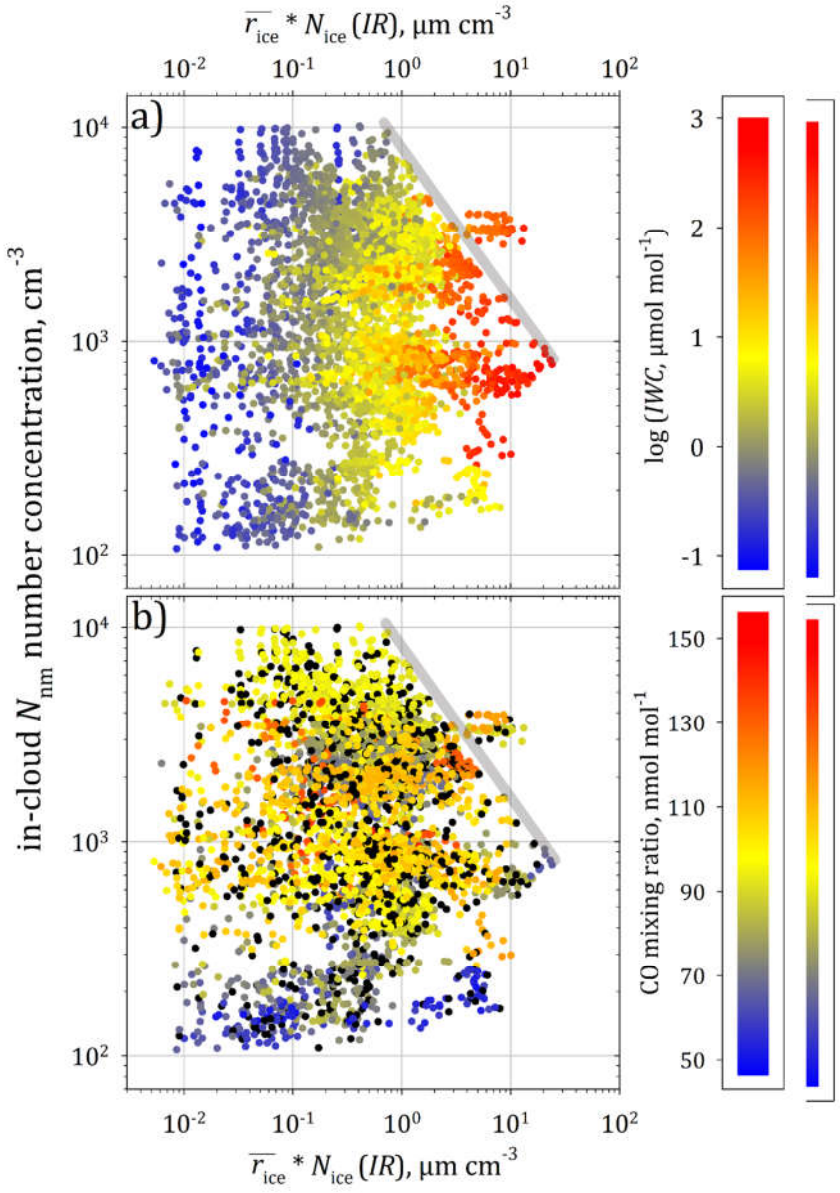
$\overline{r_{ice}} * N_{ice}(IR)$, µm cm^{-3}
10^{-2}
10^{-1}
10^{0}
10^{1}
10^{2}
a)
b)
10^{4}
10^{3}
10^{2}
in-cloud N_{nm} number concentration, cm^{-3}
log (IWC, µmol mol^{-1})
3
2
1
0
-1
CO mixing ratio, nmol mol^{-1}
150
130
110
90
70
50

Figure 8

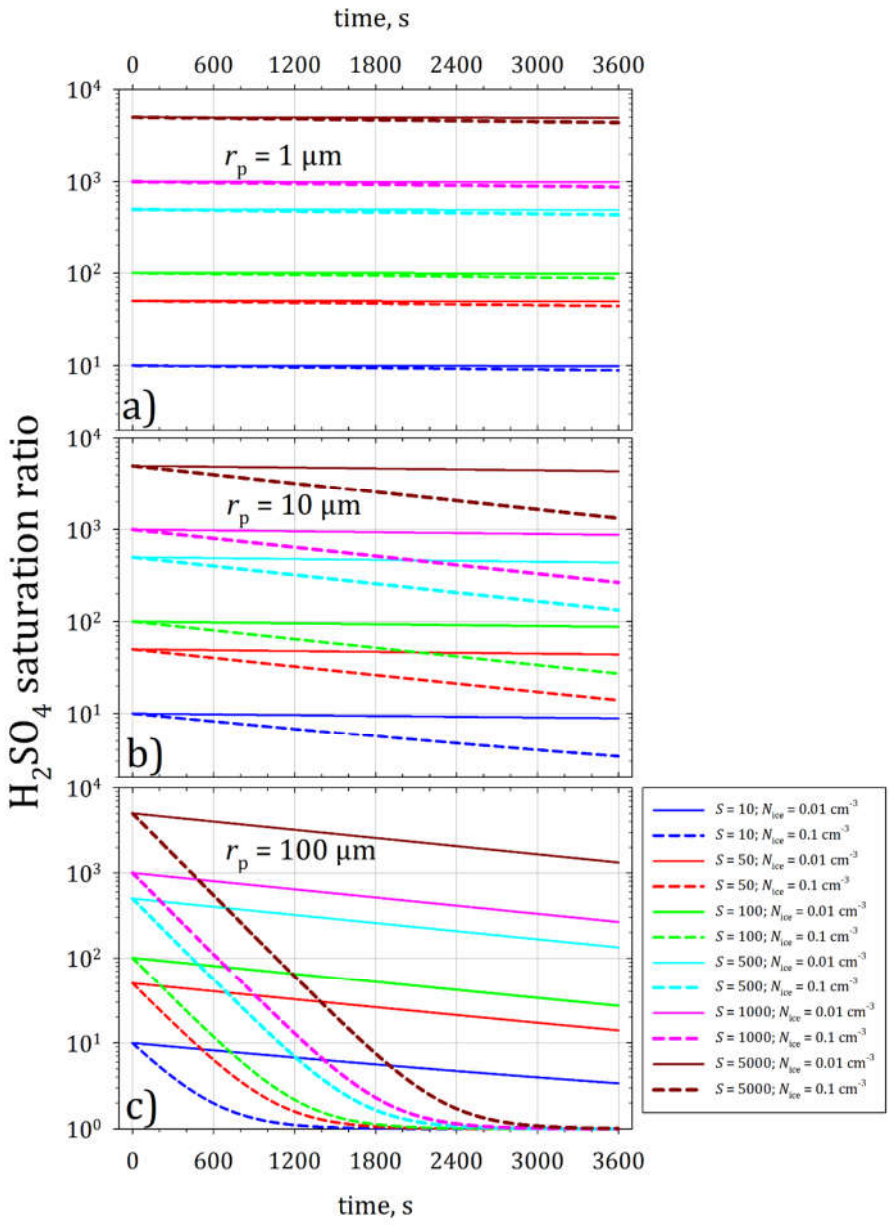
time, s
0
600
1200
1800
2400
3000
3600
10^4
10^3
10^2
10^1
10^0
r_p = 1 µm
r_p = 10 µm
r_p = 100 µm
a)
b)
c)
H_2SO_4 saturation ratio
S = 10; N_{ice} = 0.01 cm^{-3}
S = 10; N_{ice} = 0.1 cm^{-3}
S = 50; N_{ice} = 0.01 cm^{-3}
S = 50; N_{ice} = 0.1 cm^{-3}
S = 100; N_{ice} = 0.01 cm^{-3}
S = 100; N_{ice} = 0.1 cm^{-3}
S = 500; N_{ice} = 0.01 cm^{-3}
S = 500; N_{ice} = 0.1 cm^{-3}
S = 1000; N_{ice} = 0.01 cm^{-3}
S = 1000; N_{ice} = 0.1 cm^{-3}
S = 5000; N_{ice} = 0.01 cm^{-3}
S = 5000; N_{ice} = 0.1 cm^{-3}

Figure B- 1

Table 1: NPF data set of StratoClim 2017, separated by event detection under clear-air (i.e. N_{ice} = 0 cm^{-3}) and in-cloud conditions (i.e. N_{ice} > 0 cm^{-3}). Discussed in-cloud NPF events (104 ~~incidents~~ incidents that comply with introduced NPF criterion, Section 2.2) are partially embedded in larger clear-air NPF fields with continuously elevated $N_{~~uf~~nm}$. The total number of measurement seconds with NPF detections under either of both conditions is scaled to the total data set of the CN measurements and the total duration of NPF encounters. The mean horizontal distance is calculated from the event duration based on a mean flight speed of the M-55 *Geophysica* (154 ± 39 m s^{-1}) providing an equivalent horizontal extension of NPF. Geometric heights are interpolated values with maximum range of scattering from UCSE data of the eight flights.

NPF condition	total duration seconds	total duration hh : mm	percentage of NPF data	percentage of total dataset	mean horizontal distance in km
clear-air	4866	01 : 21	~ 51.2 %	~ 5.3 %	~ 750
in-cloud	4634	01 : 17	~ 48.8 %	~ 5.0 %	~ 714

		in-cloud NPF			
potential temperature	geometric altitude	total duration seconds	total duration hh : mm	percentage of in-cloud NPF	mean horizontal distance in km
355 – 360 K	~ 11 ± 2.5 km	432	00 : 07	~ 9.3 %	~ 67
360 – 365 K	~ 13.5 ± 2 km	1231	00 : 21	~ 26.6 %	~ 190
365 – 370 K	~ 15.3 ± 1 km	1455	00 : 24	~ 31.4 %	~ 224
370 – 375 K	~ 15.8 ± 1 km	1375	00 : 23	~ 29.7 %	~ 212
> 375 K	≳ 16.0 km	141	00 : 02	~ 3 %	~ 22

Formatiert: Schriftart: 11 Pt.
Formatiert: Schriftart: 11 Pt.
Formatiert: Schriftart: 11 Pt.
Formatiert: Schriftart: 11 Pt.
Formatiert: Schriftart: 11 Pt., Schriftfarbe: Automatisch, Englisch (Vereinigtes Königreich)
Formatierte Tabelle
Formatiert: Rechts
Formatiert: Englisch (Vereinigtes Königreich)